UNIVERSITY OF SALERNO

DEPARTMENT OF INDUSTRIAL ENGINEERING

Ph.D. Thesis in

MECHANICAL ENGINEERING

Cycle XII (2011-2013)

Dry clutch for automated manual transmissions

Structural analysis and control strategies

Mario Pisaturo

Supervisor	Coordinator
Prof.	Prof.
Adolfo Senatore	Vincenzo Sergi

to Alessia.

ACKNOWLEDGEMENTS

I would like to acknowledge Prof. Adolfo Senatore, my Ph.D Supervisor, both for the contributions to the development of this thesis and, mainly, for his role in my professional growth.

I would like to acknowledge Prof. Nicola Cappetti and Prof. Vincenzo D'Agostino for their support during these years. I would also like to thank all colleagues at University of Salerno for creating a positive atmosphere for research and discussions.

I would like to acknowledge Prof. Maurizio Cirrincione who has given me the opportunity to spend six months at the Université de Technologie Belfort-Montbéliard.

My parents Maria Rosalba and Emilio together with my brother Alessandro have always supported me, which has meant a lot for me. For this I will always be grateful.

Finally, I would like to express my appreciation to Alessia. Thanks for your patience and for constantly being at my side to encourage and support me. To you I dedicate this work.

Salerno, March 2014

Mario Pisaturo

Contents

List of Tables

List of Figures

Chapter 1

INTRODUCTION

The goal of this thesis is the study of the automotive push-type dry clutches used in the Automatic Manual Transmissions (AMTs) and in the Dual Clutch Transmissions (DCTs) in order to improve their performances during the engagements phases. The push-type clutch is very widespread in the automotive sector because it allows many advantages in terms of cost, reliability, isolation of vibrations to the driveline, reduced axial size and stability to the facings wear [1]. Instead, the main advantages of an AMT, respect to the Automatic Transmissions (ATs), are improvements in terms of safety, reliability, and driving performances together with the reduction of the fuel consumption and pollutant emissions [2]. For these reasons by mixing the advantages of the push-type clutch with the advantages of the AMT it is possible to attain very high performance. On the other hand, the most important drawback of the AMT is the power interruption (the so called "torque gap") during the gear shifts events. To solve this problem in the last decade the DCTs have been introduced. In fact, by applying the engine torque to one clutch just as the engine torque is being disconnected from the other one [3] the torque transmission is allowed also during the gear shift phases.

Automatic Transmissions aren't widely used, especially in the European market. But recent automotive market forecasts predict that there will be a decline of the Manual Transmissions (MTs) in favour of the AMTs and DCTs [3]. DCTs will gain market share continuously over the next few years although it depends on several circumstances based on the automakers' and transmission manufacturers' strategies. At the moment, however, Europe is the fastest growing market for DCTs. There is also significant interest at the

moment in North America. And we know that there are some programmes already released [4]. Since the recent market forecasts predict the growth

	Year		
Type	**2002**	**2008**	**2014**
AMT	1.0%	4.3%	5.5%
Automatic	12.0%	16.1%	13.5%
CVT	0.5%	1.8%	1.3%
DCT	0.0%	2.6%	11.4%
Manual	86.5%	75.2%	68.3%
Grand Total	100%	100%	100%

Table 1.1: West European Light Vehicle Production by Transmission Type. Source: CSM Worldwide [5]

both for the AMTs and DCTs, the manufactures are investing huge resource to improve the performances of this kind of transmissions and, at the same time, to reduce their cost.

In this light, the work developed in this thesis aims to give useful information both to the clutches designers and to the control algorithms designer in order to improve the performances, and consequently, the diffusion, of the AMTs and DCTs.

The thesis is organized as follows. Chapter 2 is an introductory section on the historical evolution of the clutches and of the automotive transmissions systems. Chapter 3 deals with the transmissibility torque model by considering the main factors which affect the elastic components of a push-type clutch and the friction coefficient. In the Chapter 4 application of control algorithms both for a two DoFs driveline model and for a five DoFs model are introduced. Finally, the Chapter 5 underlines the concluding remarks.

Chapter 2

HYSTORICAL EVOLUTION OF THE CLUTCH

2.1 OVERVIEW

The aim of the automotive transmissions mechanisms is to transmit the power from the engine to the wheels. Since the '800 century, with the invention of the car, numerous resource has been employed to improve the performances of these mechanisms. One of the most important component of the automotive transmissions mechanisms is the clutch. Its role is to connect the engine to the gearbox, and this latter, together to the differential, transmit the power to the wheels. Another important role of the clutch is to interrupt the torque flux in order to avoid damages to the synchronizers. The most heavy working condition for the clutch is the vehicle launch. In fact, during this phase the engine is in rotation, while the driveline (gearbox, differential and wheels) is motionless. Hence, it is the sliding between the flywheel and the clutch to permit of reaching the regime condition. The most important requirements of a clutch are to ensure the transmission of the max engine torque by limiting vibration problems during the engagement/disengagement phase.

There are two main different kinds of clutches: dry and wet. The wet clutches are used when is necessary to transmit high torque from the engine to the wheels. Moreover, they have better performance than dry clutches but on the other hand their axial size, cost and complexity are higher. So

the most commons are the dry clutches because they are more simple, less expensive, they have a reduced axial size and the last but not the least advantage is the reduced fuel consumptions and, consequently, the reduced pollutant emissions.

During the years, the clutches mechanisms have had a significant development in order to improve their efficiency, the gear shift quality and the reduction of fuel consumptions. This latter is a fundamental aspect specially in the big cities where the great number of the cars affects the air quality and, consequently, the health of the citizens.

In the next paragraphs the advantages and the disadvantages of the different kinds of clutches used in the years in the automotive sector have been analysed.

2.1.1   CONE CLUTCH

It is one of the first kind of clutches to be installed on the cars. It has had a great success during the '20 years of the last century. In Figure 2.1 is shown the first kind of the cone clutch. In this version the clutch is pushed by a coil spring forward the cone surface obtained directly in the flywheel. It is a normally closed clutch. The driver acts on the clutch pedal by winning the spring force and by disengaging the clutch. This version of cone clutch have
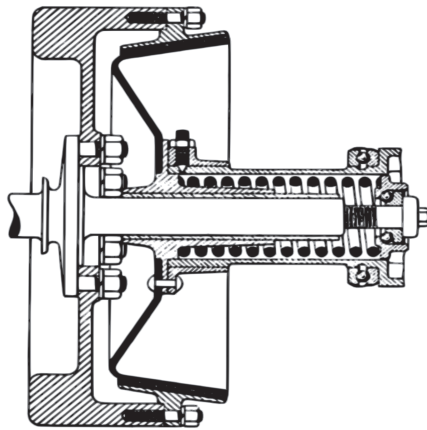
Figure 2.1: Cone clutch

many drawbacks [6]:

- The spring force acts also on the flywheel and, consequently, on the crankshaft by loading considerably the bearings;

- The cone coupling requires a great precision of the contacts surfaces to transmit the higher torque;

- The engagement phase is too abrupt and this affects the comfort perceived by the driver;

- To disengage the clutch the driver must apply steadily the max force on the clutch pedal because was used a coil spring;

- The torsional vibrations are transmitted from the engine to the gearbox without damping. In fact, the engine and the gearbox are rigidly connected;

- It is not possible to transmit high power.

To solve some of the above drawbacks have been developed different solutions as:

- Symmetric cone clutch to balance the axial load on the bearings, Figure 2.2;

- Inverse cone clutch to eliminate the axial load on the bearings, Figure 2.3.
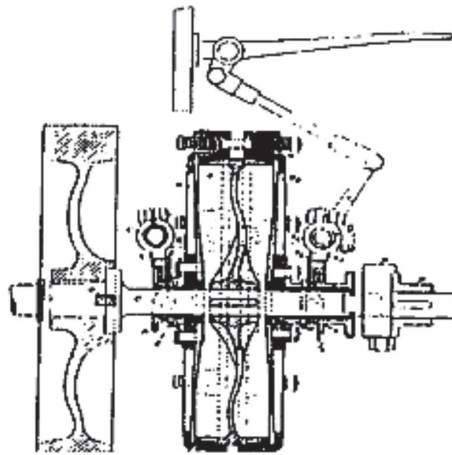
Figure 2.2: Double cone clutch, [6]
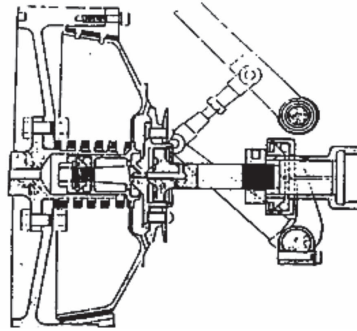
Figure 2.3: Inverse cone clutch, [6]

2.1.2 RADIAL CLUTCH

It was introduced after the cone clutch by becoming an alternative to this latter. The working principle is similar to the drum brakes and for this reason it is also called "drum clutch". Two jaws externally covered with clutch material are radially pushed forward the internal surface of the flywheel. The push force is due to the spring and, during the motion, to the centrifugal force. With this clutch there are not axial loads and it is possible to transmit a higher torque. The main drawbacks are:

- The engagement phase, like in the cone clutches, is too abrupt and this affects the comfort perceived by the driver;

- For some value of the friction coefficient, increases the tendency to lock.
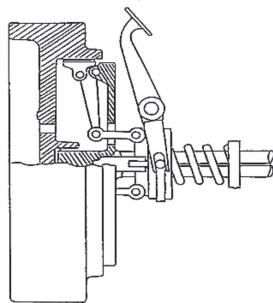
Figure 2.4: Radial clutch, [6]

2.1.3 MULTIDISK CLUTCH

The multidisk clutches was introduced in the middle of the '20 years of the last century in order to reduce the axial size by augmenting the torque transmissible. They are constituted from some discs alternatively connected on the flywheel and on the primary shaft of the gearbox, Figure 2.5. In this way it is possible to increment the number of the friction surfaces and, consequently, the max torque transmissible. There are two kinds of multidisk clutches: dry and wet. In the dry clutches it is not necessary to realize the tightness to avoid the leaks of the oil. Moreover, the friction coefficient of a dry clutch is higher respect to the wet clutch so the number of the friction pairs necessary to transmit the same torque is lesser than the wet one. In any way, the dry clutches present many disadvantages as higher wear, noise and lesser comfort perceived by the driver.
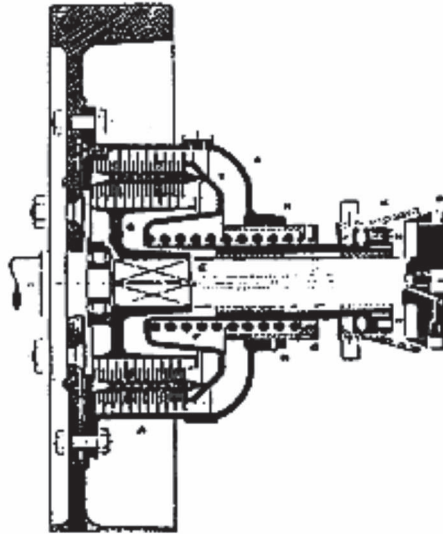
Figure 2.5: Multidisk clutch, [6]

2.1.4 COIL SPRING CLUTCH

The coil spring clutches spreads in the '20 years of the last century and since from the first versions they presented numerous advantages respect to the other kinds of clutches used in those years. They were less expensive, simple

to make, with a reduced axial size, with a less number of rotating mass and, more important thing, they had not necessity of a particular maintenance.

The first solution to exert the clamp load was to use a single coil spring which acts on some levers that pushed the clutch disk forward the flywheel, Figure 2.6. This version presents some disadvantages as:
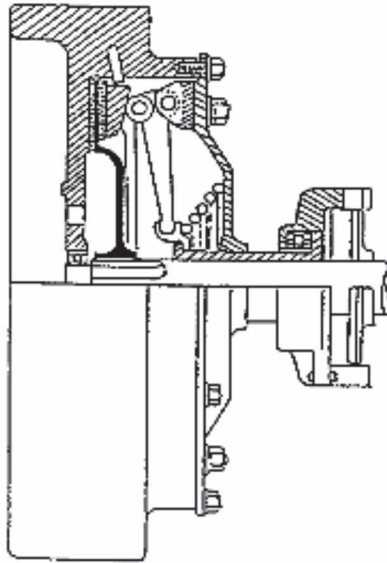
Figure 2.6: Single coil clutch, [6]

- Non-uniformities of the load distribution on the pressure plate;

- Difficulty to reach a smooth engagement phase.

To solve these drawbacks was developed a version with more parallels coil springs placed along a circumferential which act directly on the pressure plate, Figure 2.7. In this way was improved the load distribution on the pressure plate and, moreover, was reduced the axial size.

This version was adopted before the introduction of the diaphragm spring, and it had the below drawbacks:

- The force required to disengage the clutch increases with the wear;

- The little difference in the coil springs produces a non-uniform load distribution on the pressure plate;

- The centrifugal force deforms the coil springs with consequent loss of the clamp load;

- The temperatures reached during the working conditions change the elastic characteristic of the coil springs;

- Higher axial size.

All these disadvantages were eliminated by substituting the coil springs with the diaphragm spring.
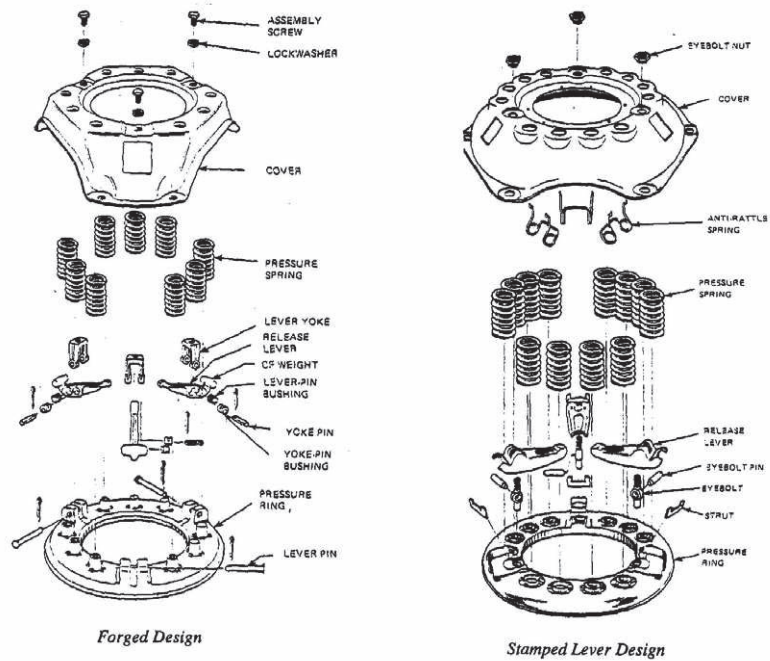
Figure 2.7: Multi coils clutch, [6]

2.1.5 DIAPHRAGM SPRING CLUTCH

As stated above, the diaphragm spring clutch solved the drawbacks of the coil springs clutches. For this reason the diaphragm spring clutch became the most spread automotive clutch.

There are two typologies of diaphragm spring clutches: the *push-type* and the *pull-type*. The *push-type* clutches are based on a first class lever

where the pressure plate fulcrum is placed at greater radius with respect to the cover fulcrum, Figure 2.8. In this way it is necessary to push the throwout bearing against the flywheel to disengage the clutch. Instead, in
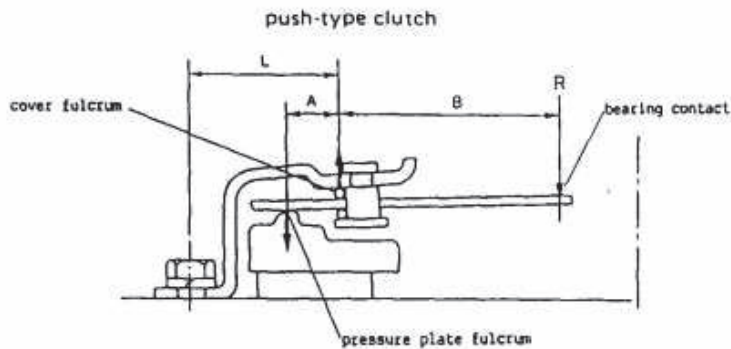
Figure 2.8: Push-type clutch, [6]

the *pull-type* clutches the fulcrums are inverted, second class lever, and the throwout bearing is pulled backward respect the flywheel, Figure 2.9. In the
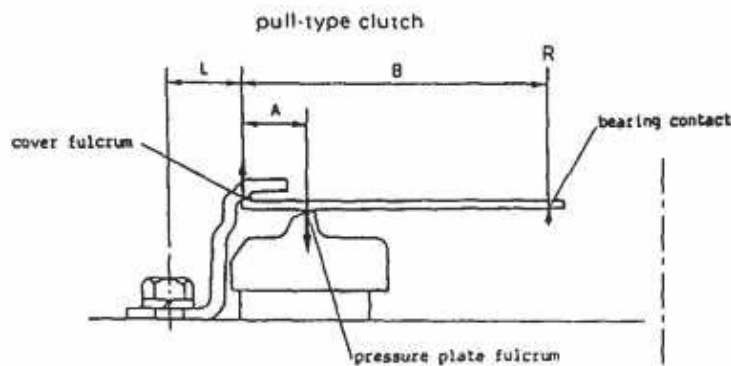
Figure 2.9: Pull-type clutch, [6]

next table are listed the comparison between the advantages and the disadvantages of the push-type and pull-type clutches. As shown in Table 2.1 the pull-type clutches have many advantages respect the push-type. Despite that, the push-type clutches have had a higher diffusion because their installation/removal from the car is very simple in comparison to the pull-type clutches.

PUSH-TYPE CLUTCH	
Advantages	**Disadvantages**
Simple release bearing design	Larger "L" dimension more cover deflection at release
Simple installation and removal in vehicle	
PULL-TYPE CLUTCH	
Advantages	**Disadvantages**
Smaller "L" dimension, less cover deflection at release	More complex release bearing design
Larger lever ratio possible, lower bearing load	More complex installation and removal procedures
Simpler, lower stress diaphragm spring design possible	
Larger O. D. possible	
No lower cover fulcrum element	
Higher clamp load design possible	

Table 2.1: Comparison between the push-type and pull-type clutches [6]

In any way, the working principle for both kinds of clutches is very similar. They are both normally closed clutches and the clamp load is given from the external rim of the diaphragm spring. The *fingers* of this latter element are the release system and they are operated by the throwout bearing.

In the next part of this paragraph the contacts points between the diaphragm spring and, respectively, the cover and the throwout bearing has been analysed. In fact, the ratio between the distance from these points defines the *lever ratio B/A*. Where B is the distance between the bearing contact and the cover fulcrum and A is the distance from the pressure plate fulcrum and the cover fulcrum. These definitions are the same for both the clutches but the related contacts points are different, Figures 2.8 and 2.9. The lever ratio is calculated after that the travels of the throwout bearing and the pressure plate have been defined. The lever ratio is chosen by considering the pedal effort, the possibility to modulate the pedal effort and

the maximum wear tolerated. Higher is the lever ratio, higher is the wear tolerated, lower is the pedal effort and higher is its modulation.

During the opening/closing phase of the clutch, the contacts radii between the different components change and it results in lever ratio modification. To avoid this drawback some solution that permit to have a steady lever ratio have been developed. In Figure 2.10 are shown two solutions developed to have a steady contact radius between the spring and the throwout bearing. For the contact between the spring and the pressure plate, the steady
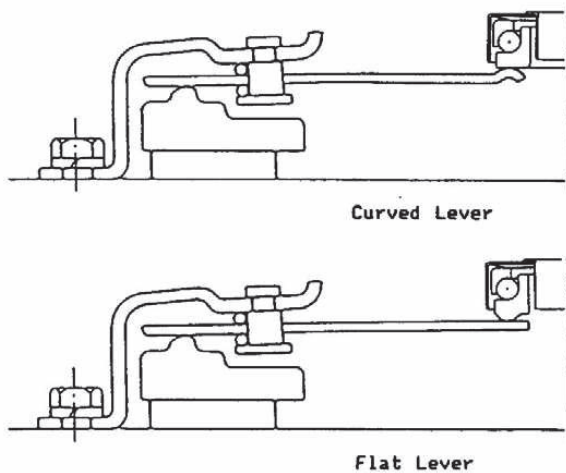
Figure 2.10: Solutions developed to achieve constant contact radius spring-throwout bearing, [6]

radius is obtained by making a curved shape on the pressure plate. This part is called *pressure plate fulcrum* so that the spring rotates by remaining in contact with this surface.

The real fulcrum of the lever, which is used to calculate the lever ratio B/A, is represented by the contact zone between the cover and the spring. In Figure 2.11 different solutions to have a steady contact radius on the lever fulcrum are shown.

(a) Riveted construction, wire ring fulcrums

(b) Bent Tab construction, wire ring fulcrums

(c) Formed in cover, upper fulcrum Belleville, lower fulcrum

(d) Formed in cover, upper fulcrum Shaped rivet head, lower fulcrum
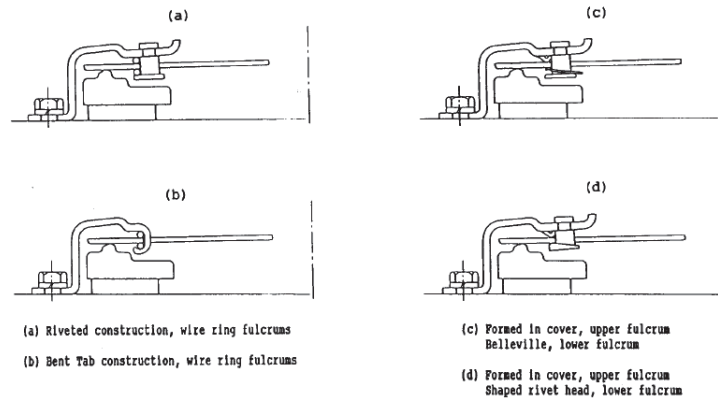
Figure 2.11: Solutions to realize the lever fulcrum, [6]

2.2 MAIN COMPONENTS OF AN AUTOMOTIVE PUSH-TYPE CLUTCH

In this paragraph the main components and the working principles of an automotive push-type clutch are described. It is possible to consider three main subsystems:

- The cover, it is in-built with the flywheel (green in Figure 2.13);

- The clutch disk, it is in-built to the gearbox primary shaft (red in Figure 2.13);

- Operating system, it permits to open/close the clutch (yellow in Figure 2.13).

In Figure 2.13 is highlighted that the engine torque is divided in two parts. The first one is transmitted from the flywheel directly to the clutch disk and the second one is transmitted from the flywheel to the cover, and from this latter to the pressure plate. Finally the pressure plate transmits the torque to the second surface of the clutch disk. In this way the clutch disk works with all the two surfaces. When the clutch is disengaged the flywheel and the cover rotate together with the crankshaft while the clutch disk, clamped to the gearbox primary shaft, rotates freely.
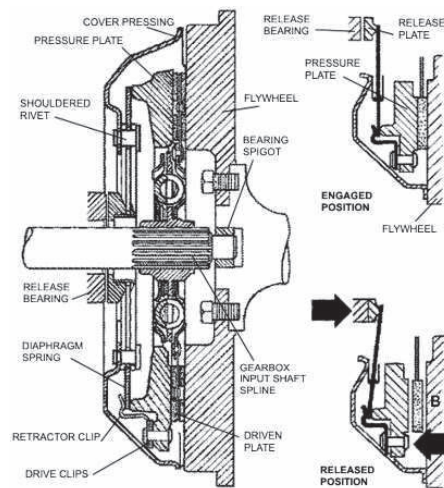
Figure 2.12: Push-type clutch: principle of operation, [7]
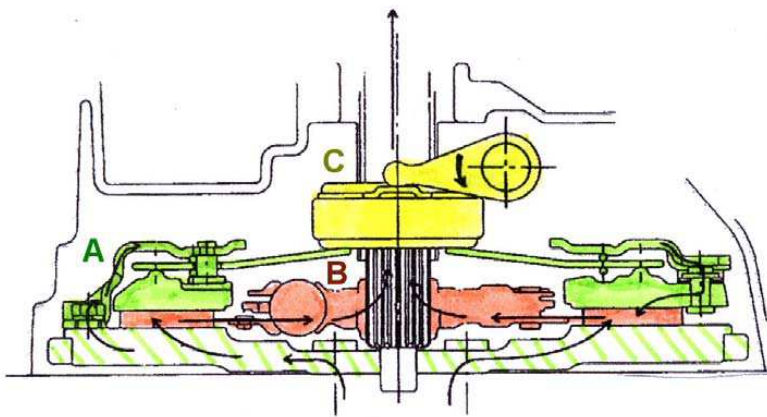
Figure 2.13: Subsystems of a push-type clutch, [6]

2.2.1   THE FLYWHEEL

The instantaneous output torque resulting from an internal combustion engine shows peaks which induce oscillations of the engine speed called engine acyclicity. In order to limit these oscillations a flywheel, i.e. a solid cast iron wheel having a big rotational inertia, is added to one end of the crankshaft [8].

Besides reducing the engine-speed oscillations the flywheel also performs three auxiliary functions [8]:

- It serves as a reduction gear for the cranking-up of the engine;

- It has on its outer perimeter a toothed target used for calculating both the engine revolution speed and the crankshaft angle for ignition and injection timing;

- The gearbox-facing side is used as a friction surface for the clutch disk.

In the first version the flywheel was made with a single mass in-built with the crankshaft. The drawbacks of this solutions were:

- The high load on the crankshaft;

- All the vibrations were transmitted integrally from the engine to the gearbox and consequently this results in discomfort perceived from the driver.

To solve these problems the dual-mass flywheel (DMFW) was introduced. The primary mass of the DMFW is much lighter than a conventional flywheel and in-built with the crankshaft. The secondary mass is only very loosely connected via the torsion damper as well as via the roller bearing to the primary flywheel mass and therefore it generates practically no reactions on the crankshaft [9]. The aim of a DMFW is to reduce the resonance frequency of the driveline under the minimum excitation frequency of the engine by augmenting the rotational inertia of the driveline. In fact, the second mass is added to the gearbox primary shaft.

The main components of a DMFW are:

- A primary mass (light blue in Figure 2.16), in-built with the crankshaft;

- A secondary mass (red in Figure 2.16), independent from the primary mass and supported by a ball bearing;

Figure 2.14: Single-mass flywheel

- A torsional damper assembled between the primary and the secondary masses;

- A pressure plate and a clutch disk that, after its engagement, are connected with the secondary mass.

In a first phase the DMFW had a slow development due to its high cost and complexity. But after a deep analysis it has been understood that the introduction of the DMFW to reduce the vibrational drawback, both torsional and bending, was strictly related to the reduction of the warranty costs due to the customers claims.

In Figure 2.16 is depicted the development history of the DMFW.

Figure 2.15: Dual-mass flywheel (DMFW)

1985

1987

1989

1995

planned for 2000
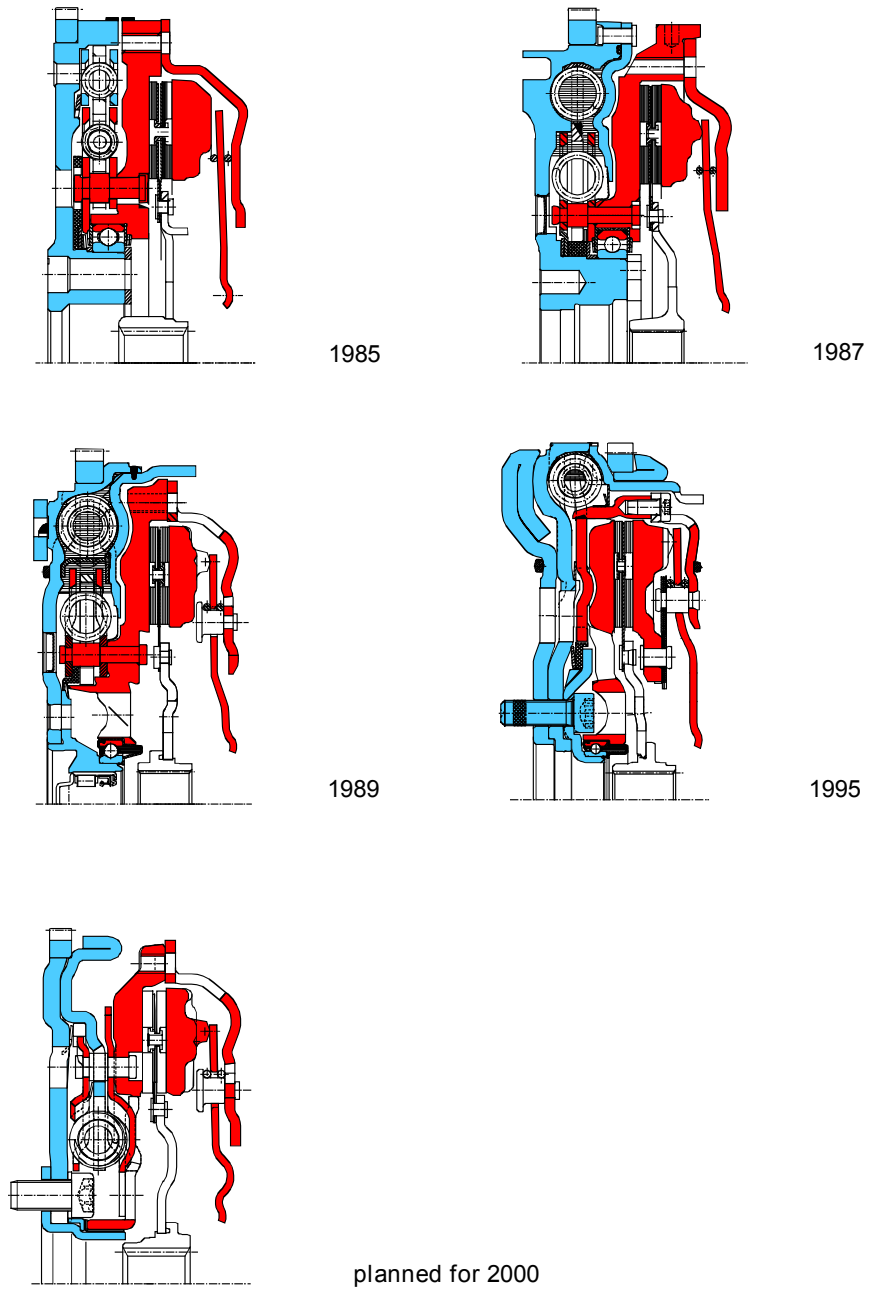
Figure 2.16: Development history of the DMFW, [9]

2.2.2   THE DIAPHRAGM SPRING

The diaphragm spring is one of the fundamental part of the modern clutches. In fact, numerous advantages of the modern clutches are due to this spring. It derives from a belleville spring with the addition of some fingers which have the function of lever that operate the same spring, Figure 2.17. By

Figure 2.17: Diaphragm spring

studying the elastic characteristic of the diaphragm spring is possible to note an increasing clamping load for clutch disk worn. This means that it can transmit a higher torque ever for reduced thickness of the frictional facings, inversely to the coil spring clutches. In fact, in these latter the clamp load is smaller when the clutch disk is worn and, consequently, also its transmissibility is lower. Another advantage of the diaphragm spring is that to disengage the clutch it is necessary a lower force, i.e. a lower pedal effort in the manual transmissions. This factor improves the ergonomics and the effort required to the driver to keep the clutch in the open position is lower [6]. It is important to note that it is possible to get the desired elastic characteristic of a belleville spring by changing the ratio between the height and the thickness (h/t in Figure 2.19).

2.2.3   PRESSURE PLATE, COVER, CLIPS AND DRIVE STRAPS

The pressure plate (or push plate) is in-built with the cover by the drive straps and the clips. It is mounted on the gearbox primary shaft free to translate and rotate [6]. The pressure plate is released mainly by the action of the cushion spring. Also the drive straps and the clips give a contribute to release the pressure plate. But the main aim of the drive straps is to transmit
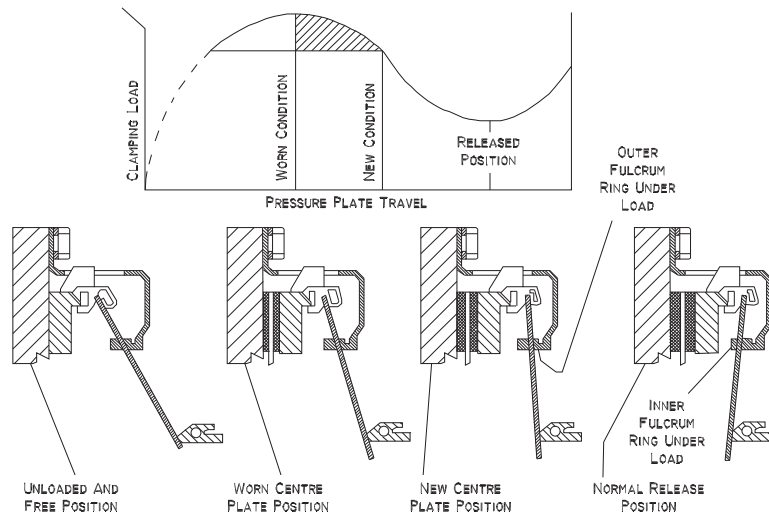
Figure 2.18: Diaphragm spring phases
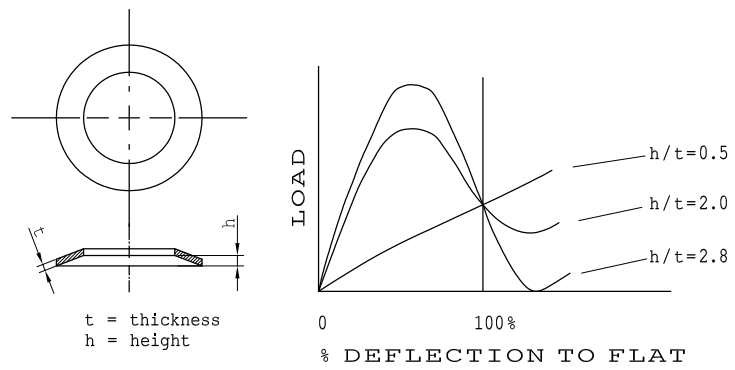
Figure 2.19: Elastic characteristic as function of the ratio h/t, [6]

the engine torque from the cover to the pressure plate. When the release load is calculated it is important also to take into account the contribute of the drive straps and clips. The role of the pressure plate is to push the clutch disk forward the flywheel to transmit the torque from the engine to the gearbox. In Figure 2.20 is shown the pressure plate assembled to the cover. The

Figure 2.20: Pressure plate

cover is torsionally in-built with the flywheel, it is also the component where is riveted the diaphragm spring. This latter is operated by the throwout bearing to release the pressure plate and to disengage the clutch. Sometimes, the drive straps are not able to provide force to release and to keep distant the pressure plate from the clutch disk during the opening phase. For this reason, the clips are mounted on the cover, Figure 2.22. The role of the drive straps and of the clips are very important to avoid that the pressure plate comes in contact with the clutch disk during the opening phase due to the bending vibration of the crankshaft. The cover also acts as travel end of the clutch both during the opening phase and during the closing phase. In fact, when a new clutch is designed, it is very important to ensure the full closing when it is new and a full opening when it is worn. If this is not adequately taken into account it could be possible to damage the clutch components.
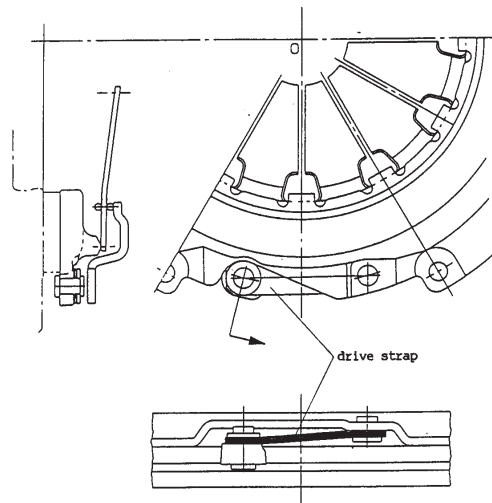
Figure 2.21: Drive straps, [6]
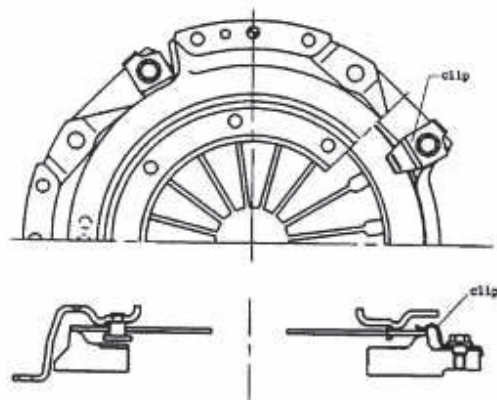
Figure 2.22: Clips, [6]
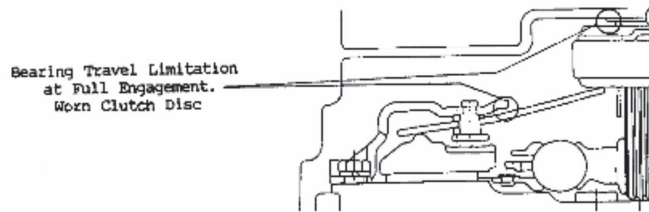
Figure 2.23: Travel end of a push-type clutch during the closing phase, [6]
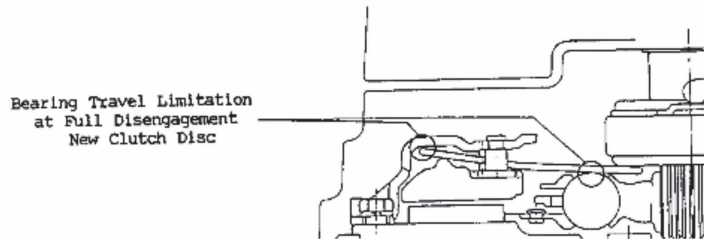
Figure 2.24: Travel end of a push-type clutch during the opening phase, [6]

2.2.4   SELF-ADJUSTING CLUTCH (SAC)

The Self-Adjusting Clutch (SAC©, LuK patents) [10], was introduced on the vehicles with high power engine where, due to the clutch wear, the pedal effort increases considerably. The SAC is a system that permits to compensate the clutch wear. In this way, the clutch works ever in the same conditions so that the pedal effort is ever the same. In fact, with conventional clutches, the actuation force increases with increased facing wear. Instead, with the SAC©, the progressive facing wear is compensated by means of a wear adjusting system. In this way the actuation force does not change [10].

   The SAC© differs from the conventional clutch by adjusting the position of the diaphragm spring during wear, Figure 2.26. The adjustment occurs such that the angle position of the diaphragm spring, and hence the actuation and clamp load, remain constant regardless of wear (primarily facing wear). In order to realize this wear compensation, the main diaphragm spring is not permanently riveted to the clutch cover or mounted with keyhole tabs, as with conventional clutch assemblies, but is only retained axially against the cover by a defined force (sensor force). A ramp ring, which extends into the ramp of the cover, is located between the diaphragm spring

and the clutch cover, and is rotated by the coil springs [10].
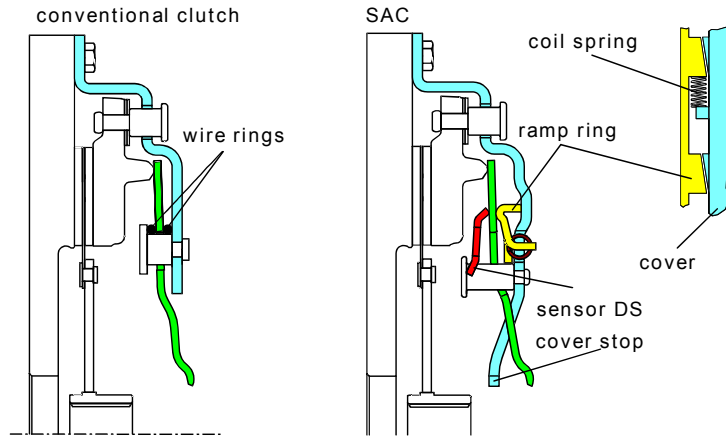
Figure 2.25: Comparison of a conventional clutch to a SAC, [10]
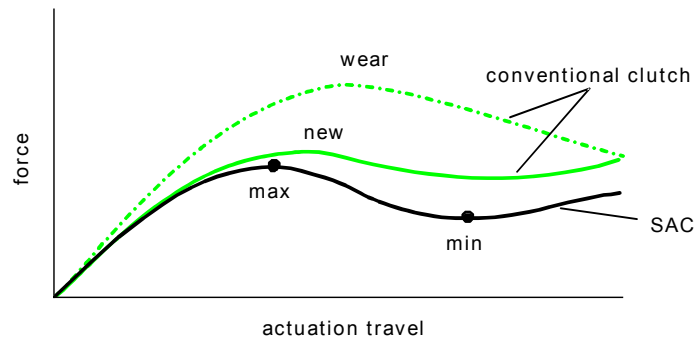
Figure 2.26: Comparison of the actuation force characteristic curve of a conventional clutch to a SAC, [10]

2.2.5 FACING MATERIALS

The facing material is the heart of the clutch [11]. In the past facings were produced with beech and oak wood. Clutch facings as we know them today have been manufactured since around 1930 [11]. It is very hard to choose the good facing material because the facing requirements are numerous and in contrast each other. The main characteristics of a good facing material are listed below:

- High friction coefficient;

- Wear resistance;

- Comfort;

- Mechanical resistance;

- Low rotational mass;

- Low cost;

- Thermal resistance;

- Good thermal conductivity;

- Lifetime;

- Good feasibility.

- Environment compatibility
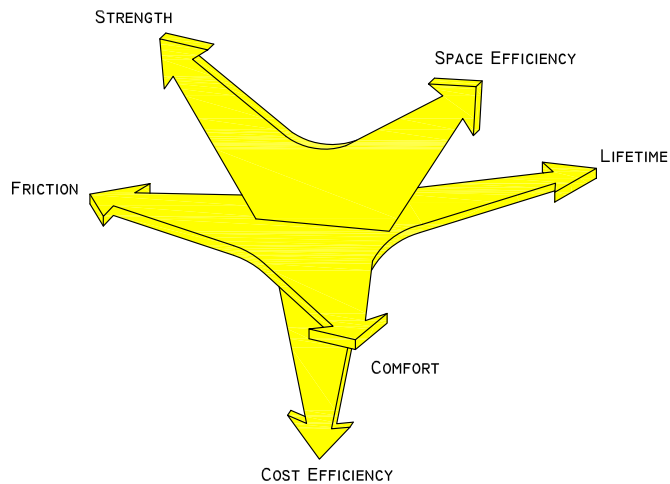
Figure 2.27: Conflicting goals in facing development, [11]

To attain all these goals, the facings have been made of phenolic resin and exposed to strict tests. The Figure 2.28 shows the production cycle of a typical facing.
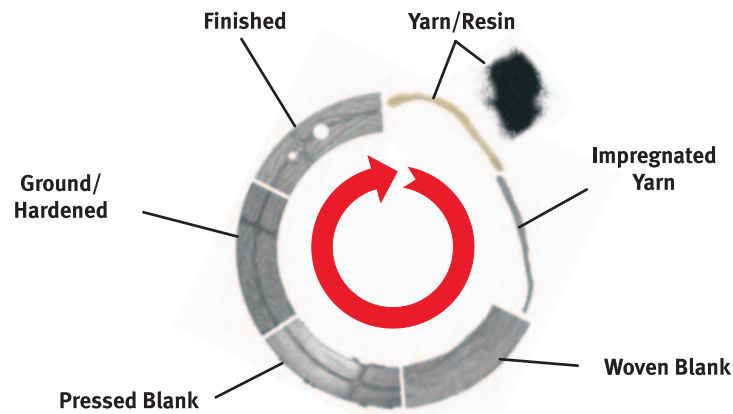
Figure 2.28: Production cycle, [11]

2.2.6 CLUTCH DISK

The clutch disk is connected to the gearbox primary shaft by the hub. It
is placed between the flywheel and the pressure plate so that it works with
both its surfaces. The aim of the clutch disk is to smoothly connect and
disconnect the engine to the driveline [8]. In Figure 2.29 is depicted a typical
clutch disk. The main components of a clutch disk are:

- The facings;

- The hub;

- The torsional dampers;

- The cushion spring or flat spring.

The role of the facings has been analysed in the previous paragraph. The
hub has the goal to rigidly connect the clutch disk with the gearbox primary
shaft. The torsional damper has the important function to filter the torsional
vibrations due to the engine speed fluctuation. But due to the increasing
need of acyclicity filtering, the more powerful engines are equipped with a
DMFW that assures a better filtering action. In this latter case the clutch
disk presents no damping springs [8]. The most important component which,
as it will be analysed in details in the next paragraphs, determines the torque
characteristic exhibited from a given clutch is the cushion spring, or flat
spring [2]. It is placed between the two friction surfaces, and usually it is
composed by a number of a cushion segments, Figure 2.30.
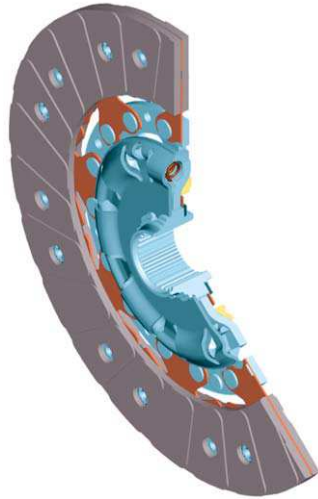
Figure 2.29: Clutch disk, [12]
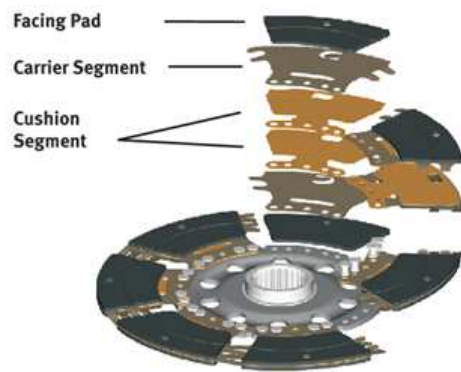
Figure 2.30: Explose of a clutch disk, [12]

2.2.7   HYDRAULIC ACTUATOR

In an MT vehicle the hydraulic cylinder connects the clutch pedal to the
clutch washer-spring fingers through a hydraulic circuit composed of a mas-
ter cylinder called concentric master cylinder (CMC) directly connected to
the pedal, several pipe sections one of which is flexible to allow the movement
of the engine on its suspensions, an optional vibration filter and, finally, a
slave cylinder called concentric slave cylinder (CSC) that, placed between
the gearbox carter and the clutch, pushes directly the diaphragm fingers [8].

This hydraulic circuit also assures an effort reduction through the com-
bined effect of the surface ratio between the CMC and CSC and the lever
effect given by the clutch pedal. An additional compensation spring is also
present in order to further reduce the force necessary for opening the clutch
[8].

In an AMT vehicle the CSC position is directly controlled by the trans-
mission control unit through an electro-valve. Since no effort is required by
the driver neither an effort-reduction nor a compensating spring are used
[8].
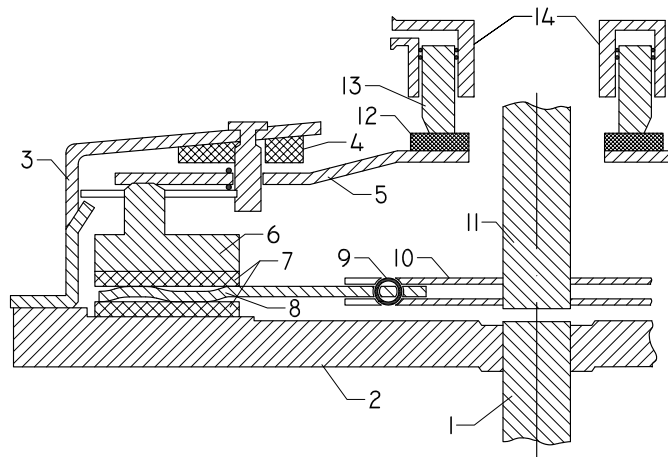
Figure 2.31: Clutch structure, axial cut. 1 crankshaft 2 flywheel 3 clutch
external structure 4 wear-compensation system 5 washer spring 6 pressure
plate 7 friction pads 8 flat spring 9 spring damper 10 clutch disk 11 gearbox
primary shaft 12 needle roller bearing 13 concentric slave cylinder (CSC)
piston 14 concentric slave cylinder (CSC), [8]

2.3 AUTOMOTIVE TRANSMISSIONS SYSTEMS

In this paragraph the different solutions adopted in automotive transmissions systems are analysed.

2.3.1 MANUAL TRANSMISSION (MT)

An automotive manual transmission is usually used with a driver-operated clutch which is engaged or disengaged by a foot pedal. Its aim is to adjust the torque transfer from the engine to the transmission. The driver chooses the gear by using a gear stick.

The first kind of a manual transmission is thought to have been invented by Louis-René Panhard and Emile Levassor in the late 19th century. This type of transmission offered multiple gear ratios and, in most cases, reverse. The gears were typically engaged by sliding them on their shafts (hence the phrase shifting gears), which required careful timing and throttle manipulation when shifting, so the gears would be spinning at roughly the same speed when engaged; otherwise, the teeth would refuse to mesh. These transmissions are called sliding mesh transmissions or sometimes crash boxes, because of the difficulty in changing gears and the loud grinding sound that often accompanied the gear shifts [13].

In a non-synchronous transmission, to shift to a higher gear, the transmission is put in neutral and the engine allowed to slow down until the transmission parts for the next gear are at a proper speed to engage. The vehicle also slows while in neutral and that slows other transmission parts; thus the time in neutral depends on the road slope, wind, and other such factors. To shift to a lower gear, the transmission is put in neutral and the throttle is used to speed up the engine and thus the relevant transmission parts, to match speeds for engaging the next lower gear. For both up-shifts and down-shifts, the clutch is released (engaged) while in neutral. Some drivers use the clutch only for starting from a stop, and shifts are done without the clutch. Other drivers will disengage the clutch, shift to neutral, then engage the clutch momentarily to force transmission parts to match the engine speed, then disengage the clutch again to shift to the next gear, a process called double clutching. Double clutching is easier to get smooth, as speeds that are close but not quite matched need to speed up or slow down only transmission parts, whereas with the clutch engaged to the engine, mismatched speeds are fighting the rotational inertia and power of the

engine [13].

Modern manual-transmission vehicles are equipped with a synchronized gearbox. Transmission gears are always in mesh and rotating, but gears on one shaft can freely rotate or be locked to the shaft. The locking mechanism for a gear consists of a collar (or dog collar) on the shaft which is able to slide sideways so that teeth (or dogs) on its inner surface bridge two circular rings with teeth on their outer circumference: one attached to the gear, one to the shaft. When the rings are bridged by the collar, that particular gear is rotationally locked to the shaft and determines the output speed of the transmission. The gearshift lever manipulates the collars using a set of linkages, so arranged so that one collar may be permitted to lock only one gear at any one time; when "shifting gears", the locking collar from one gear is disengaged before that of another is engaged. One collar often serves for two gears; sliding in one direction selects one transmission speed, in the other direction selects another [13].

The modern cone system was developed by Porsche and introduced in the 1952 Porsche 356; cone synchronisers were called Porsche-type for many years after this. In the early 1950s, only the second-third shift was synchromesh in most cars, requiring only a single synchro and a simple linkage; drivers' manuals in cars suggested that if the driver needed to shift from second to first, it was best to come to a complete stop then shift into first and start up again. With continuing sophistication of mechanical development, fully synchromesh transmissions with three speeds, then four, and then five, became universal by the 1980s. Many modern manual transmission cars, especially sports cars, now offer six speeds. The 2012 Porsche 911 offers a seven-speed manual transmission, with the seventh gear intended for cruising-top speed being attained on sixth [13].

Figure 2.32: Synchronized gearbox, [14]

2.3.2   AUTOMATED MANUAL TRANSISSION (AMT)

The first version of Automated Manual Transmission (AMT) was introduced in the 1988 for the F1 cars. Successively a version which used the synchronized gearbox for the standard cars was developed. The rapid development of the AMTs is due to the fact that it is directly derived from a manual one through the integration of actuators. For these reasons, development and production costs are generally lower than other automatic transmissions, while the reliability and durability are at highest level. For high class sport cars, vehicle dynamic performances and driving quality can be strongly improved with respect to automatic transmissions [15]. AMTs systems are generally constituted by a dry or wet clutch assembly and a multi-speed gearbox, both equipped with electro-mechanical or electro-hydraulic actuators, which are driven by a control unit, the transmission control unit (TCU), Figure 2.33. The operating modes of AMTs are usually two: semiautomatic or fully automatic. In both cases, after the gear shift command, the TCU manages the shifting steps according to current engine regime, driving conditions and selected program. An important way to reduce the engage-
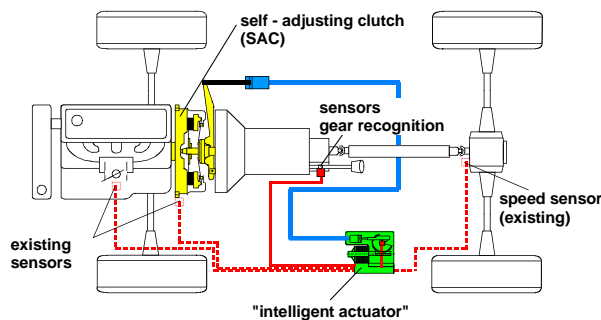
Figure 2.33: Scheme of a typical AMT, [16]

ments/disengagements times is the torque tracking. Usually the clutch is designed to transfer the engine torque in any working conditions with a sufficient additional reserve. For these reasons a fully closed clutch can transfer 1.5 to 2.5 times the engine torque. The basic idea of the torque tracking is to adjust the clutch torque by considering the current engine torque. In Figure 2.34 is explained the working principle of the torque tracking. Figure 2.35 illustrates the advantage during a shifting cycle. With a conventional system without torque tracking, the clutch torque remains much higher than
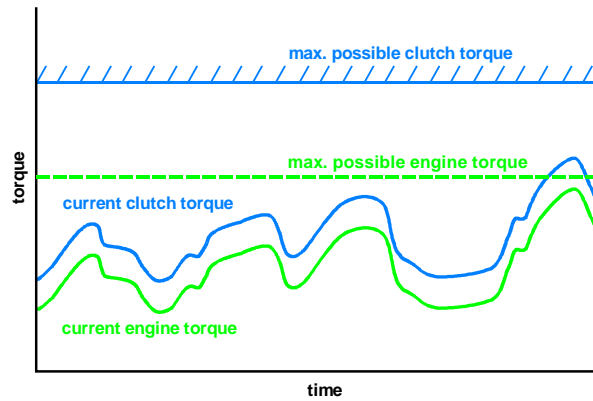
Figure 2.34: Time curve torque tracking, [16]

the engine torque. If the driver wants to change gears and lets up on the
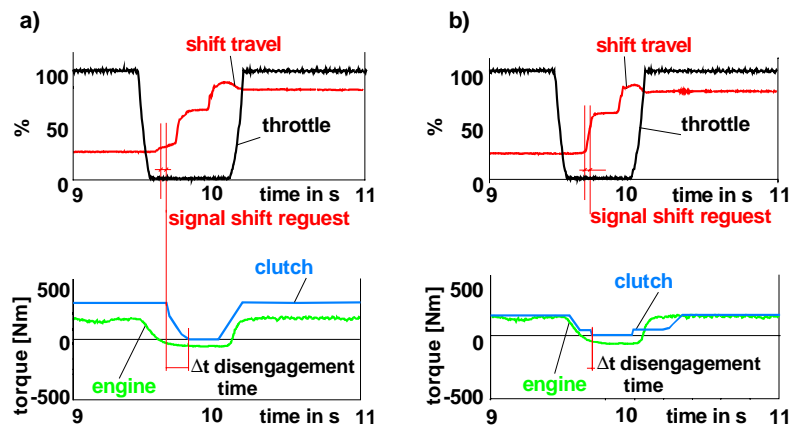
Figure 2.35: The shifting process a) without torque tracking and b) with torque tracking, [16]

gas pedal, the engine torque decreases. When he/she moves the shift lever, the intention to switch gears is triggered and the clutch must now go from "completely closed" to "completely open". This defines the disengagement time. This must not be too long or else the clutch still transfers torque during the synchronization of the next gear, which can lead to transmission chatter or damage. Figure 2.35b) illustrates the same process with torque

tracking. The clutch torque is only slightly higher than the engine torque. Thus the travel to "completely open" is already significantly less than with a conventional sequence. If the driver then lets up on the gas because he wants to change gears, the engine torque and thus also the clutch torque decrease immediately. By triggering the intent to switch, the clutch is thus already almost open and the rest of the disengagement occurs very quickly. Even very sudden gear changes are thus possible without transmission noise or damage [16]. Another important advantage of the torque tracking is the reduction of the vibrations during the gear shifts, Figure 2.36.
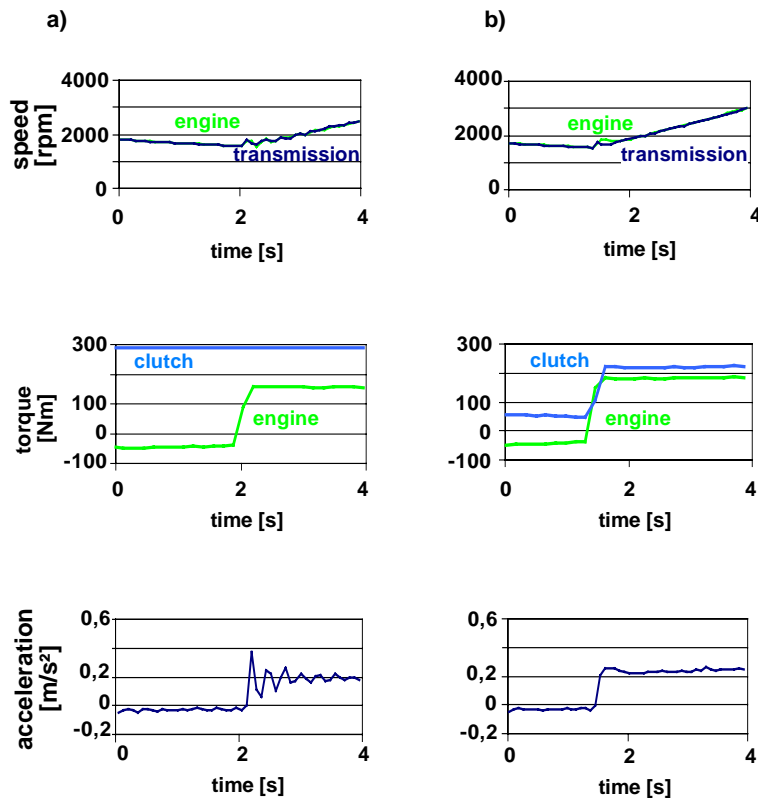
Figure 2.36: Load cycle a) without torque tracking and b) with torque tracking, [16]

2.3.3 DUAL-CLUTCH TRANSMISSION (DCT)

A dual-clutch transmission (or twin-clutch gearbox or double clutch transmission or synthetically DCT) offers the function of two manual gearboxes in one. The DCT is a semi-automatic gearbox assembly with separate clutches for odd and even gears [3]. Figure 2.37 shows together two DCT sketches for dry (above) and wet (below) clutches, in which: A and B are the two independent clutch discs, C is the outer clutch output shaft, D the inner one [17].
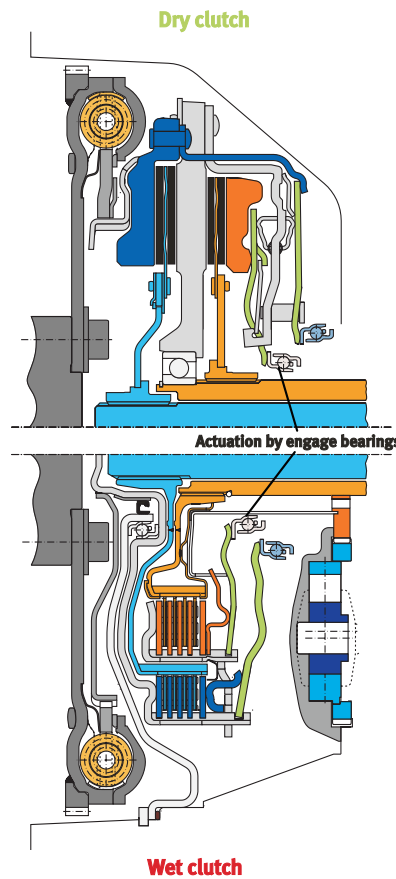
Figure 2.37: Dual-Clutch Transmission: dry system (upper) and wet system (bottom), [17]

The main advantage of a DCT is that the shifts can be achieved without

sensible torque gap. In fact, with this system is possible to apply the engine torque to one clutch just as the engine torque is being disconnected from the other clutch. The result is gentle, jerk-free gear changes with the same relaxed driving style found in an automatic combined with the efficiency of a manual transmission [3]. It is as smooth as the most sophisticated automatic, but more economical than a conventional automatic; it is as easy to drive as a standard auto, faster and more responsive than manual gearbox on high performance cars [3].

Another important advantage of the DCT is the reduction of fuel consumptions. In fact, by eliminating the torque gap the efficiency of the system is improved. Some experts say that by comparing a 5-gears AT and a 6-gears DCT, this latter improves of the 10% the efficiency of fuel. Nowadays the diffusion of the DCT is limited to the high class vehicles because their costs are higher respect to the AMT or MT. On the other hand, market forecasts say that in the next years the vehicles equipped with DCT will attain more than 10% of the market shares.

2.3.4   AUTOMATED TRANSMISSION (AT)

The first automatic transmission was invented in 1921 by Alfred Horner Munro of Regina, Saskatchewan, Canada, and patented under Canadian patent CA 235757 in 1923. (Munro obtained UK patent GB215669 215,669 for his invention in 1924 and US patent 1,613,525 on 4 January 1927). Being a steam engineer, Munro designed his device to use compressed air rather than hydraulic fluid, and so it lacked power and never found commercial application [18]. The first automatic transmissions using hydraulic fluid were developed by General Motors during the 1930s and introduced in the 1940 Oldsmobile as the "Hydra-Matic" transmission. They were incorporated into GM-built tanks during World War II and, after the war, GM marketed them as being "battle-tested" [18].

In a modern AT the engine is connected to the gearbox by the torque converter. It takes the place of a mechanical clutch, allowing the transmission to stay in gear and the engine to remain running while the vehicle is stationary, without stalling [18]. A set of planetary gears provide a range of gear ratio. To effect gear changes, one of two types of clutches or bands are used to clamp a particular member of the planetary gear to the (fixed) frame, while allowing another member to rotate, thereby transmitting torque and producing gear reductions or overdrive ratios. These clutches are actuated by the valve body, their sequence controlled by the transmission's internal

programming [18].

Hydraulic automatic transmissions are almost always less energy efficient than manual transmissions due mainly to viscous and pumping losses, both in the torque converter and the hydraulic actuators [18].
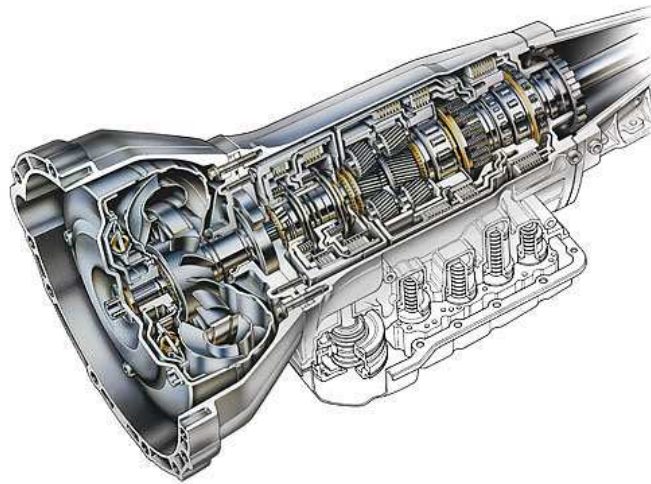
Figure 2.38: Automatic Transmission, torque converter (left) and planetary gearbox (right) [19]

2.3.5 CONTINUOUSLY VARIABLE TRANSMISSION (CVT)

Another kind of automated transmission is the Continuously Variable Transmission (CVT). The main difference with other mechanical transmissions, which offer a fixed number of gear ratios, is that it can change steplessly through an infinite number of effective gear ratios between maximum and minimum values.

The typical CVT system is composed by two V-belt pulleys that are split perpendicular to their axes of rotation, with a V-belt running between them. The gear ratio is changed by moving the two sheaves of one pulley closer together and the two sheaves of the other pulley farther apart. Due to the V-shaped cross section of the belt, this causes the belt to ride higher on one pulley and lower on the other. In this way the effective diameters of the pulleys, which in turn changes the overall gear ratio. The distance between the pulleys does not change, and neither does the length of the

belt, so changing the gear ratio means both pulleys must be adjusted (one bigger, the other smaller) simultaneously to maintain the proper amount of tension on the belt [20]. The V-belt needs to be very stiff in the pulley's
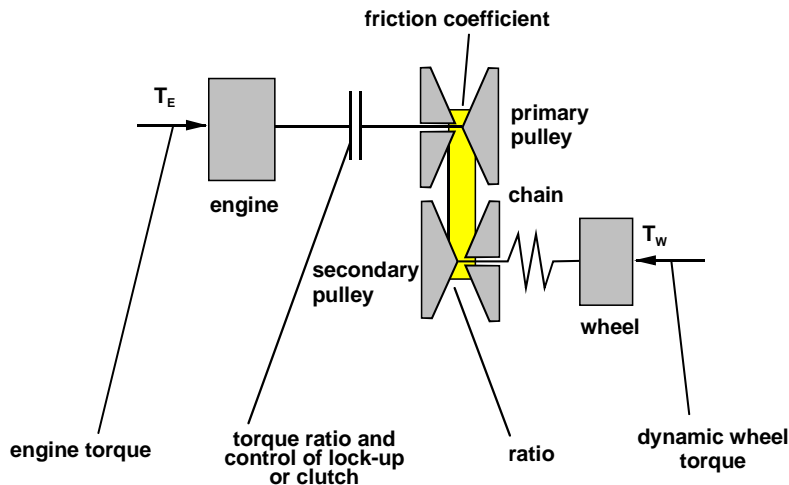
Figure 2.39: CVT scheme, [21]

axial direction in order to make only short radial movements while sliding in and out of the pulleys. This can be achieved by a chain and not by homogeneous rubber. To dive out of the pulleys one side of the belt must push. This again can be done only with a chain. Each element of the chain has conical sides, which perfectly fit to the pulley if the belt is running on the outermost radius. As the belt moves into the pulleys the contact area gets smaller. The contact area is proportional to the number of elements, thus the chain has lots of very small elements. The shape of the elements is governed by the static of a column. The pulley-radial thickness of the belt is a compromise between maximum gear ratio and torque. For the same reason the axis between the pulleys is as thin as possible. A film of lubricant is applied to the pulleys. It needs to be thick enough so that the pulley and the belt never touch and it must be thin in order not to waste power when each element dives into the lubrication film [20]. One of the most advantage of CVT is that it can provide better fuel economy than other transmissions by enabling the engine to run at its most efficient revolutions per minute (RPM) for a range of vehicle speeds [20].
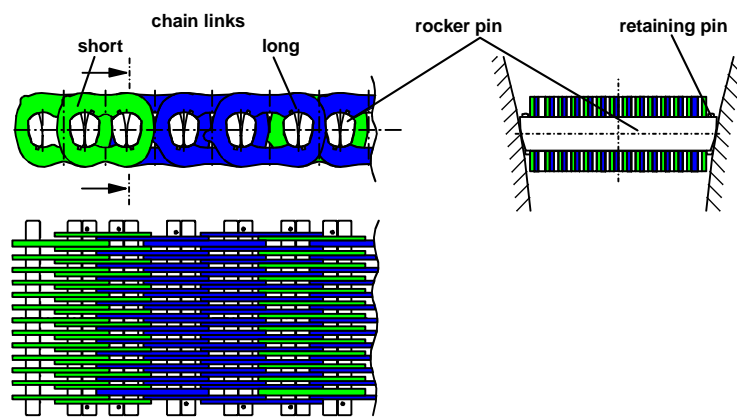
Figure 2.40: Design and components of the LuK-P.I.V. CVT chain, [21]

Chapter 3

TORQUE TRANSMISSIBILITY

The aim of this chapter is to clarify how the different driveline components of a dry-clutch system explicitly influence the transmissibility. The analysis of functional and structural links between the clutch engagement system and other driveline components is the first fundamental step for solving the modeling issues [22]. Recent studies have shown that the availability of phenomenological model of the torque transmissibility implemented in the TCU is fundamental to improve the performances of the automated dry clutch. Until now the control strategies implemented in the TCUs take into account a simplified model of the friction phenomena and without considering the influence of the clutch components [2]. Indeed, these latter have a remarkable influence on the shifting quality of the gear shifts and consequently on the performances of the automated transmission. By describing a typical engagement process it has been illustrated how the diaphragm spring [23–25] and the cushion spring [26–29] take part in the transmissibility characteristic. Even though the torque transmitted through a dry-clutch influences and is influenced by driveline components and diaphragm spring, the torque transmissibility proposed model shows that the two main elements to be considered are the cushion spring load and the dry friction phenomenon. In the next sections, how these two elements enter separately into the proposed torque transmissibility model is shown. In such model the influence of the temperature [30–33], of the slip speed and of the contact pressure [34–37] has been taken into account. Finally a novel torque transmissibility model to implement in the Transmission Control Unit (TCU) of the automated dry

clutch such as AMT and DCT has been defined. In the next paragraphs the non linearity of the clutch torque characteristic shown by the push-type dry clutch has been highlighted and explained.
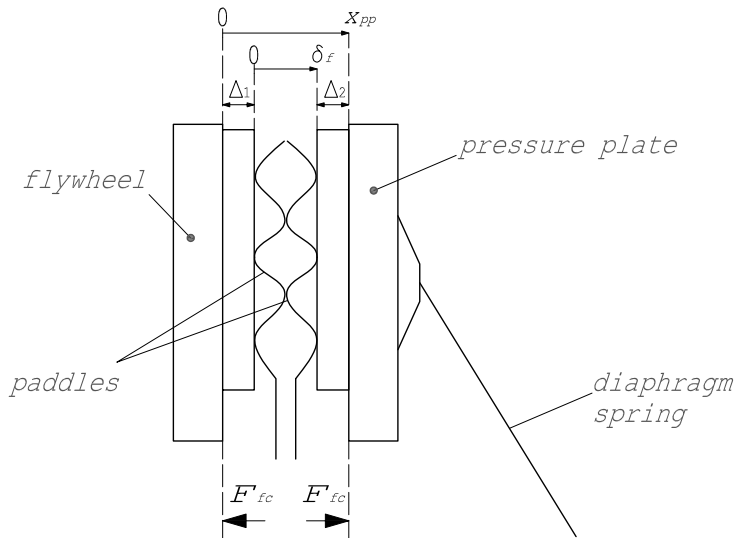
Figure 3.1: Particular of a dry clutch system in the open position: $\delta_f = \Delta_f$ when the clutch is open and $\delta_f = 0$ when the clutch is closed

3.1 LOAD-DEFLECTION CHARACTERISTICS OF THE MAIN ELASTIC COMPONENTS

3.1.1 DRIVE STRAPS

As explained in the previous paragraphs the role of the drive straps is to transmit the engine torque from the cover to the pressure plate. When the release load is calculated it is important to take into account also the contribute of the drive straps. Its secondary role is to give a contribute to disengage the pressure plate during the opening phase. For this reason, it is important to take into account also the contribute of the drive straps when the release load is calculated.

The drive straps can be modelled as a cantilever beam so the elastic

characteristic is linear.

$$K = \frac{3EI}{L^3 \cos(\alpha)} \tag{3.1}$$

where $E = 206$ GPa is the Young's module, $I = \frac{bs^3}{12}$ is the figure inertia and the geometrical parameters are reported in Figure 3.2. Typical characteristic
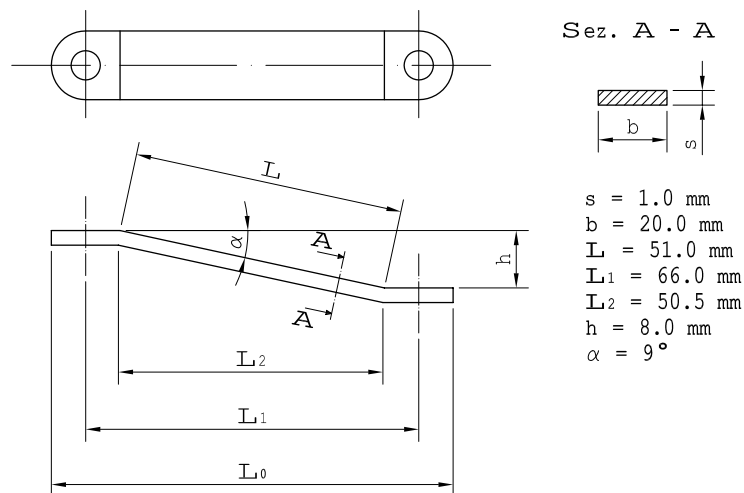
Figure 3.2: Drive straps scheme

of the drive straps is reported in Figure 3.3. It is obtained by considering that the drive straps are mounted like parallel springs. It is important to note that its contribute to the release load is minimal in comparison to the contribute to the cushion spring.

3.1.2   DIAPHRAGM SPRING

The diaphragm spring is the component threw by the throwout bearing to engage or disengage the clutch. Its characteristic is strongly non-linear and in Figure 3.5 the force vs. deformation dimensionless curve is shown. The diaphragm spring load-deflection curve with constant thickness can be
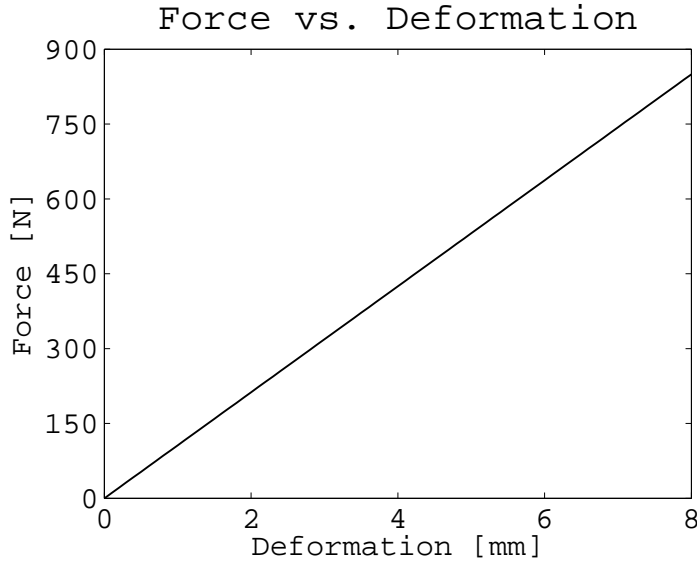
Figure 3.3: Drive straps alsatic characteristic

obtained using the theory of Almen and Laszlo, equation (3.2).

$$F = \frac{4E}{1-\nu^2} \frac{t^4}{K_1 D_e^4} \frac{s}{t} \left[\left(\frac{h_0}{t} - \frac{s}{t} \right) \left(\frac{h_0}{t} - \frac{s}{2t} \right) + 1 \right] \tag{3.2}$$

$$\delta = \frac{D_e}{D_i}$$

$$K_1 = \frac{1}{\pi} \frac{\left(\frac{\delta-1}{\delta} \right)^2}{\frac{\delta-1}{\delta+1} - \frac{2}{\ln \delta}}$$

where E is the Young's module, ν is the Poisson's coefficient, t is the thickness of the diaphragm spring, h_0 is the height of the diaphragm spring, D_e is the outer diameter and D_i is the inner diameter, for details see Figure 3.4. Another important feature is the relationship between the throwout bearing position x_{to} and the push plate position x_{pp}, Figure 3.6. In fact, by means of this connection it is possible to determine the so called "kiss point", i.e. the stroke point of the throwout bearing where the clutch disk comes in contact with the push plate and on the other side with the flywheel. Theoretically the relationship between the throwout bearing position and the push plate position should be linear and dependent only by the lever ratio B/A. Moreover, this latter should represent the segment slope [6].
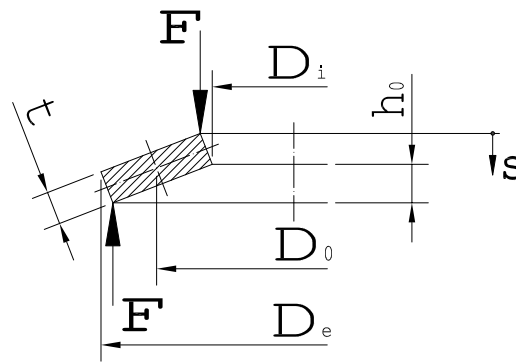
Figure 3.4: Method of loading in the Almen and Laszlo theory
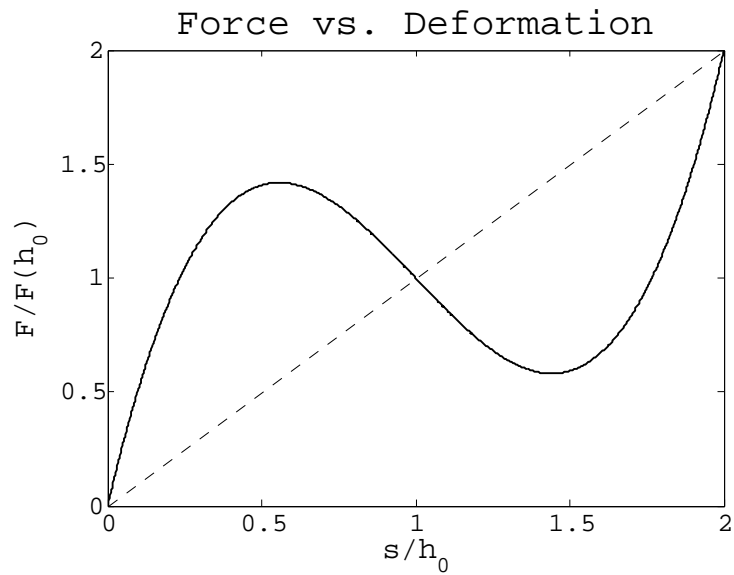
Figure 3.5: Dimensionless diaphragm spring load-deflection characteristic
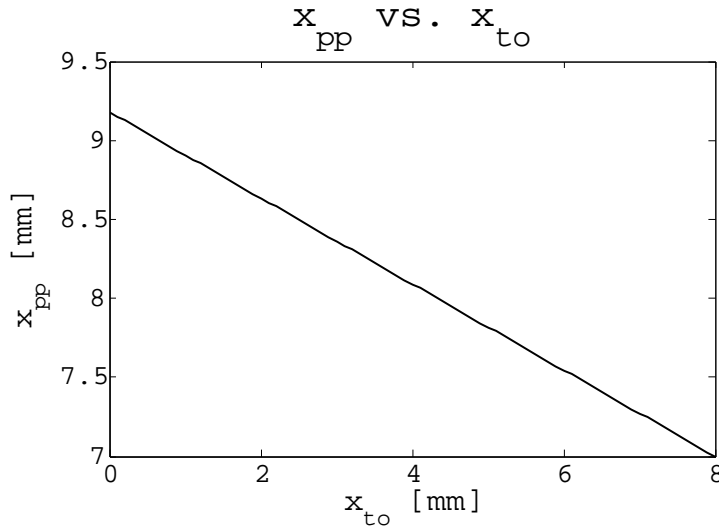
Figure 3.6: Theoretical push plate position vs. throwout bearing position

The lower bound Δ of the push plate travel is represented by the depth of the friction pads because, when the clutch is fully closed, the cushion spring is compressed and its thickness is negligible. Typical value for Δ are $6-7$ mm for a new clutch disk. Instead, in the real system when the clutch is in the closing phase there is a significantly delay in the push plate travel due to the elastic deformation of the mechanical components. In any way, in the first part, the trend is nearly linear and its slope is approximately equal to the lever ratio like as the ideal case. In Figure 3.7 is evident that it is possible to approximate the last part of the curve to an horizontal segment.

WEAR EFFECT

The most important wear effect on the clamp/release load is due to the wear of the facing materials. The characteristic of clamp/release load of a diaphragm spring clutch is very similar to the characteristic of a belleville spring. Normally the clamp load F_{pp} is given as function of the push plate travel x_{pp}, or directly as function of the throwout bearing travel x_{to}, Figure 3.8. In Figure 3.8 is shown the characteristic of the diaphragm spring without the clutch disk, the so called *free position curve*. Instead, the *new gage curve* is obtained by considering also the thickness of a new clutch disk
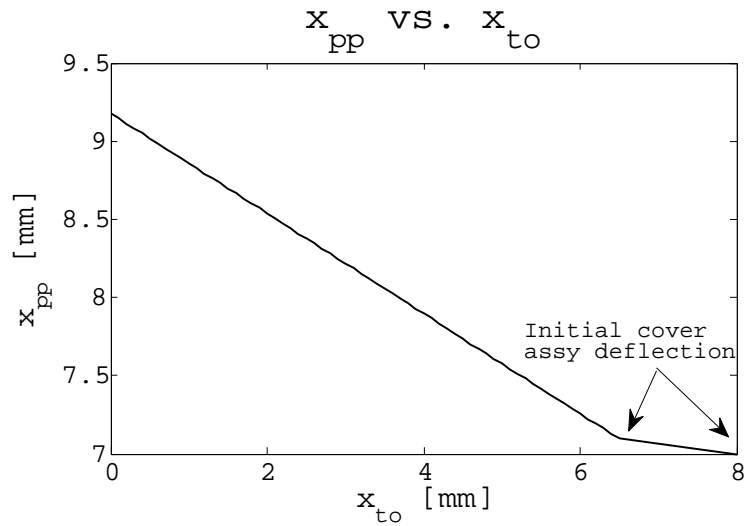
Figure 3.7: Measured push plate position vs. throwout bearing position
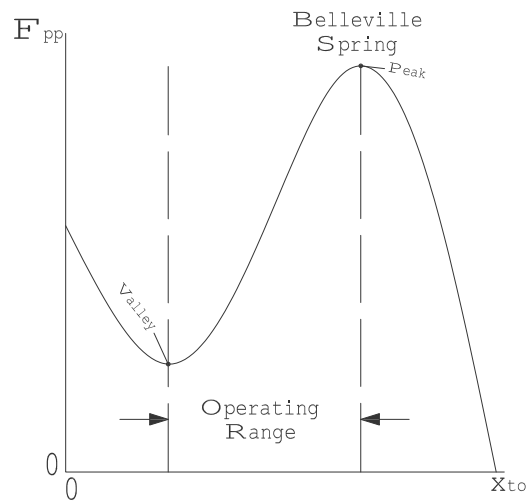
Figure 3.8: Clamp load of a diaphragm spring clutch in *free position*

mounted under the pressure plate Figure 3.9. It is important to highlight that these curves have been obtained by considering a clutch disk rigid axially and by excluding the hysteresis phenomenons [6]. When the *new gage*
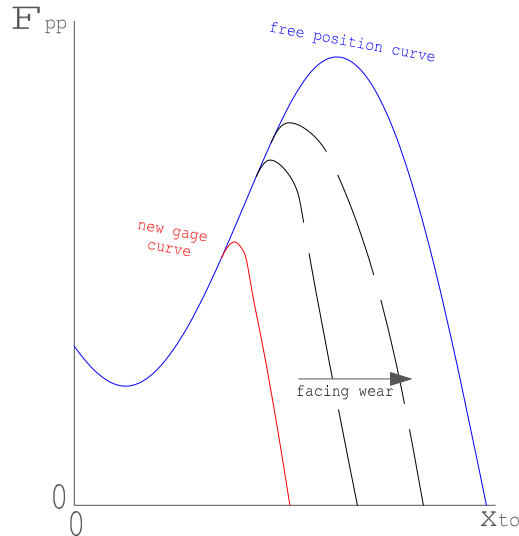
Figure 3.9: Clamp load of a diaphragm spring clutch with a new clutch disk

curve and the *free position curve* are plotted together, the intersection point represents the clamp load for a totally closed clutch with a new clutch disk. These two curves represent, respectively, the condition without wear (new clutch disk) and the condition with a clutch disk totally worn. In Figure 3.9 is shown how change the clamp load by considering the wear on the facing materials. In fact, the clamp load tends to increase with the wear. The maximum tolerable wear condition is identified with the smallest facing thickness before the direct contact between rivets and push-plate. It is possible to modify the diaphragm spring characteristic and, consequently, the maximum tolerable wear by tuning the diaphragm spring elasticity: higher is the elasticity higher is the wear travel [6].

In addition to the clutch facings wear there is another wear effect that modifies the clamp/release load: it is the wear of the diaphragm spring. This effect is due both to the thermal effects and to the ageing that results in a decline of the mechanical characteristics. The most dangerous consequence is the reduction of the clamp load curve Figure 3.10.
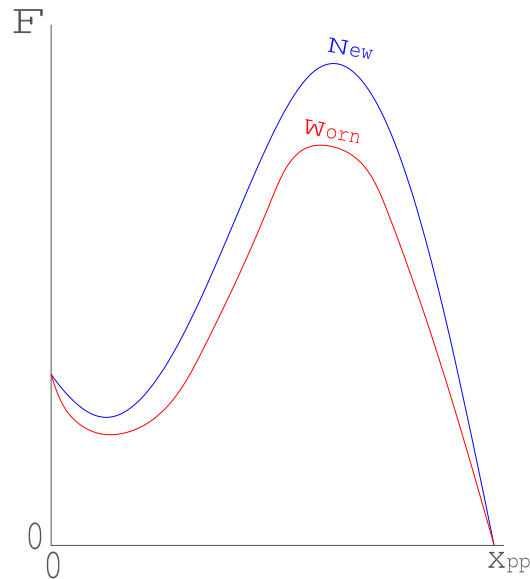
Figure 3.10: Wear effect on the diaphragm spring

HYSTERESIS

All the curves shown in the previous paragraphs have been obtained in the ideal condition without taking into account the hysteresis effect. In Figure 3.11 the new gage curve and the free position curve are represented by also considering the hysteresis effect.

FINITE ELEMENT ANALYSIS

A finite element analysis (FEA) to determine the diaphragm spring load-deflection characteristic has been carried out by using commercial software. Reverse engineering method to import the real diaphragm spring geometry into CAD file has been used. The acquiring was made with digital scanner in equipment of Department of Industrial Engineering of University of Salerno, Figure 3.12. In Figure 3.13 the result of the acquired diaphragm spring after suitable manipulations is shown. Indeed, the achieved result is a cloud of points and, after appropriate adjustments, a mesh for finite element analysis has been generated. Under the hypothesis of axial symmetry the deflection behaviour of one finger of the diaphragm spring has been simulated through FE analysis [25, 38].
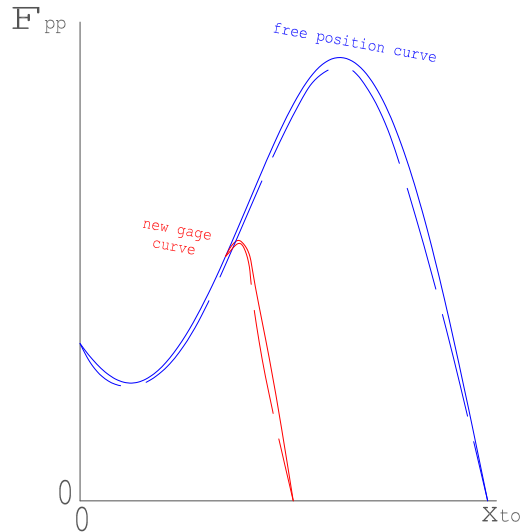
Figure 3.11: Hysteresis effect on the diaphragm spring

The diaphragm spring finger geometry has been meshed with solid elements (SOLID 185 of the ANSYS library) and computed using a linear elastic material law variable with the temperature. The throwout bearing displacement has been modelled by imposing a displacement on the nodes in contact with it, see Figure 3.13. On the nodes in contact with the cover fulcrum a zero axial displacement has been imposed, leaving to these nodes a free rotation. On the two surfaces cut to isolate the finger from the whole diaphragm spring have been imposed axial symmetry conditions, i.e. by fixing the circumferential direction. The FE results has been compared with the Almen and Laszlo theory in order to validate the proposed finite element method (FEM). In Figure 3.14 the compared dimensionless results are illustrated. It shows that the theory results have been well reproduced by the FE simulation, especially in the clutch operative range. This spring features a non-linear load-deflection curve with the advantage to disengage the clutch by exerting a decreasing force. Another important feature is the relationship between the throwout bearing position x_{to} and the push plate position x_{pp}. In fact, by means of this connection it is possible to determine the so called "kiss point", i.e. the stroke point of the throwout bearing where the clutch disk comes in contact with the push plate and on the other side with the flywheel.

Figure 3.12: Acquiring system
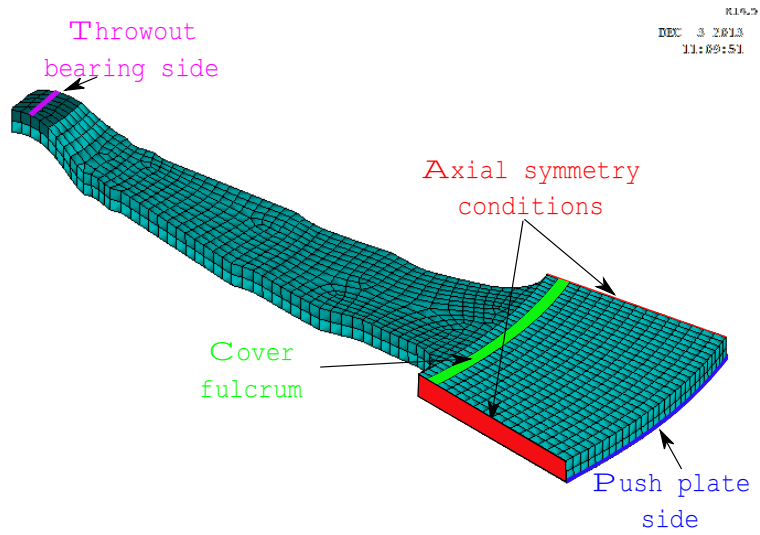
Figure 3.13: Diaphragm spring finger: FE model
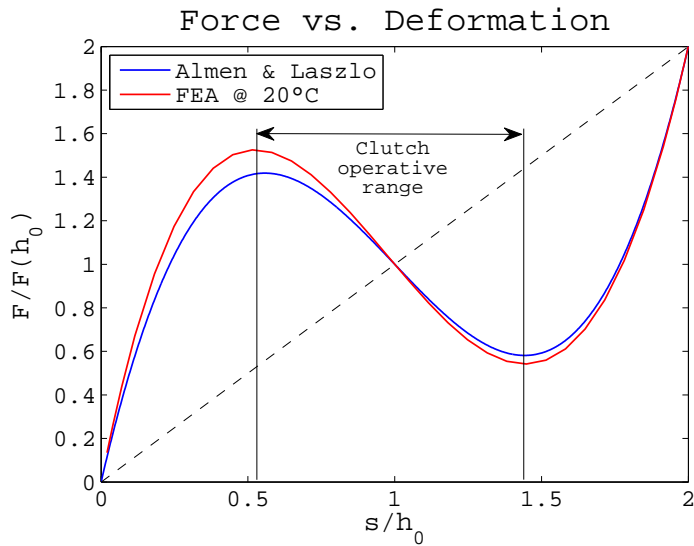
Figure 3.14: Comparison between the Almen and Laszlo theory and FE results
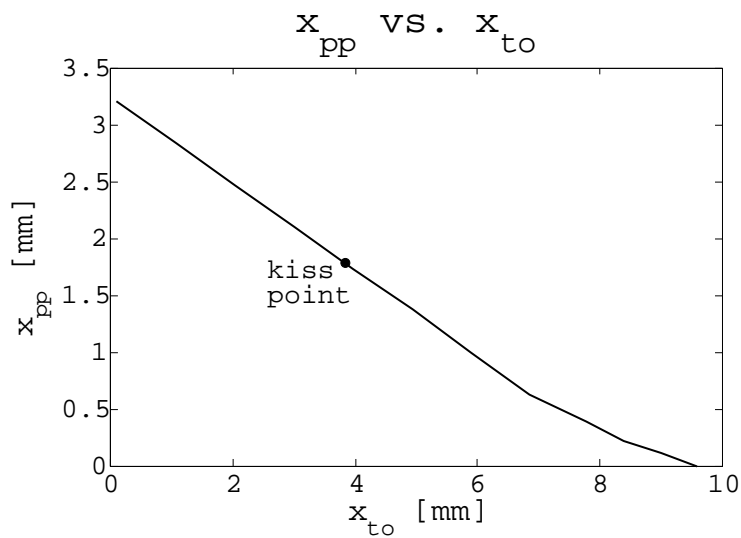
Figure 3.15: Relationship between the pressure plate position x_{pp} and the throwout bearing position x_{to}

3.1.3 CUSHION SPRING

The cushion spring is a thin steel disk placed between the clutch friction pads and it is designed with different radial stiffness to ensure the desired smoothness of engagement [2]. When the cushion spring is completely compressed by the pressure plate we say that the clutch is closed, whereas when the pressure plate position is such that the cushion spring is not compressed we say that the clutch is open. We say that the clutch is in the engagement phase when is going form open to locked-up. The cushion spring is composed by n pairs of paddles (or cushion segments) as shown in Figure 3.16. A single pair of cushion segments can be considered as two series springs and the whole system can be considered as parallels springs. Under the hypothesis
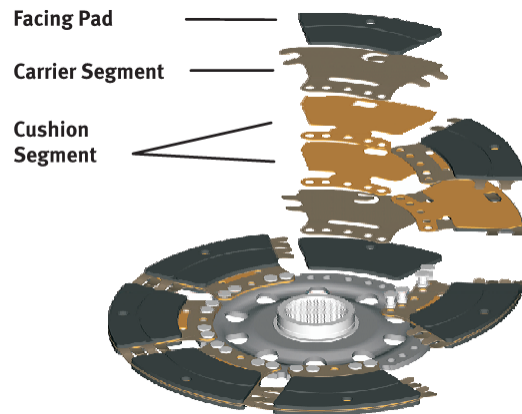
Figure 3.16: Cushion spring segments, [12]

Figure 3.17: Paddle of the cushion spring

that all the paddles have the same proprieties it is possible to get the cushion

spring load-deflection characteristic by multiplying the load-deflection characteristic of a single pairs of paddle for the number of pairs which compose the cushion spring. Logically, the hypothesis that all the paddles have the same proprieties is an approximation. In fact, by considering the differences of the material, the flaws of the assembly, etc. no component could never be equal to another component and, consequently, to have the same proprieties. It is also true that the differences between two paddles can be considered irrelevant as shown in Figure 3.18, [1]. Under these assumptions the cushion spring load-deflection characteristics both experimental and simulate have been obtained. The experimental results have been done by using a testing machine of the Department of Industrial Engineering of the University of Salerno. The parameters used to attain the experimental results are:

- maximum load cell capacity: 30 kN;

- speed of the crosshead: 0.5 mm/min;

- sampling time: 5 Hz.

The zero displacement was assumed when the cushion spring reaction force is around 10 N to cancel out the resolution uncertainty due to the testing system. In Figure 3.18 are shown the experimental results of the cushion spring load-deflection characteristic. In order to reproduce the experimental results a finite element analysis of the cushion spring has been developed. Only one pairs of paddles has been modelled according to the symmetry assumption described above. Reverse engineering method has been used to import tested cushion spring geometry into CAD file. The acquiring was made with digital scanner in equipment of Department of Industrial Engineering of University of Salerno. In Figure 3.19 the acquired cushion spring segment (a) and the obtained result (b) are shown, [28]. The achieved result is a cloud of points and, after appropriate adjustments, it has been used for the FEA. During the acquisition phase a portion of the paddle tail was covered by pin and consequently it has not been possible to earn it, Figure 3.19(b). This is not a problem because the "tail" of the cushion spring is used to fix it to the clutch disk and so it is not compressed by clutch facings. In fact, the load-deflection characteristic is due only to the waved zone of the cushion spring. Between clutch facings there are two paddles besides a symmetry plane. To find this plane, a MATLAB algorithm has been implemented that receives as input the cloud of points and the result is a plane that has all points on or over it, Figure 3.20. The cushion spring
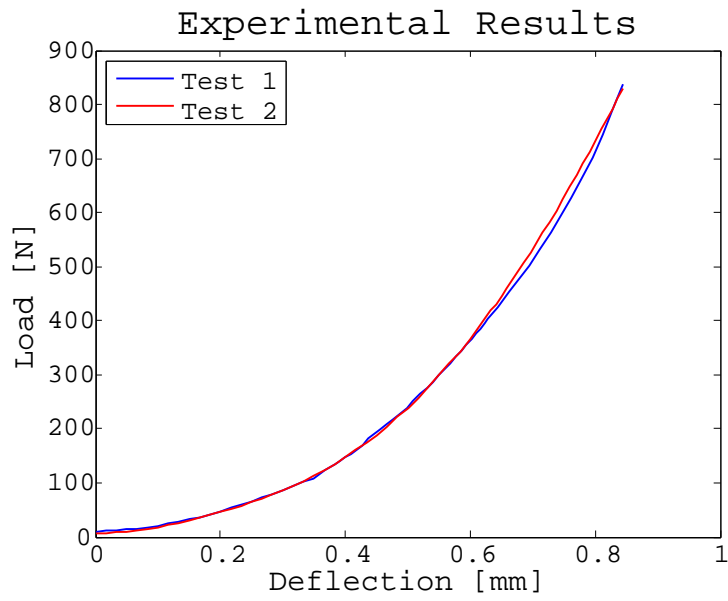
Figure 3.18: Load−deflection curves from the experiments
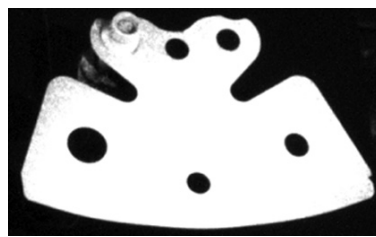
(a) Acquired cushion spring segment
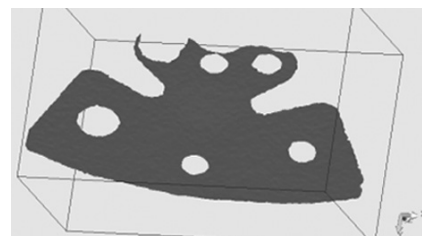
(b) Obtained cushion spring segment

Figure 3.19: Comparison between the acquired and obtained cushion spring segment

geometry has been meshed with shell elements (SHELL 181 of the ANSYS$^{©}$ library) according to its thin thickness (0.4 mm) and computed using a linear elastic material law. The thickness of the cushion spring has been measured both with digital scanner after the acquiring and with digital calibre, in different points, and with both methods the same thickness value has been obtained. The clutch facings and pressure plates have been modelled by flat rigid plates. The axial compression of the clutch disk during the gear re-engagement has been simulated in this way. Surface-to-surface contact has
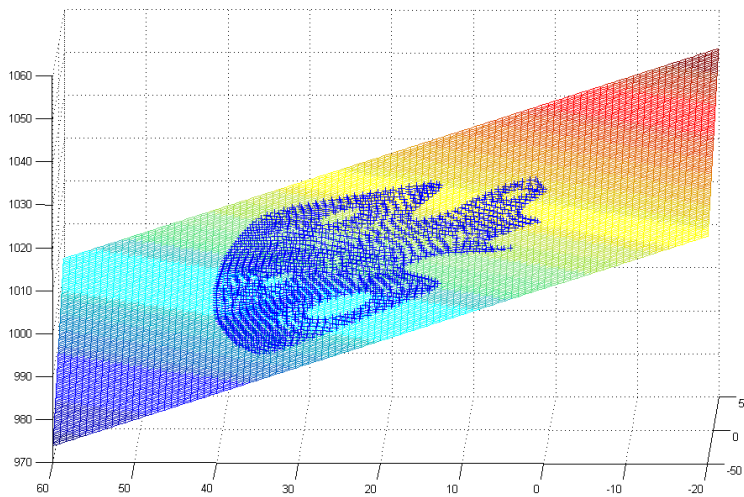
Figure 3.20: Plane of symmetry for the cushion spring

been used to simulate cushion disk phenomena compression. Each contact pairs needed of a master (contact element "CONTA 174") and slave (target element "TARGET 170") surface. The augmented Lagrangian algorithm has been chosen to solve the contact problem. In this work the only real constants (RC) used are: normal contact stiffness factor named FKN and penetration tolerance factor named $FTOL$. FKN represents the stiffness of a fictive springs disposed between the two surfaces in contact [26]. Its default value is 1 but it could range between 0.01 and 100 [39]. A high value of FKN gives good solution accuracy but can lead to ill-conditioning of the global stiffness matrix causing convergence difficulty [26, 39, 40]. On the other hand a too low contact stiffness value can lead to a bad solution [26]. $FTOL$ default value is 0.1 and if it is too small, i.e. small penetration, the FE analysis can fail. On the other hand if $FTOL$ is too large, i.e. high penetration, can lead to a bad solution [26, 39]. Lower pressure plate is

fixed in all directions while the upper one moves axially compressing the paddles. The plate motion is controlled by displacement in order to limit convergence problem. The cushion spring paddles are clamped on the clutch disk by rivets; in the FE model this condition has been simulated by locking the nodes of the holes where they are housed [28]. In Figure 3.21 the ANSYS model used is shown.

Two different mesh densities have been chosen to validate the model: 0.5 mm and 2.0 mm. Furthermore, the ANSYS default convergence criterion has also been used. The best results have been achieved with this factor values: $FKN = 0.9$; $FTOL = 0.1$. The zero position was assumed when the cushion spring reaction force is equal to 10 N to compare FE results with experimental ones. In Figure 3.22, the experimental load-deflection curve is compared with the result of the simulation [28].
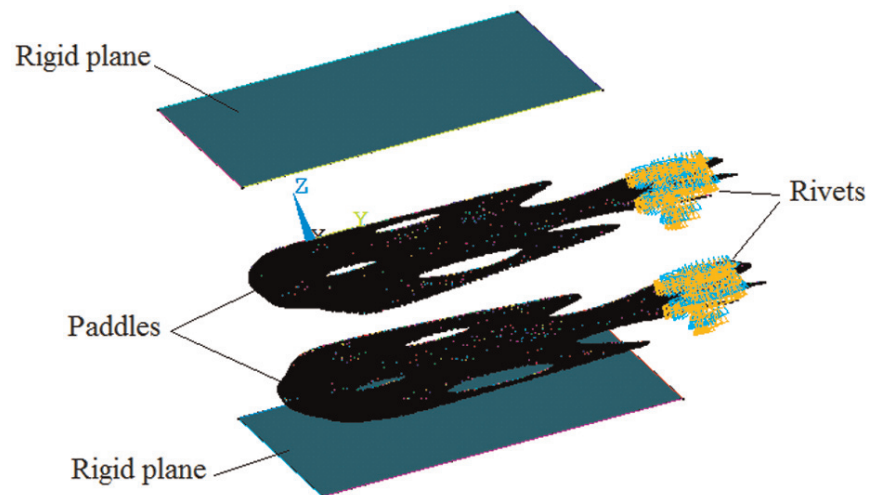
Figure 3.21: ANSYS model for the simulation of the compression of the paddles

3.2 THE ROLE OF THE TEMPERATURE

Temperature plays an important role on the engagement phase in a dry clutch system. In fact, repeated gear shifting induce a rise of the temperature due to the friction between the flywheel and a clutch facing on one side and between the push plate and the second clutch facing on the other
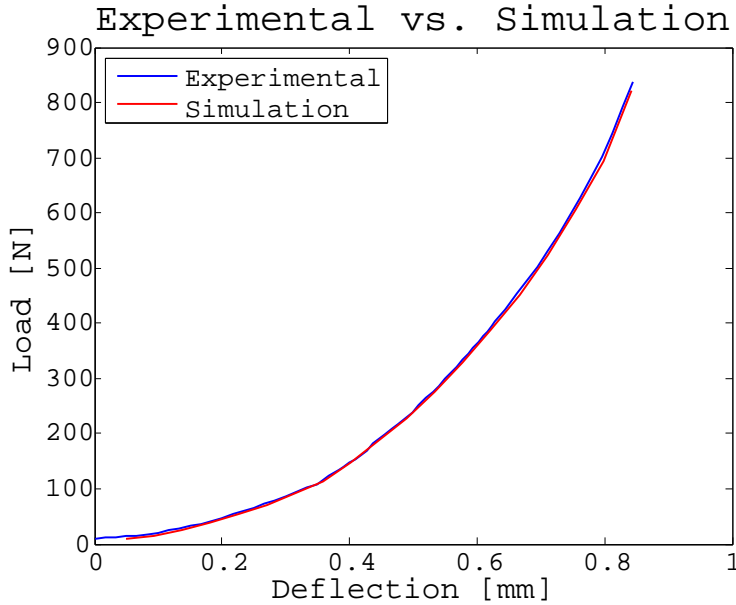
Figure 3.22: Load−deflection curves: experimental and simulation results

side. This thermal effect has strong influence on the behaviour of the main components of the dry clutch assembly. Therefore, if they have not taken into account accurately, they could lead to a poor engagement. For example, after repeated clutch engagement the temperature on the clutch facing could attain very high values, around 300-350 °C and, above 350-400 °C, the friction system starts to suffer permanent damage [17].

A simplified heat transfer model has been assumed to calculate the average temperature of the cushion spring θ_{cs}. The two clutch facings on flywheel side and pressure plate side have been assumed at the same temperature levels. Say C the thermal capacity of the cushion spring, the heat transfer mechanism through the facing materials is mainly given by conductive flux; the heat transfer can be modelled as the conductance U times the temperature difference $(\theta_{cm} - \theta_{cs})$. A more detailed model should take into account the actual heat patterns through the rivets or other metal joints between the facings and the cushion spring. Furthermore, a convective radial heat flux toward an ambient at room temperature θ_a is modelled by way of the transfer coefficients H [25].

On the base of these hypotheses, the simplified thermal dynamics of the

cushion spring is provided by a first order differential equation where U has value of 0.1 WK^{-1}, H of 0.04 WK^{-1} and C of 1.0 JK^{-1}:

$$U(\theta_{cm}(t) - \theta_{cs}(t)) + H(\theta_a(t) - \theta_{cs}(t)) = C\dot{\theta}_{cs}(t) \tag{3.3}$$

$$C\dot{\theta}_{cs}(t) + (U + H)\theta_{cs}(t) = U\theta_{cm}(t) + H\theta_a(t) \tag{3.4}$$

$$\frac{C}{U + H}\dot{\theta}_{cs}(t) + \theta_{cs}(t) = \frac{U}{U + H}\theta_{cm}(t) + \frac{H}{U + H}\theta_a(t) \tag{3.5}$$

The temperature of the facing material has been simulated aiming at reproducing literature results [17, 31] by considering repeated clutch engagements with 60 seconds period. The previously described model has been implemented in Matlab/Simulink©; the results are depicted in Figure 3.23. In ad-
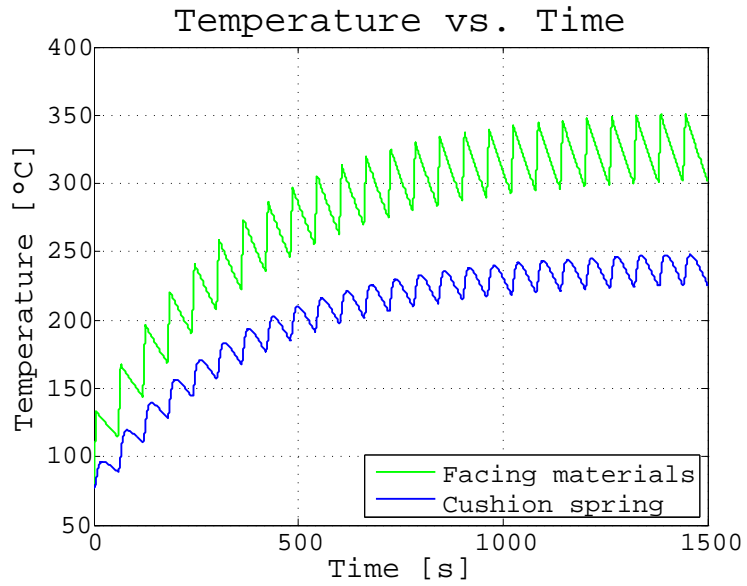
Figure 3.23: Clutch facings and cushion spring temperature after repeated starts, [25]

dition to these phenomena the temperature also modifies the load-deflection curve of the cushion spring and consequently also the clutch transmission characteristic is affected by the temperature.

In the below paragraphs the temperature effects on the crucial components of a dry clutch system have been analysed. Therefore, it is necessary

to implement in the TCU a model which takes into account the role of the temperature on each components to improve the automation of the AMTs.

3.2.1 DIAPHRAGM SPRING

A finite element analysis (FEA) to evaluate the influence of the temperature on the diaphragm spring load-deflection characteristic has been carried out. By using the FE model developed previously a thermal load step has been added before to determine the load deflection characteristic. In this way, with the first load step the thermal effects has been taken into account whereas with the second load step the load-deflection characteristic is calculated.

In Figure 3.24, the results at different temperatures of the FE simulation are depicted. These curves have been obtained by considering the diaphragm spring as standalone system. It is important to underline the weak influence of the temperature on the diaphragm spring characteristic. As previously ex-
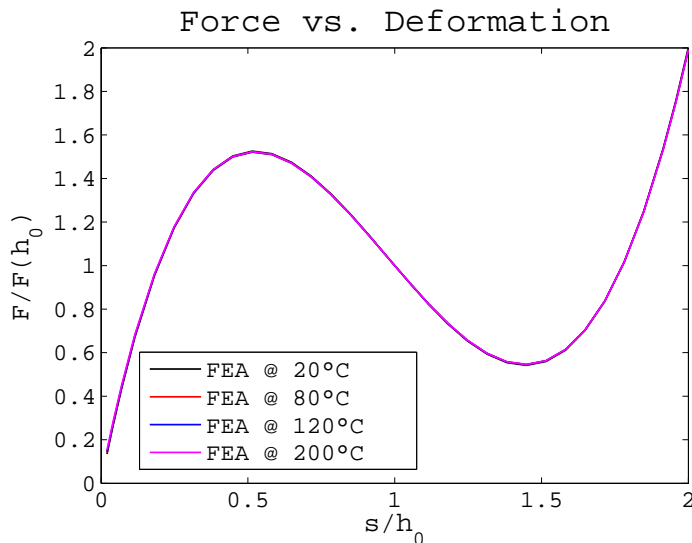
Figure 3.24: Dimensionless diaphragm spring characteristic at different temperature, FE results

plained another important feature is the relationship between the throwout bearing position x_{to} and the push plate position x_{pp} because it is useful to determine the "kiss point". The position of the kiss point changes during the clutch operation both due to the clutch facings wear and the axial thermal

expansion of the components of the clutch disk. These two phenomena have an opposite effect on the kiss point; in fact, the axial thermal expansion reduces the gap required to get the kiss point, whereas the wear increases this gap. In Figure 3.25, the clutch facings wear and the axial thermal expansion influence on the position of the kiss point are shown. The results of the FE analysis of this section have pointed out that the temperature has irrelevant effects on the diaphragm spring characteristic and consequently also on the relationship $x_{pp}(x_{to})$.
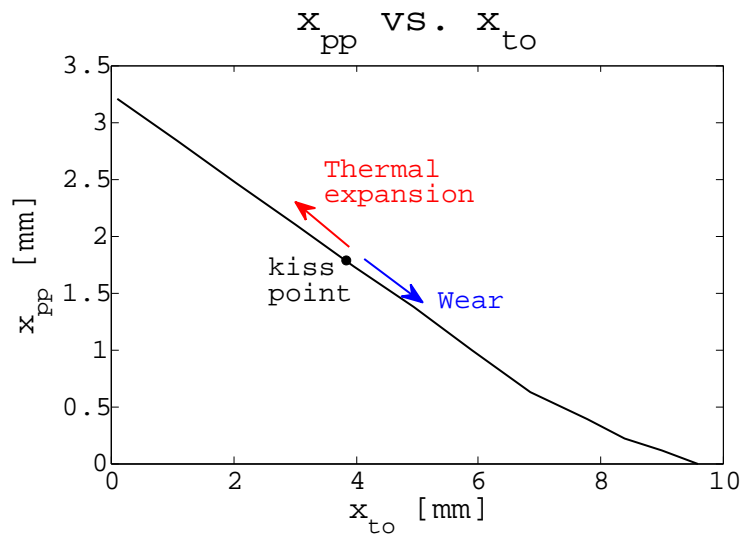
Figure 3.25: Variation of the kiss point due to the temperature and to the wear of the clutch facings

3.2.2 CUSHION SPRING

A finite element analysis to predict the influence of the temperature on the cushion spring load-deflection characteristic has been performed, using above mentioned ANSYS© FE model. The analysis aimed at investigate the temperature influence on the cushion spring characteristic modification and how this affects the torque transmissibility curve. The knowledge of these effects could provide useful data for a real-time adaption of TCU control through the measurement of the estimation of clutch system average temperature.

As first simulation step, an uniform temperature field has been applied to the cushion spring paddle to calculate the thermal distortion and the modified material properties. As second step, a controlled displacement of rigid planes to induce axial compression has been simulated. Both the steps involves non-linear shape modifications since the analysis faces with contact problems. In fact, the first analysis is non-linear because during the thermal strain the paddles get in contact both each other and with the rigid plane that simulate the clutch facings. In this analysis an isotropic linear elastic material, characterised by a Young's module depending on the temperature and a constant expansion coefficient, has been used to model the material behaviour. The Table 3.1 shows the material proprieties used for the analysis. Because the clutch system, during its life, could work

Parameter	Parameter values
Temperature (°C)	20, 80, 200, 350
Young's modulus (GPa)	206, 202, 196, 186
Expansion coefficient (°C^{-1})	$1.12 \cdot 10^{-6}$

Table 3.1: Properties of the materials

in a wide range of temperatures as explained previously, in this analysis the cushion spring behaviour at several temperature levels (80 °C; 120 °C; 200 °C; 250 °C; 300 °C; 350 °C) has been analysed, in addition to the room one. In Figure 3.26, the cushion spring load-deflection curve depending on the temperature has been obtained by considering the thermal expansion in a first load step and the compression phase in a second load step. It is important to note that with the numeric analysis, in contrast with the experimental tests, the zero displacement can be assumed when the incipient contact between rigid plane and cushion spring occurs. In the results of this analysis has been assumed a whole throwout bearing travel of 8 mm and a reference load-deflection curve at 20 °C which starts at a throwout bearing position of 4 mm [33]. It shows that temperature influences in two ways the cushion spring characteristic. In fact, by increasing the temperature level, the material stiffness changes and this results in local modification of the load-deflection characteristic slope. Conversely, the thermal load induces a thermal expansion that results in axial size increase and consequently in a change of the *kiss point* position. These two effects together lead to an uncertainty during the engagement phase. Indeed, the position of the kiss point changes and if this issue is not taken into account during the
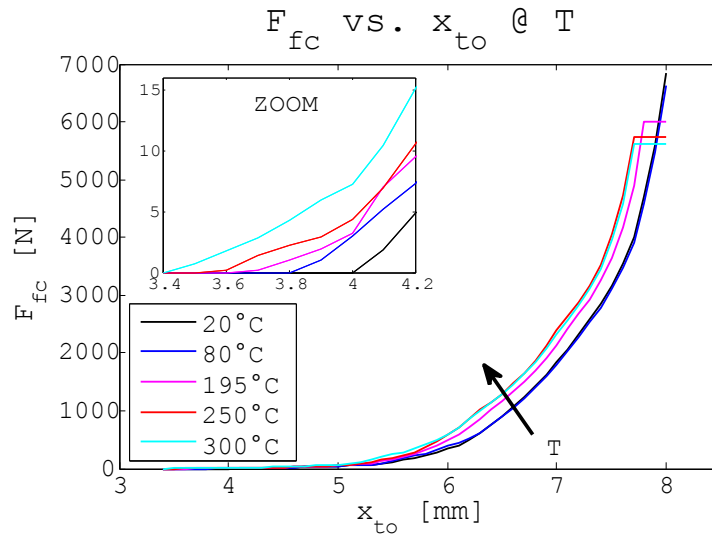
Figure 3.26: Load−deflection curve at increasing temperature levels

engagement phase the TCU could lead to a wrong position of the throwout bearing [25, 33].

3.2.3   LEVER SPRING

Due to the construction of powershift transmissions, in DCT safety reasons dictate that the clutches must open automatically if the clutch actuation system fails [17]. This can be achieved very easily through the use of so-called "actively closed clutches". In actively closed clutches, the contact force is equal to zero if there is little or no force acting on the diaphragm spring fingers. Conversely, in passively closed clutches the full contact force is present on the clutch linings if there is no force acting on the diaphragm spring fingers. In this condition, the maximum torque is transmitted [17]. In Figure 3.27 is shown the cross-section of an actively closed clutch. Since, in actively closed clutches, the diaphragm spring is used mainly as a lever to transmit the engage force to the contact plate, this is described as a lever spring [17]. The particular requirement is that the lever spring fingers must be extremely rigid in the axial direction to minimise travel losses. The lever spring is also designed such that throughout the working range of the engage bearing there is always low return force and so the opening of the clutch is ensured. A finite element analysis has been carried out to explore
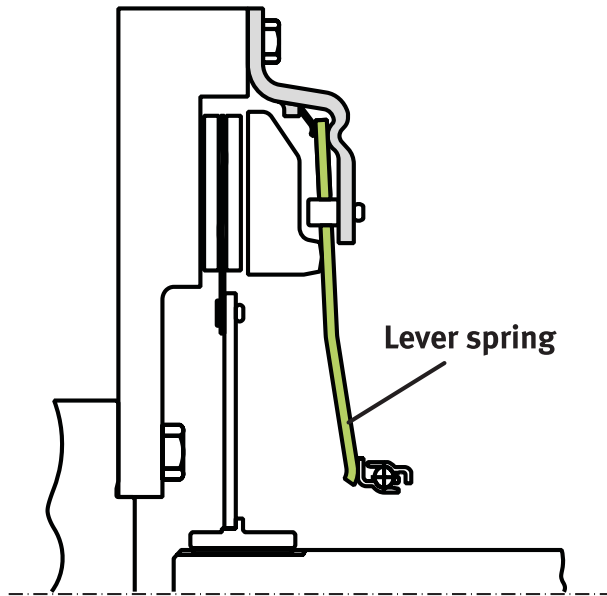
Figure 3.27: Lever spring, [17]

the temperature influence on the relationship between the throwout bearing force F_{to} and the pressure plate force F_{pp}. Since this relationship is strongly dependent from the cushion spring reaction it has been assumed that the temperature affects only the cushion spring characteristic whereas it has a weak influence on the lever spring as shown in the previous sections. On the throwout bearing side a displacement x_{to} has been imposed and, by using a linear spring with a high stiffness, which works as a force sensor, the relative F_{to} has been measured. Instead, on the pressure plate size a displacement x_{pp} has been imposed, and after a given gap the lever spring begins to compress the cushion spring. The latter has been modelled by using an element type which represents a non-linear spring [41]. The FE model is shown in Figure 3.28. These curves have been obtained by considering the lever spring as standalone system. It is worth to note that the change of the curve slope in Figure 3.29 results in a change of the curve slope in all curves of Figure 3.30. These curves are also influenced by the backward travel of the kiss point which reduces the gap between the pressure plate and the begin of compression of the cushion spring.
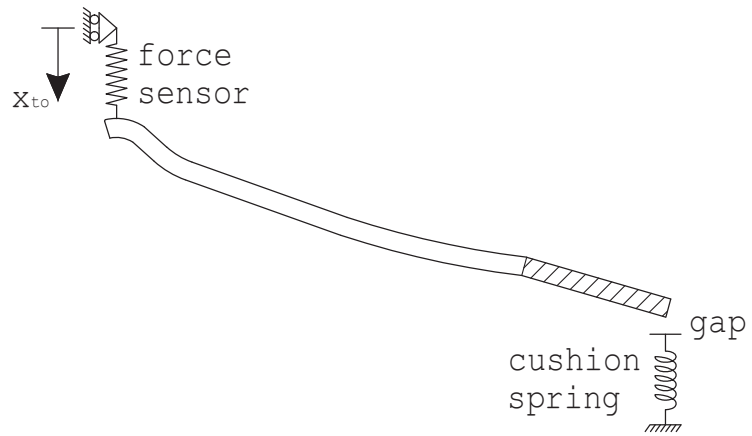
Figure 3.28: FE model
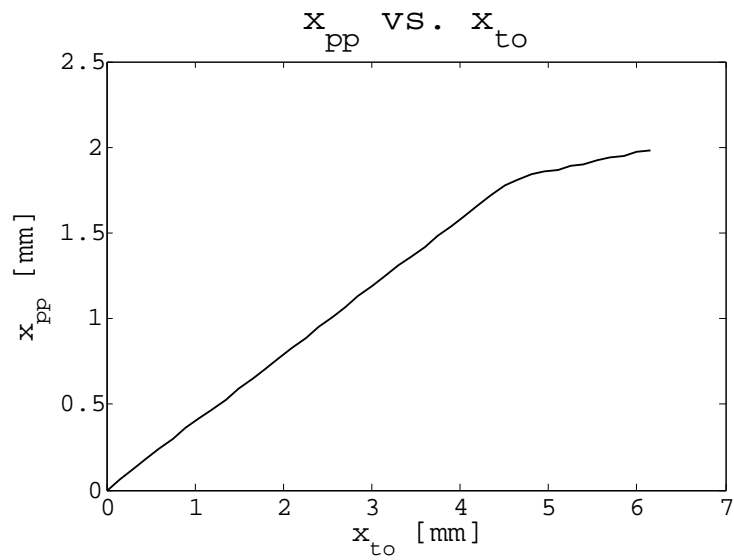
Figure 3.29: Relationship between pressure plate lift vs. throwout bearing motion, [41]
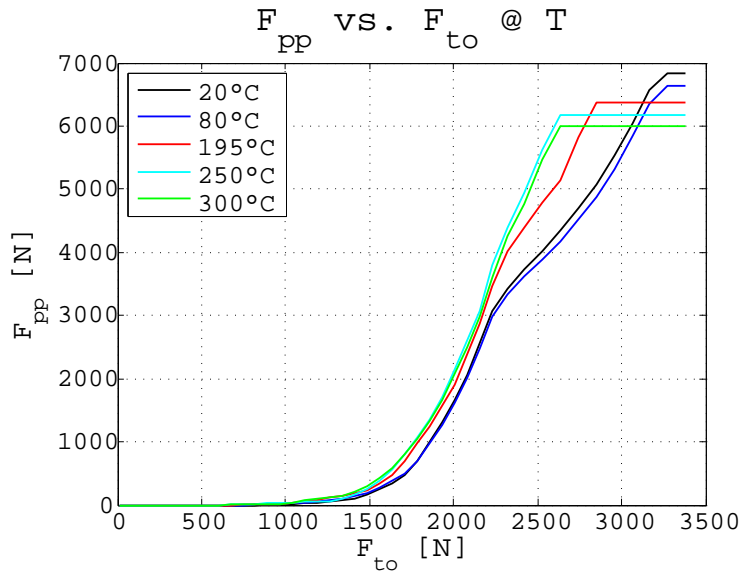
Figure 3.30: Pressure plate force vs. throwout bearing force at increasing temperature levels, [41]

3.3   FRICTION COEFFICIENT

The friction coefficient has a strong effect on the clutch torque characteristic as explained in the next paragraphs. For this reason a deep analysis on its variation during the engagement phase is fundamental to improve the performance of an actuated dry clutch. In fact, effective controllers are difficult to be designed without having a dependable frictional map of the clutch-torque transmissibility characteristic [35]. The modelling of friction variation during the clutch engagement process has been studied by numerous authors. The relationship between the static and/or dynamic friction coefficient and the sliding speed has been extensively studied in [42–44]. Raghavan and Jayachandran [45] have considered that the coefficient of friction varies with the sliding speed as well as with the generated contact pressure and the number of clutch engagements due to the thermal effect. The thermal effect was also approached through FE analysis for ceramic clutch in [31]. In [30], instead, tests on automotive clutch facings have been carried out to analyse the temperature effect. Poser et al. [46] investigated the dependence of friction coefficient of clutch conventional and innovative facings on the sliding

speed. In order to ascertain the rise up of the judder phenomenon during the engagement process, Centea et al. [47] and Maucher [48] investigated the gradients of the friction coefficient with slip speed.

3.3.1   THERMAL EFFECTS

In this section the thermal impact on the frictional behaviour of the clutch disk facings has been analysed. In fact, during the engagement phase the friction between the clutch facings and the flywheel on one side and the push plate on the other side brings about a rise of the temperature, especially after repeated engagements, see Figure 3.23. In [30] tests on automotive clutch facings have been carried out to analyse the temperature effect, whereas in [49] a similar analysis has been carried out on a disk brake. In [32] is reported the technical data sheet of a typical automotive clutch facings. It shows how the friction coefficient exhibits a smooth variation within the temperature range from $100\,^\circ$C to $250\,^\circ$C, whereas it begins to decline sharply after $250\,^\circ$C, Figures 3.31(a) and 3.31(b). This typical behaviour is shown also in [30, 49]. This effect is due to the decomposition of the phenol resin of the clutch facings at high temperature. In fact, when the temperature is higher than $330\,^\circ$C, a severe thermal decomposition produces fluids and gas emissions. This effect induces not expected phenomena transition from dry friction to lubricated friction. For this reason the friction coefficient drops [30, 49].

3.3.2   CONTACT PRESSURE AND SLIDING SPEED

In this section the influence of the sliding speed, at different contact pressure, on the friction coefficient has been analysed. In [35] tests on commercial clutch facings have been carried out to investigate how these parameters affect the friction coefficient. The results as function of the sliding speed and for two contact pressure levels are shown in Figure 3.32. It is evident that for both contact pressure level the friction coefficient tends to an asymptotic value at higher sliding speeds. The friction coefficient asymptotic value is higher for higher contact pressure. Moreover, the contact pressure has a nearly linear influence on the friction coefficient, according to the results in [35], achieved on a tribometer at room temperature, Figure 3.32. Thus, the dependence of the friction coefficient on sliding speed, average contact pressure and facing temperature is given by the equations (3.6) and (3.7)

$$\mu_\infty\left(p, \theta_{cm}\right) = \alpha + \beta \frac{p}{p_0} + f\left(\theta_{cm}\right) \qquad (3.6)$$
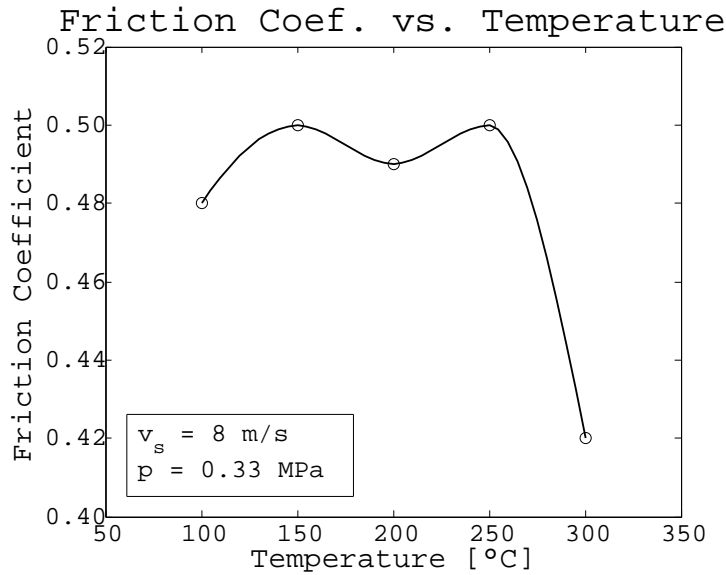
(a) Friction coefficient vs. average facing temperature θ_{cm}, [32]
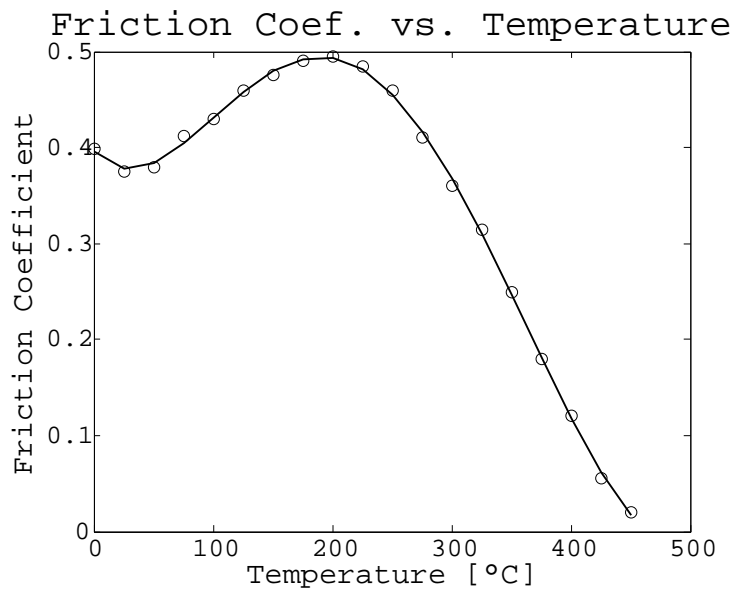
(b) Friction coefficient vs. average facing temperature θ_{cm}, [30]

Figure 3.31: Friction coefficient vs. average facing temperature θ_{cm}

where α and β have been identified from the Figure 3.32 in the plateau region and the corresponding values are: $\alpha = -0.110$, $\beta = 0.110$; the reference pressure is $p_0 = 0.33\ MPa$, i.e. the same average contact pressure of the experiments in Figure 3.31(a), [32]. The function f is derived from the data in Figure 3.31(a).

The equation (3.7) is based on the experimental results in [35] for strictly positive slip speed:

$$\mu\left(v_s, p, \theta_{cm}\right) = \mu_{\infty}\left(p, \theta_{cm}\right) + \mu_{\Delta}\left(\tanh\left(\frac{v_s}{v^*}\right) - 1\right) \tag{3.7}$$

In equation (3.7), $v_s = R_m\left|\omega_e - \omega_c\right|$ is the sliding speed given by the product between the difference between engine and clutch angular speed $\left|\omega_e - \omega_c\right|$ and mean radius R_m. μ_{Δ} and v^* have been identified and the corresponding values are 0.09 and 0.5 m/s, respectively.
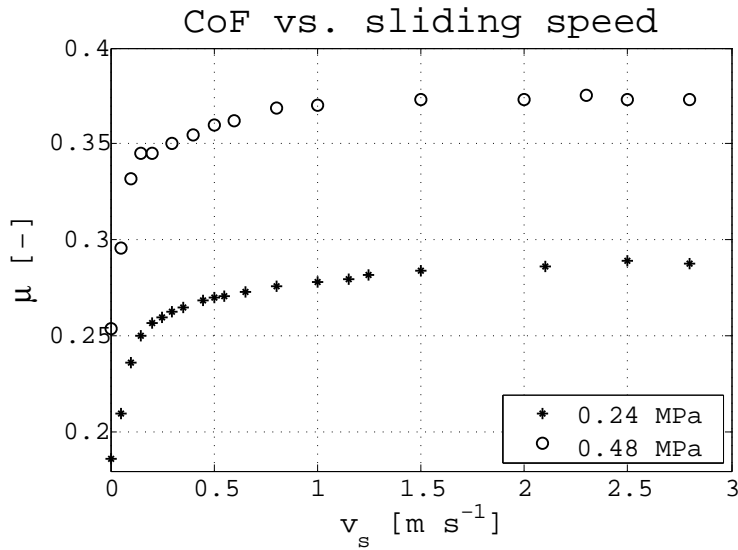
Figure 3.32: Friction coefficient vs. sliding speed at different contact pressure: 0.24 MPa, 0.48 MPa, [35]

3.4 MATHEMATICAL MODEL

The torque transmitted by a dry clutch is generated by the friction phenomenon between the friction pads mounted on the two sides of the clutch

disk and the flywheel and pressure plate. In [2] a model of dry clutch torque transmissibility has been proposed; it explains the role of clutch springs and how they influence the torque transmissibility. The connection between torque transmissibility and cushion spring force obtained in [2] is given by equation (3.8).

$$T_{fc}(x_{to}) = n\mu R_{eq}F_{fc}(\delta_f(x_{pp}(x_{to}))) \tag{3.8}$$

where n ($n = 2$ in our case) is the number of pairs of contact, μ is the dynamic friction coefficient, R_{eq} is the equivalent radius of the contact surface and F_{fc} is the cushion spring reaction. From equation (3.8) it is clear that the cushion spring compression δ_f and the corresponding force $F_{fc}(\delta_f)$ determine the torque transmissibility [2]. Below is reported a more detailed analysis on the equivalent radius presented in [2].

The force applied by the flat spring on the friction surfaces (by assuming symmetry of the n contact surfaces and by omitting for simplicity the dependence on x_{to}) can be written as:

$$F_{fc} = \int_0^{2\pi} \int_{R_1}^{R_2} \sigma\left(\rho, \varphi, \delta_f\right) \rho d\rho d\varphi \tag{3.9}$$

where ρ and φ are the radial and angular geometric variables of the friction pad surface ($\rho = 0$ at the center of the clutch disk), the parameters R_1 and R_2 are the inner and outer radii of the clutch friction pads, and σ is the pressure distribution on the friction pads. Within the above geometric framework the friction torque can be written as:

$$T_{fc} = n \int_0^{2\pi} \int_{R_1}^{R_2} \tau\left(\rho, \varphi, \delta_f\right) \rho^2 d\rho d\varphi \tag{3.10}$$

where τ is the distribution of tangential stress along the friction surfaces of clutch. It is possible to define the parameter:

$$R_\mu = \frac{\int_0^{2\pi} \int_{R_1}^{R_2} \tau\left(\rho, \varphi, \delta_f\right) \rho^2 d\rho d\varphi}{\int_0^{2\pi} \int_{R_1}^{R_2} \sigma\left(\rho, \varphi, \delta_f\right) \rho d\rho d\varphi} \tag{3.11}$$

By multiplying and by dividing the equation (3.10) with the equation (3.9) and by highlighting the parameter (3.11) the transmitted torque can be rewritten as:

$$T_{fc} = nR_\mu F_{fc} \tag{3.12}$$

An uniform distribution along the angular direction can be usually assumed, i.e. σ and τ do not depend on φ. Therefore the parameter (3.11) becomes:

$$R_\mu = \frac{\int_{R_1}^{R_2} \tau\left(\rho, \delta_f\right) \rho^2 d\rho}{\int_{R_1}^{R_2} \sigma\left(\rho, \delta_f\right) \rho d\rho} \tag{3.13}$$

To obtain an expression for T_{fc} one must now detail the tangential stress τ and the normal pressure σ. To this aim a typical assumption made in friction mechanics is:

$$\tau\left(\rho, \delta_f\right) = \mu\left(\rho \omega_{sl}\right) \sigma\left(\rho, \delta_f\right) \tag{3.14}$$

Where $\mu\left(\rho \omega_{sl}\right)$ is the friction function and it depends from the tangential velocity $v = \rho \omega_{sl}$. Precisely $\omega_{sl} = \omega_f - \omega_c$ represents the slip speed and it is defined as the difference between the flywheel angular speed and the clutch disk angular speed and it is different for each radius of clutch disk, [2]. In a simplified friction model is assumed that the friction function depends only on the signum of the velocity, i.e. Coulomb's friction law, or is modelled by using a smooth approximation of the signum function to avoid the numerical problems due to the simulation of discontinuities in Coulomb's friction law at zero velocity [50]. Note that by considering $\mu\left(\rho \omega_{sl}\right)$ as a signum function and ω_{sl} positive, μ will not depend on ρ thus simplifying the computation of the equation (3.11). By using (3.14) and μ constant in (3.14), (3.13) becomes

$$R_\mu = \mu \frac{\int_{R_1}^{R_2} \sigma\left(\rho, \delta_f\right) \rho^2 d\rho}{\int_{R_1}^{R_2} \sigma\left(\rho, \delta_f\right) \rho d\rho} \tag{3.15}$$

The only function still to be defined is the pressure distribution σ. If σ is assumed to be constant the equation (3.15) becomes:

$$R_\mu = \mu \frac{2}{3} \frac{R_2^3 - R_1^3}{R_2^2 - R_1^2} \tag{3.16}$$

Conversely, under the assumption of uniform wear of pads during contacts σ will be proportional to the inverse of ρ [51] and (3.15) becomes:

$$R_\mu = \mu \frac{1}{2}\left(R_1 + R_2\right) \tag{3.17}$$

During the closing phase of the clutch engagement, the contact between the clutch disk and the flywheel is designed to begin at the outer sector of the

flywheel and to continue towards the inner area, with a consequent increase of the contact surface area, i.e. the contact occurs for $\rho \in [r_i(F_{fc}), R_2]$. Remembering the hypothesis made previously it is possible to define the follows expressions for the transmitted clutch torque:

- Constant contact pressure

$$T_{fc} = n\mu \frac{2}{3} \frac{R_2^3 - r_i^3(F_{fc})}{R_2^2 - r_i^2(F_{fc})} F_{fc}(\delta_f) \tag{3.18}$$

- Uniform wear

$$T_{fc} = n\mu \frac{2}{3} \frac{R_2^3 - r_i^3(F_{fc})}{R_2^2 - r_i^2(F_{fc})} F_{fc}(\delta_f) \tag{3.19}$$

In the Figure 3.33(a) the cushion spring load-deflection curve is depicted whereas, in Figure 3.33(b) the torque characteristic is shown. It is evident that the shape of the cushion spring curve has a strong inference on the torque characteristic. In fact, for a given clutch architecture with n frictional surfaces, μ and R_{eq} vary in narrow ranges or under opportune hypotheses they could be considered as constants [2, 22]. Thus, bearing in mind the equation (3.8), the clutch torque characteristic is substantially provided by the cushion spring load-deflection curve multiplied by a constant value [29]. By considering the results shown in the previous paragraphs on the cushion spring and on the friction coefficient it has been developed a more complex clutch torque transmissibility model by modifying the equation (3.8) in the equation (3.20), [36] under the assumption of uniform wear of pads during contacts.

$$T_{fc}(x_{to}, \theta_{cs}, \theta_{cm}, v_s, p) = n\mu(v_s, p, \theta_{cm}) R_m F_{fc}(\delta_f(x_{pp}(x_{to}, \theta_{cs}), \theta_{cs})) \tag{3.20}$$

In this section the clutch torques at various values of θ_{cs} and θ_{cm} are obtained by equation (3.20) are reported in Figure 3.34. In particular, the curve Torque 1 has been obtained by considering $\theta_{cs} = 80\,°\mathrm{C}$ and $\theta_{cm} = 80\,°\mathrm{C}$, the curve Torque 2 has been obtained by considering $\theta_{cs} = 110\,°\mathrm{C}$, $\theta_{cm} = 144\,°\mathrm{C}$ and the curve Torque 3 has been obtained by considering $\theta_{cs} = 213\,°\mathrm{C}$ and $\theta_{cs} = 275\,°\mathrm{C}$.
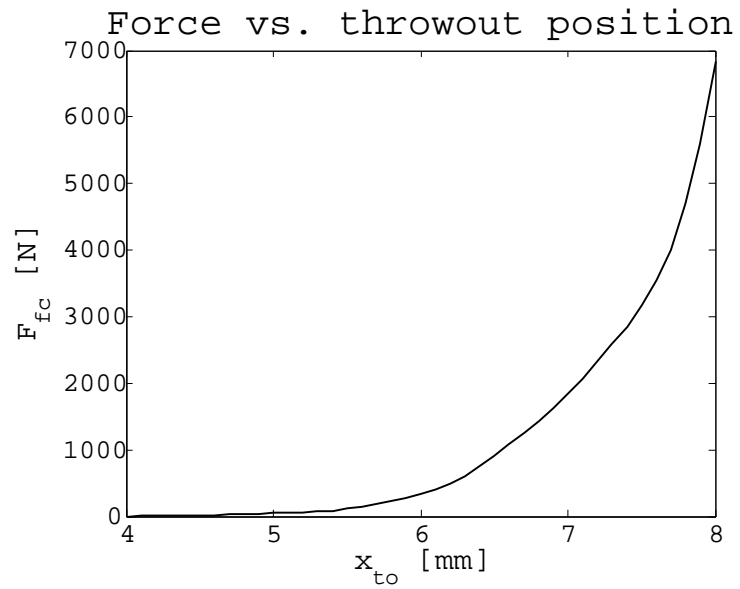
(a) $F_{fc}(x_{to})$
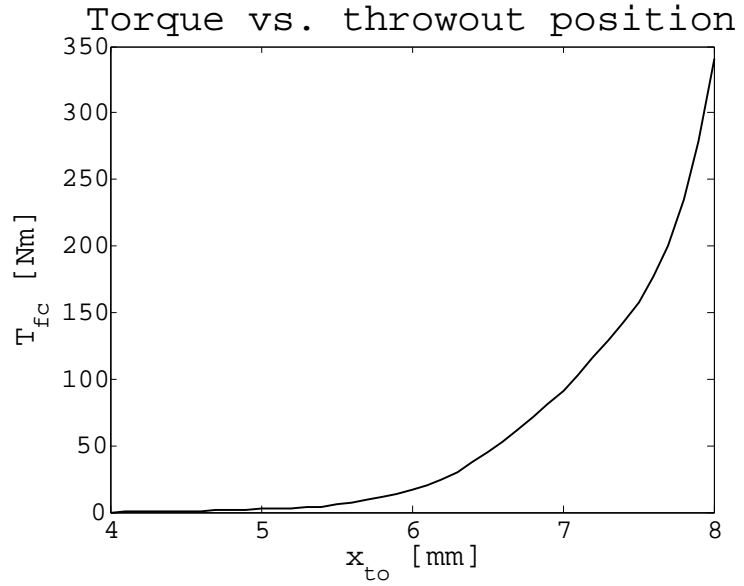
(b) $T_{fc}(x_{to})$

Figure 3.33: Comparison between $F_{fc}(u)$ and $Torque(x_{to})$
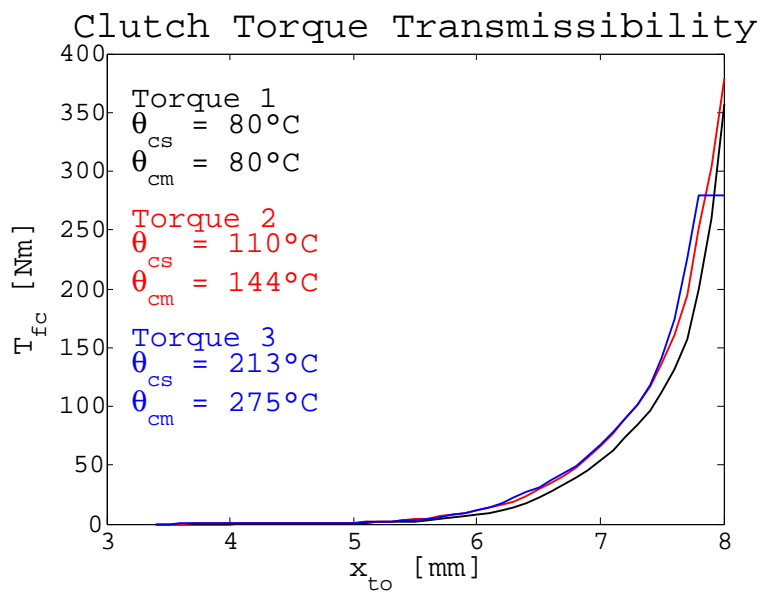
Figure 3.34: Clutch torque characteristic at different temperature levels, [36]

Chapter 4

DRIVELINE MODEL AND CONTROL ALGORITHMS

As explained in the previous Chapter the clutch torque transmissibility is influenced by numerous factors:

- friction phenomena;

- load-deflection characteristic of the elastic components;

- temperature;

- geometry of the clutch assembly;

- wear of the clutch facings;

- wear of the elastic components;

- hysteresis of the elastic components.

Of course these factors have different importance. Indeed, the geometry can be considered fixed for a given clutch assembly. Also the hysteresis and the wear of the elastic components are secondary factors because usually they are substituted before that they reach critical conditions. The wear of the clutch facings is a main factor in a dry clutch system but its effect can be compensate by using suitable solution, Chapter 2. So, the main factors that affect the clutch torque transmissibility are:

- friction phenomena;

- load-deflection characteristic of the cushion spring;

- temperature.

The temperature has an indirect effect on the clutch torque transmissibility because, as explained in the Chapter 3, it influences both the friction coefficient and the cushion spring load-deflection characteristic. Under this light, these latter are the main phenomena to be considered in order to improve the performances of an AMT during the engagement phase. In Figure 4.1 is highlighted the role of the cushion spring map and of the friction map in the TCU.
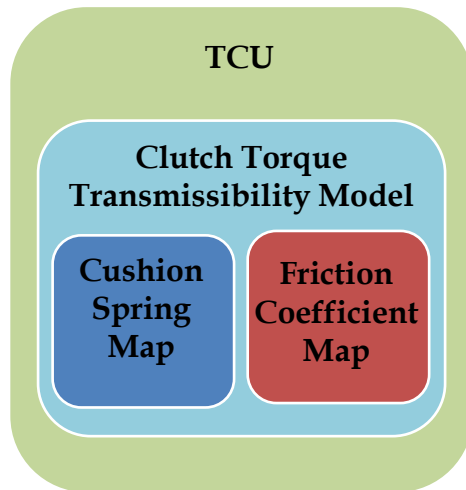
Figure 4.1: Role of the clutch torque transmissibility model in the TCU

If in the TCU is not implemented a good clutch torque transmissibility model the engagement manoeuvre could result in a *poor engagement* reducing the comfort perceived by the driver and vehicle car passengers. In fact, in an automated system such as an AMT the control strategy is fundamental to accomplish good performances. The poor engagement problems occur mainly either non-accurate model is used to schematize the behaviour of the clutch system or bad control strategy is implemented in the TCU. The effect of a poor engagement could result in: engine speed spikes and consequent noise, engine switching off or lack of torque transmission to the driveline during the engagement phase. A possible cause of poor engagement could be an inadequate assessment of the thermal effect on the dry clutch

system after repeated engagements. This condition could lead to a wrong throwout bearing position with imperfect tracking of the reference torque demand. Consequently, the clutch torque corresponding could be either too high or too low and therefore to bring about vibrations, discomfort or even the switching off of the engine.
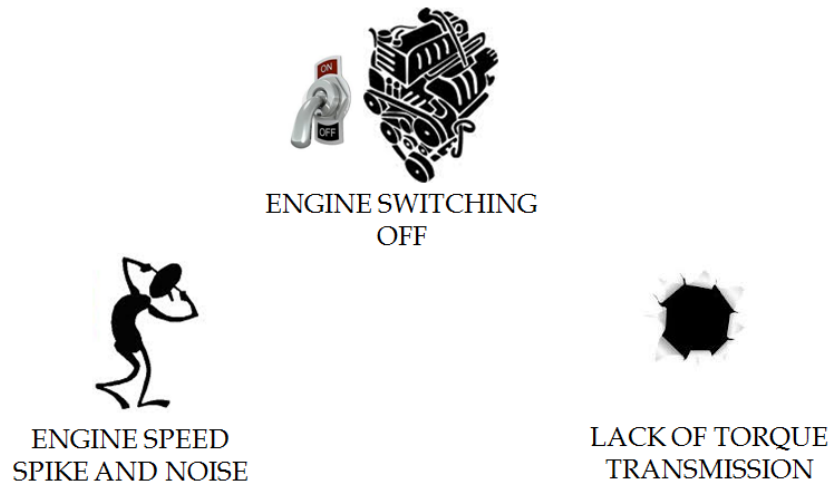
Figure 4.2: Common poor engagement conditions

Once the role of the clutch torque transmissibility model has been explained, in the next paragraphs the mathematical model and different control strategies have been analysed for the engagement phase of the AMT.

4.1   MATHEMATICAL MODEL

This section describes a model for simulating the driveline dynamic behaviour and the Figure 4.3 shows the driveline scheme, where the subscripts e, f, c, g, w indicate engine, flywheel, clutch disc, (primary shaft of) gearbox, and wheels, respectively. A dynamic model of the driveline can be obtained by applying the torque equilibrium at the different nodes of the driveline scheme, where T indicates the torques, J the inertias and ϑ the angles.
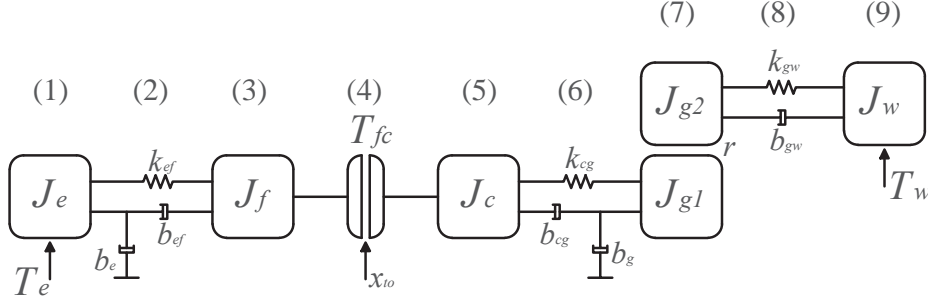
Figure 4.3: Driveline scheme: 5 DoF

The equations which model the driveline are:

$$J_e \dot{\omega}_e = T_e (\omega_e) - b_e \omega_e - T_{ef} (\vartheta_{ef}, \omega_{ef}) \tag{4.1}$$

$$J_f \dot{\omega}_f = T_{ef} (\vartheta_{ef}, \omega_{ef}) - T_{fc} (x_{to}) \tag{4.2}$$

$$J_c \dot{\omega}_c = T_{fc} (x_{to}) - T_{cg} (\vartheta_{cg}, \omega_{cg}) \tag{4.3}$$

$$J_g (r) \dot{\omega}_g = T_{cg} (\vartheta_{cg}, \omega_{cg}) - b_g \omega_g - \frac{1}{r} T_{gw} (\vartheta_{gw}, \omega_{gw}) \tag{4.4}$$

$$J_w \dot{\omega}_w = T_{gw} (\vartheta_{gw}, \omega_{gw}) - T_w (\omega_w) \tag{4.5}$$

and the angle dynamics are:

$$\dot{\vartheta}_e = \omega_e \tag{4.6}$$

$$\dot{\vartheta}_{ef} = \omega_{ef} = \omega_e - \omega_f \tag{4.7}$$

$$\dot{\vartheta}_{cg} = \omega_{cg} = \omega_c - \omega_g \tag{4.8}$$

$$\dot{\vartheta}_{gw} = \omega_{gw} = \omega_g - \omega_w \tag{4.9}$$

where T_e is the engine torque (assumed to be a control input of the model), T_{fc} is the torque transmitted by the clutch (the second control input), x_{to} is the throwout bearing position, and T_w is the equivalent load torque at

the wheels (a measured disturbance). The gear ratio is r (which here includes also the final conversion ratio), and J_c is an equivalent inertia, which includes the masses of the clutch disc, friction pads and the cushion spring. Furthermore the following equations also hold:

$$J_g\left(r\right) = J_{g1} + \frac{J_{g2}}{r^2} \tag{4.10}$$

$$T_{ef}\left(\vartheta_{ef}, \omega_{ef}\right) = k_{ef}\vartheta_{ef} + b_{ef}\omega_{ef} \tag{4.11}$$

$$T_{cg}\left(\vartheta_{cg}, \omega_{cg}\right) = k_{cg}\vartheta_{cg} + b_{cg}\omega_{cg} \tag{4.12}$$

$$T_{gw}\left(\vartheta_{gw}, \omega_{gw}\right) = k_{gw}\vartheta_{gw} + b_{gw}\omega_{gw} \tag{4.13}$$

$$T_w\left(\omega_w\right) = T_{w0} + \frac{1}{2}\rho_a A c_d R_w^3 \omega_w^2 \tag{4.14}$$

where k are torsional stiffness coefficients, b viscous dampings, T_{w0} a constant load torque, ρ_a the air density, A the front surface vehicle area, c_d the drag resistance coefficient, R_w the wheels radius. These equations represent the driveline system during the slipping phase, whereas, during the engaged phase, the flywheel angular speed ω_f and the clutch angular speed ω_c are the same: thus the equations (4.2) and (4.3) can be summed each other, which yields:

$$(J_c + J_f)\dot{\omega}_c = T_{ef}\left(\vartheta_{ef}, \omega_{ef}\right) - T_{cg}\left(\vartheta_{cg}, \omega_{cg}\right) \tag{4.15}$$

4.2 TWO DoF MODEL

A reduced-order model can be obtained from this complex model by assuming the rigidity of the crankshaft $\omega_e = \omega_f$, of the main-shaft $\omega_c = \omega_g$ and of the driveshaft $\omega_g = r\omega_w$. In Figure 4.4 the reduced-order model is shown. A reduced-order model has been used to focus on the control scheme performances by avoiding the expected oscillations of higher order driveline which might mask the difference between engagement at different temperature levels and the poor control outcomes.

The equations of the reduced-order model are derived from (4.1)-(4.15)
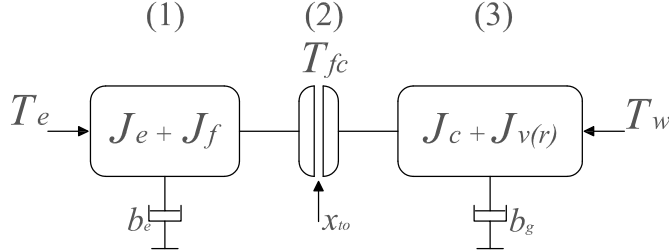
Figure 4.4: Driveline scheme: 2 DoF

with the assumption of the rigid shafts as explained above:

$$(J_e + J_f)\,\dot{\omega}_f = T_e\,(\omega_{ef}) - b_e\omega_f - T_{fc}\,(x_{to}, \omega_{fc}) \tag{4.16}$$

$$(J_c + J_v(r))\,\dot{\omega}_c = T_{fc}\,(x_{to}, \omega_{fc}) - b_g\omega_c - \frac{1}{r}T_w\left(\frac{\omega_c}{r}\right) \tag{4.17}$$

where:

$$J_v(r) = J_g(r) + \frac{1}{r^2}J_w \tag{4.18}$$

The equation of the "locked up" model is obtained by adding the equations (4.16) to (4.17) and by considering $\omega_f = \omega_c$:

$$(J_e + J_f + J_c + J_v(r))\,\dot{\omega}_f = T_e\,(\omega_f) - (b_e + b_g)\,\omega_f - \frac{1}{r}T_w\left(\frac{\omega_f}{r}\right) \tag{4.19}$$

4.2.1   OPEN LOOP CONTROL

In this section an analysis of open loop motion strategy of the throwout bearing in presence of uncertainties about the dry-clutch torque transmissibility characteristic during the vehicle launch manoeuvre is proposed. This control strategy is adopted where cost reason and complexity do not permit the use of displacement sensor. The driveline model parameters are shown in Appendix A. The simulation are carried out by considering as inputs the T_e^{ref} and the T_{fc}^{ref}, see Figure 4.5 for details. The reference clutch torque T_{fc}^{ref} is inverted using the cushion spring load-deflection characteristic and the friction coefficient at $20\,^\circ\text{C}$ to obtain the reference throwout bearing position. This latter is actuated by means of a controlled actuator which is

represented in the control scheme by a unitary gain first-order transfer function $A(s)$ with a time constant of 0.1 s. The output of $A(s)$ is the throwout bearing position which is used, along with the temperatures, as input of the clutch torque map to get the clutch torque to use in the dynamic model. The other input of the dynamic model is the reference engine torque T_e^{ref}. The clutch torque map consists in a series of cushion spring characteristics function of the temperature θ_{cs}, they are depicted in Figure 3.26, and they have been obtained by the FE analysis. Also the friction coefficient is a function of the temperature θ_{cm}, it is depicted in Figure 3.31(b). The open loop control scheme is shown in Figure 4.5.
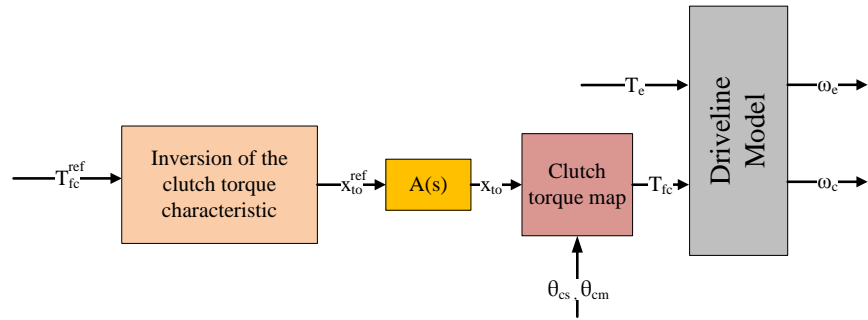
Figure 4.5: Open loop control scheme

SIMULATIONS RESULTS: VEHICLE LAUNCH

This section introduces the results of the simulations carried out in order to empathize the engagement uncertainty during the vehicle launch. Two typical start up manoeuvres with slow-torque and fast-torque requests have been considered for the simulations. The clutch is considered closed when the slip speed is less than 1 $rads^{-1}$. Once the clutch is closed, the throwout bearing position x_{to} is quickly moved to its maximum position. The Figures below show the results for a slow-torque request and for a fast-torque request during launch manoeuvres. In particular the Figure 4.6 exhibits a slow-torque request manoeuvre at reference temperature both for the clutch facings and for the cushion spring. In this case the results display that at reference temperature the start-up manoeuvre is good. As reported in the Chapter 3 after repeated starts the temperatures of the cushion spring and of the clutch facings increases and could reach values higher than 200 °C. So, in the Figures 4.7 and 4.8 are reported the results at higher temperatures

(a) Torques vs. time

(b) Throwout bearing position vs. time

(c) Angular velocity vs. time

(d) Lock up condition vs. time
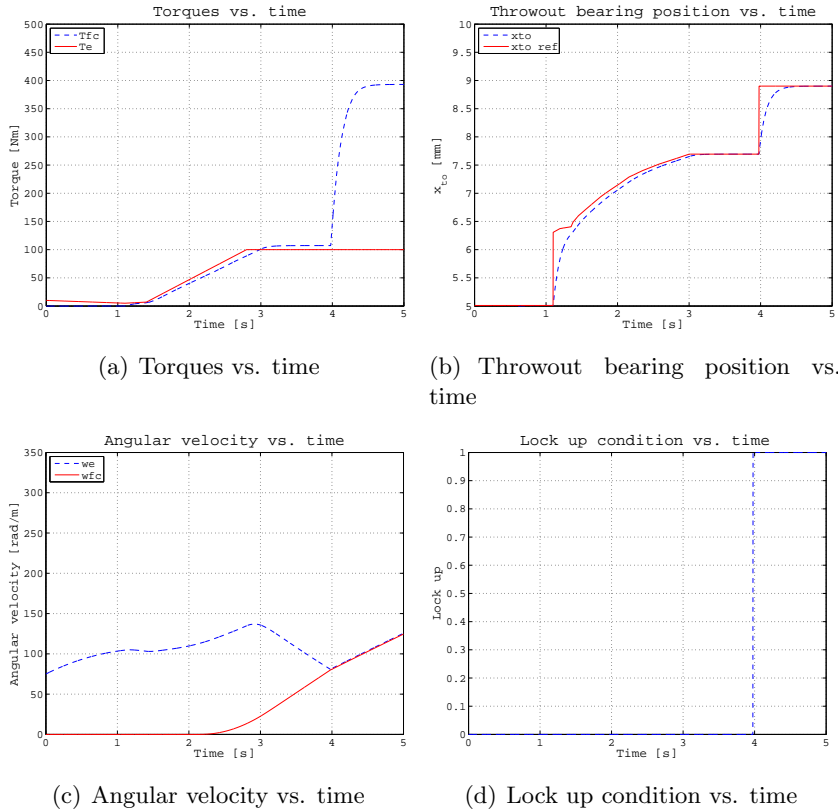
Figure 4.6: Slow-torque request at $\theta_{cs} = 80\,^{\circ}\mathrm{C}$ and $\theta_{cm} = 80\,^{\circ}\mathrm{C}$

than references one both on the cushion spring and on the clutch facings. The throwout bearing reaches a position which correspond to a clutch torque higher than the expected one, Figures 4.9(a) and 4.10(a) respectively. This is due to the fact that in the inversion of the clutch torque characteristic it has not been taken into account the backward travel of the kiss point due to the thermal effects. Consequently, this issue would lead to the switching off of the engine because the engine angular velocity reaches the so called *kill condition* [52]. The Figures show a fast-torque request manoeuvre both at reference temperatures, Figure 4.11, and considering a cushion spring temperature $\theta_{cs} = 110\,^{\circ}\mathrm{C}$ and a clutch facings temperature $\theta_{cm} = 144\,^{\circ}\mathrm{C}$, Figure 4.12. Also in this situation, at temperatures higher than reference one, the throwout bearing reaches a position which corresponds a too high
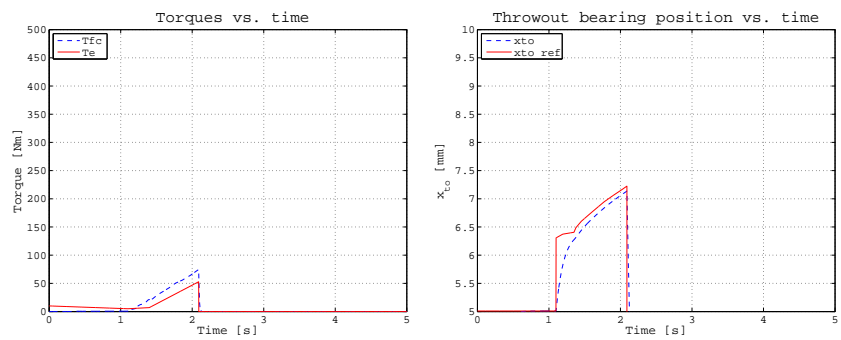
(a) Torques vs. time

(b) Throwout bearing position vs. time
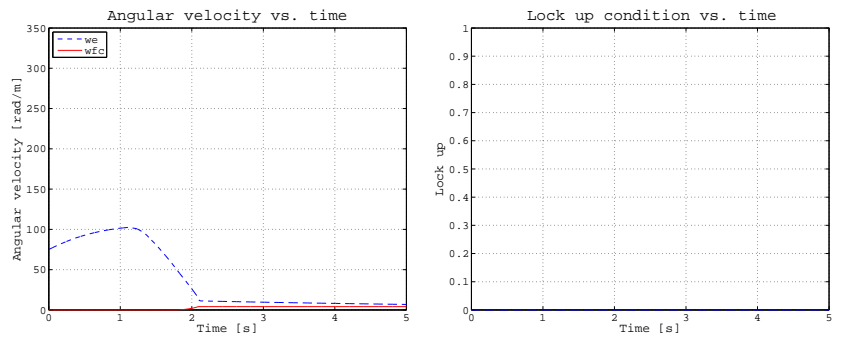
(c) Angular velocity vs. time

(d) Lock up condition vs. time

Figure 4.7: Slow-torque request at $\theta_{cs} = 110\,^{\circ}\mathrm{C}$ and $\theta_{cm} = 144\,^{\circ}\mathrm{C}$

(a) Torques vs. time

(b) Throwout bearing position vs. time

(c) Angular velocity vs. time

(d) Lock up condition vs. time
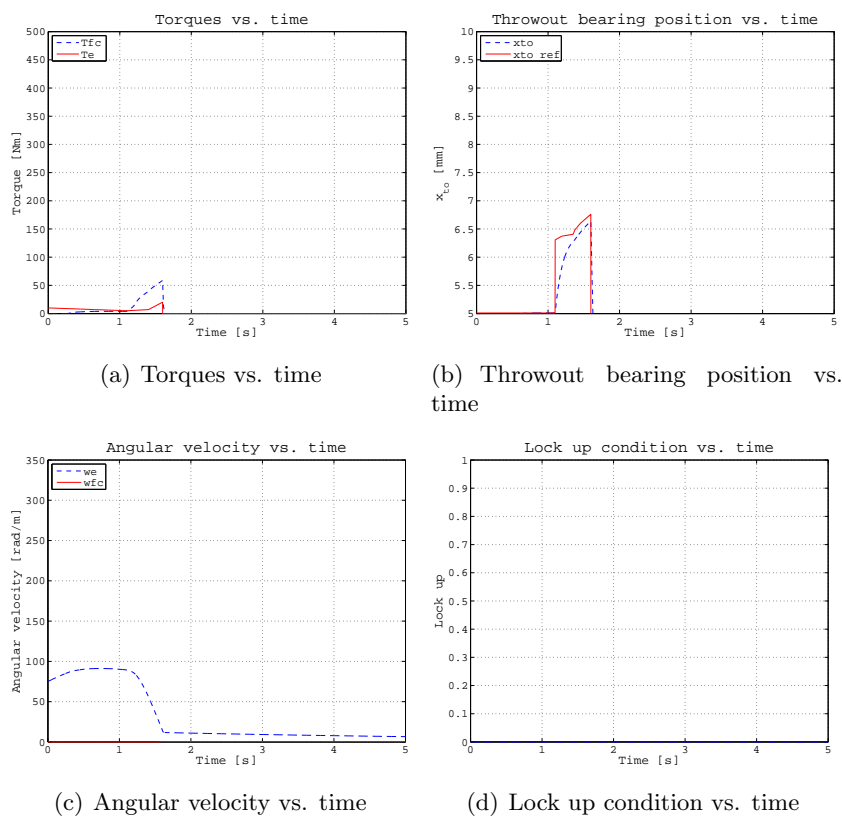
Figure 4.8: Slow-torque request at $\theta_{cs} = 213\,^{\circ}\mathrm{C}$ and $\theta_{cm} = 275\,^{\circ}\mathrm{C}$
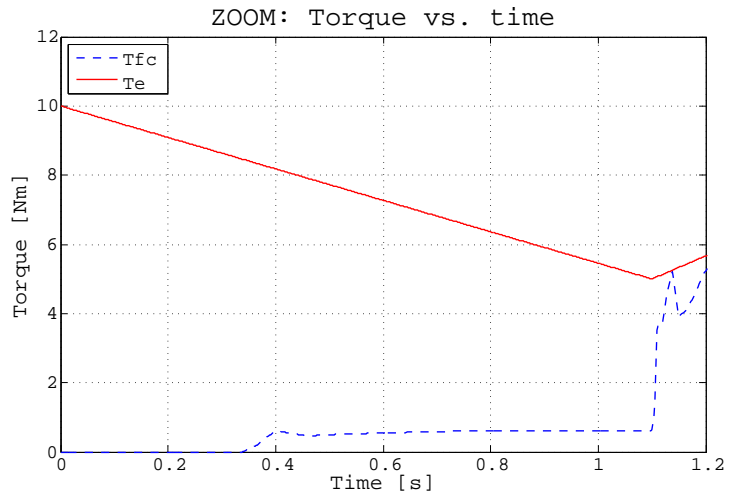
(a) Zoom: Torques vs. time
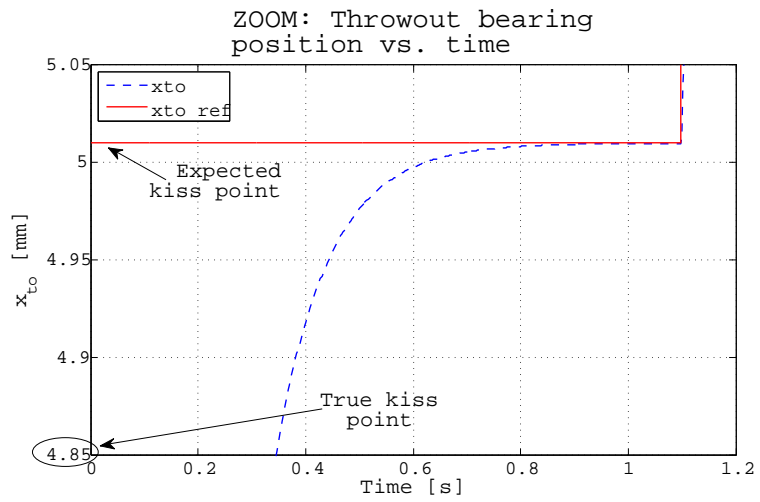
(b) Zoom: Throwout bearing position vs. time

Figure 4.9: Zoom: Slow-torque request at $\theta_{cs} = 110\,^{\circ}\mathrm{C}$ and $\theta_{cm} = 144\,^{\circ}\mathrm{C}$
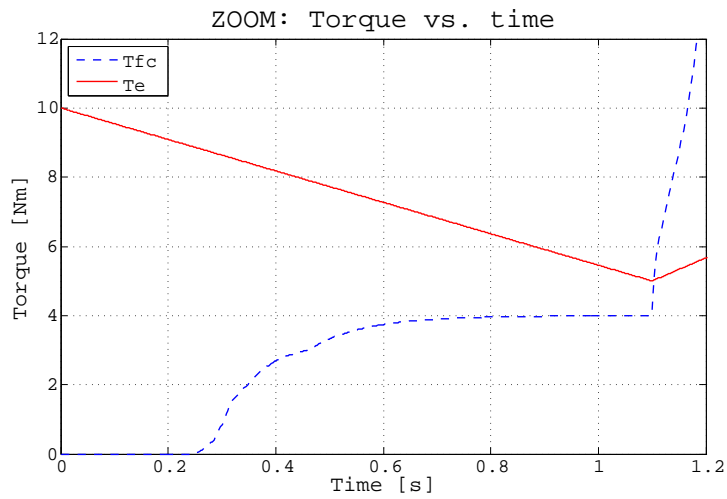
(a) Zoom: Torques vs. time
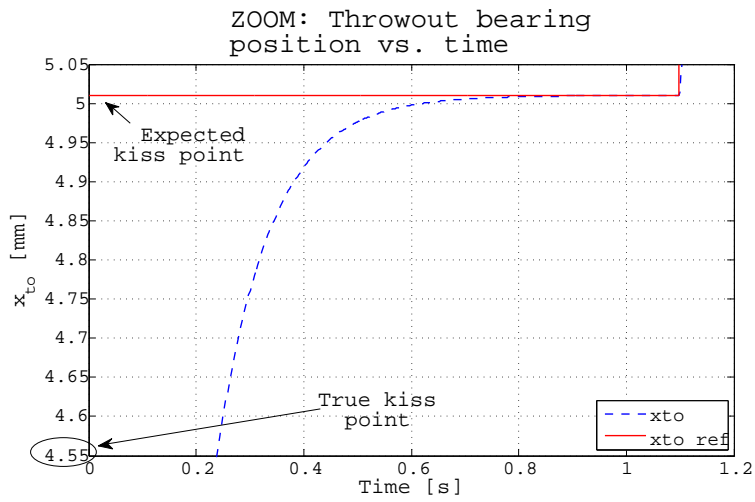
(b) Zoom: Throwout bearing position vs. time

Figure 4.10: Zoom: Slow-torque request at $\theta_{cs} = 213\,^{\circ}\mathrm{C}$ and $\theta_{cm} = 275\,^{\circ}\mathrm{C}$

clutch torque, Figure 4.12(a); in this case the fast-torque request manoeuvre prevents the switching off of the engine. The result is a very fast manoeuvre, about a third shorter than to the same manoeuvre at reference temperature. Consequently the manoeuvre perceived by the driver is uncomfortable.

(a) Torques vs. time

(b) Throwout bearing position vs. time

(c) Angular velocity vs. time

(d) Lock up condition vs. time
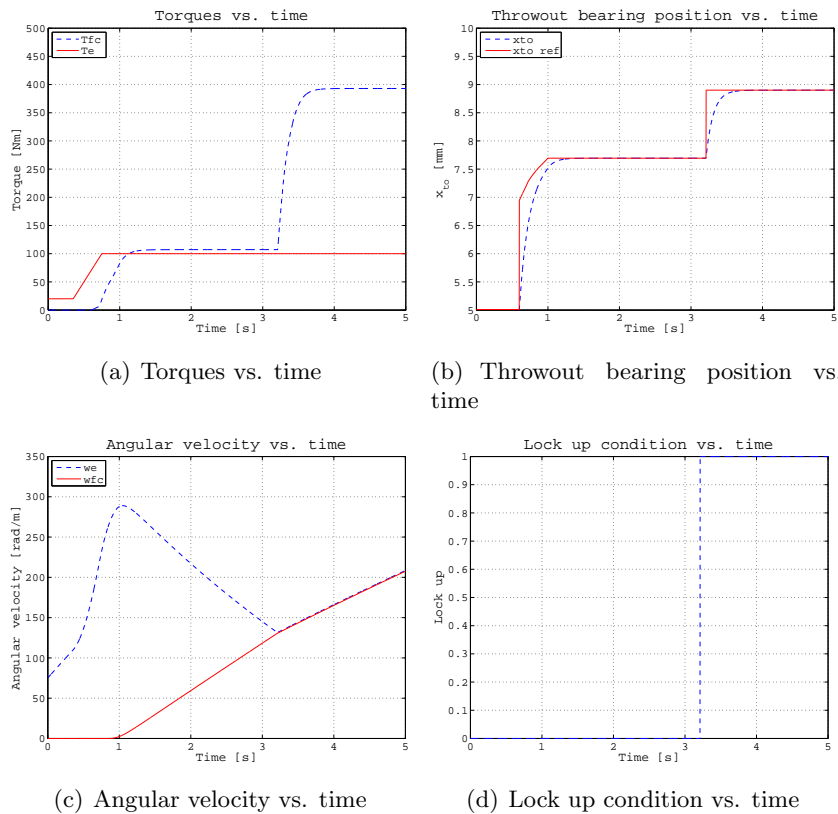
Figure 4.11: Fast-torque request at $\theta_{cs} = 80\,°\mathrm{C}$ and $\theta_{cm} = 80\,°\mathrm{C}$

(a) Torques vs. time

(b) Throwout bearing position vs. time

(c) Angular velocity vs. time

(d) Lock up condition vs. time
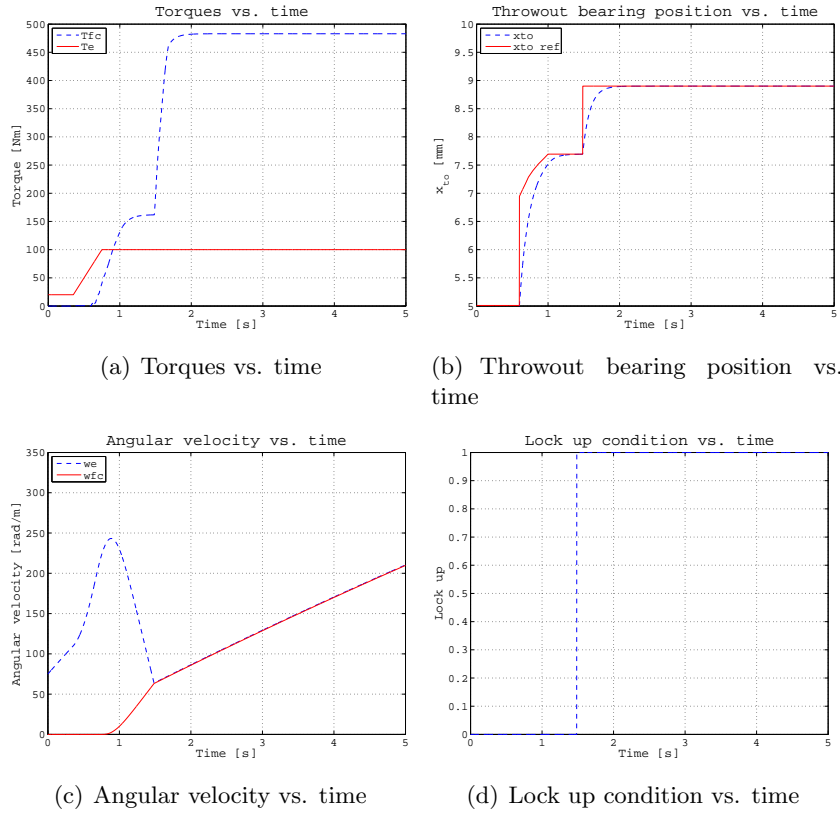
Figure 4.12: Fast-torque request at $\theta_{cs} = 110\,^\circ\text{C}$ and $\theta_{cm} = 144\,^\circ\text{C}$

4.2.2   CLOSED LOOP CONTROL (PI)

In this section an analysis on the AMT closed loop control scheme in presence of uncertainties about the dry-clutch torque transmissibility characteristic is proposed. The driveline model parameters are shown in Appendix A. The simulations are carried out by using a closed loop system with decoupling controller for the engine and the clutch [53], where the input are the ω_e^{ref} and the ω_c^{ref}, see Figure 4.13 for details. The reference clutch angular speed ω_c^{ref} and reference engine speed ω_e^{ref} are compared with the output of the driveline model. The parameters of the engine speed control loop PIe are respectively 2.67 $Nmrad^{-1}s$ and 0.4 $Nmrad^{-1}$, while the parameters of the clutch speed control loop PIc are 2.33 $Nmrad^{-1}s$ and 1.8 $Nmrad^{-1}$ and they have been obtained as in [53]. The output of the PIe is added to the reference

clutch torque to have the reference engine torque which has been assumed equal to the engine torque as input of the dynamic model. The output of the PIc is the reference clutch torque T_{fc}^{ref} which is inverted by using the cushion spring load-deflection characteristic and the friction coefficient at $20\,°\text{C}$ to obtain the reference throwout bearing position x_{to}^{ref}. This latter is actuated by means of a controlled actuator which is represented in the control scheme by a unitary gain first-order transfer function $A(s)$ with a time constant of 0.1 s. The output of $A(s)$ is the throwout bearing position which is used, together to the temperatures, as input of the clutch torque map to get the clutch torque to use in the dynamic model. The other input of the dynamic model is the engine torque. The clutch torque map is given by equation (3.20) where: the cushion spring characteristics, function of the temperature θ_{cs}, is a look-up table obtained by the FE analysis and depicted in Figure 3.26. Instead, the friction coefficient, function of the temperature θ_{cm}, of the contact pressure and of the sliding speed, has been obtained as shown in the Chapter 3. The closed loop control scheme is shown in Figure 4.13.
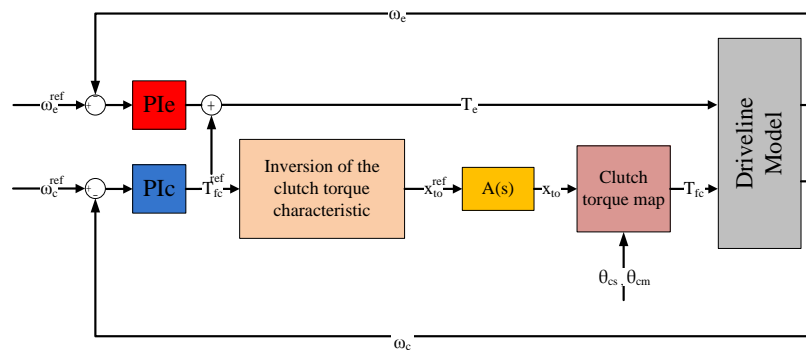
Figure 4.13: Closed loop control scheme

SIMULATIONS RESULTS: VEHICLE LAUNCH

This section introduces the results of the simulations carried out to empathize the engagement uncertainty during the vehicle launch. The clutch is considered closed when the slip speed is less than 1 $rads^{-1}$. Once the clutch is closed, the throwout bearing position x_{to} is forced to move to its maximum position. The Figures below show the results for two pairs of temperatures for launch manoeuvres. In particular, the Figure 4.14 shows

the launch manoeuvre by considering the cushion spring at 80 °C and the clutch facing at 80 °C. Instead, Figure 4.15 shows the launch manoeuvre by

(a) Torques vs. time

(b) Throwout bearing position vs. time

(c) Angular velocity vs. time

(d) Lock up condition vs. time
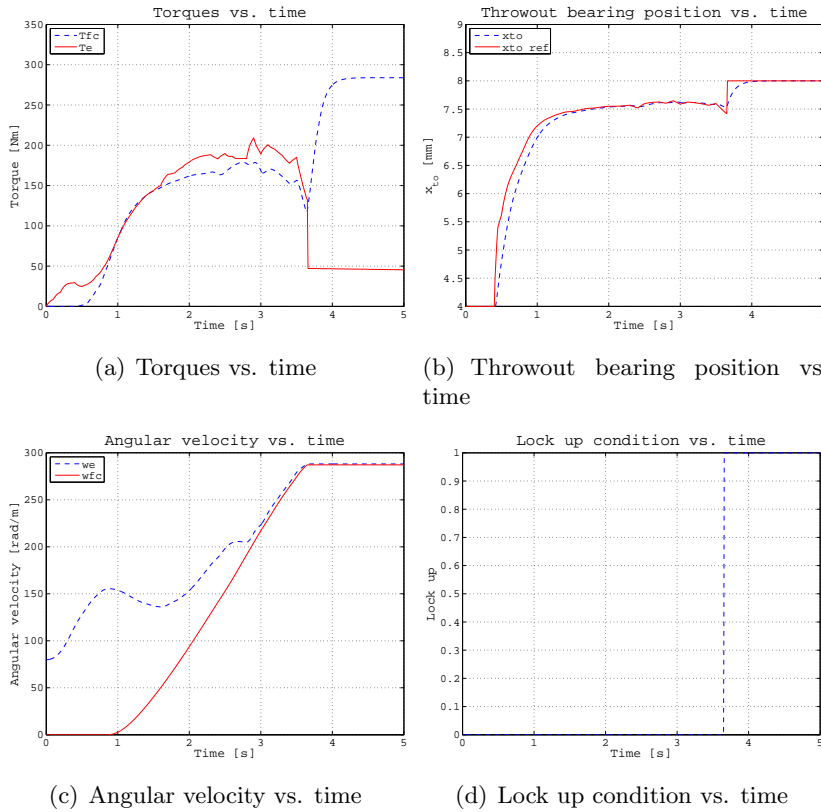
Figure 4.14: Start up manoeuvre at $\theta_{cs} = 80$ °C and $\theta_{cm} = 80$ °C

considering a cushion spring temperature $\theta_{cs} = 110$ °C and a clutch facing temperature $\theta_{cm} = 144$ °C. These results showed that at higher temperature the engagement time is shorter. The explanation of this outcome could be found in the kiss-point position travelling due to the axial thermal expansion of the cushion spring. Consequently, at higher temperature the TCU, which does not take into account the thermal effects, assigns a given position of the throwout bearing to which corresponds an unexpected higher torque value.

(a) Torques vs. time

(b) Throwout bearing position vs. time

(c) Angular velocity vs. time

(d) Lock up condition vs. time
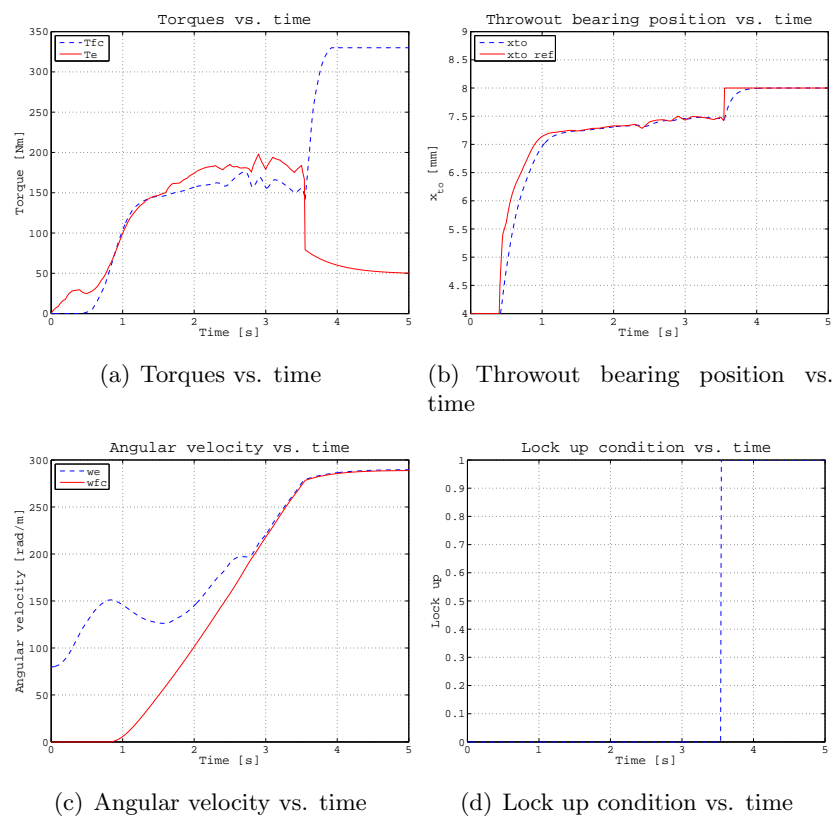
Figure 4.15: Start up manoeuvre at $\theta_{cs} = 110\,^{\circ}\mathrm{C}$ and $\theta_{cm} = 144\,^{\circ}\mathrm{C}$

SIMULATIONS RESULTS: UP-SHIFT

In this section the results concerning an up-shift manoeuvre from $2nd$ to $3rd$ gear ratio at different temperatures will be shown. An up-shift manoeuvre consists in a first phase where the clutch is engaged at the previous gear. After a driver gearshift request there is a switching from the engaged phase to the slipping opening phase. When the new gear is synchronized the slipping closing phase begins. The manoeuvre ends when slip angular speed between the flywheel and the clutch reaches a value less than $1\ rads^{-1}$. The Figure 4.16 show the up-shift manoeuvre by considering a temperature of the cushion spring $\theta_{cs} = 80\,°C$ and a temperature of clutch facing $\theta_{cm} = 80\,°C$. Instead, the Figure 4.17 displays the results at a cushion spring temperature $\theta_{cs} = 213\,°C$ and a temperature $\theta_{cm} = 275\,°C$.

(a) Torque vs. time

(b) Throwout bearing position vs. time

(c) Angular velocity vs. time

(d) Lock up condition vs. time
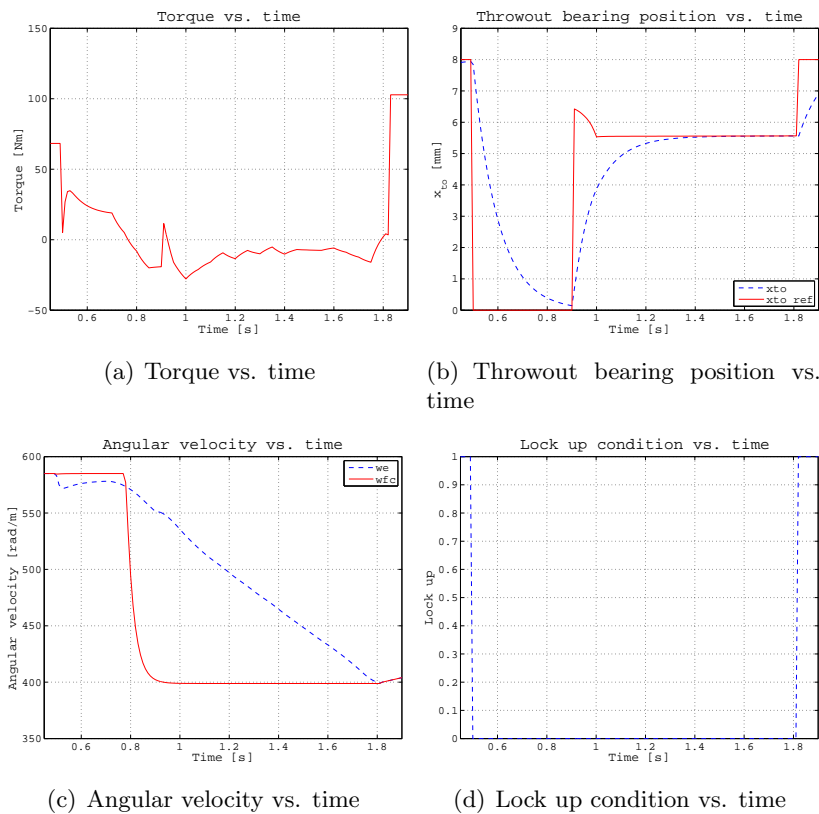
Figure 4.16: Up-shift manoeuvre at $\theta_{cs} = 80\,°C$ and $\theta_{cm} = 80\,°C$

(a) Torque vs. time

(b) Throwout bearing position vs. time

(c) Angular velocity vs. time

(d) Lock up condition vs. time
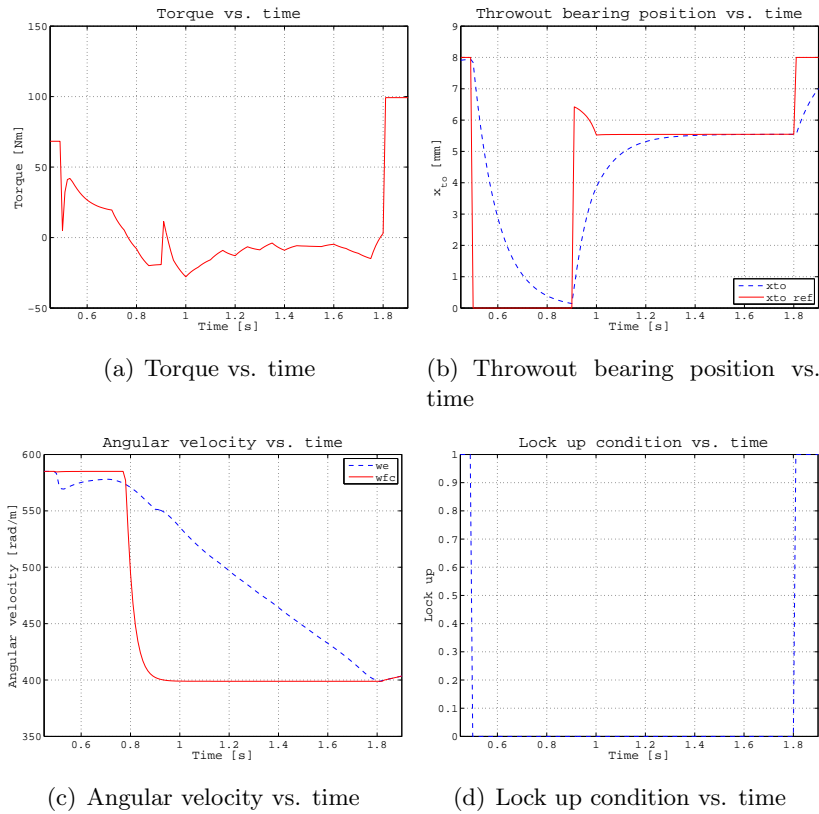
Figure 4.17: Up-shift manoeuvre at $\theta_{cs} = 213\,^{\circ}\mathrm{C}$ and $\theta_{cm} = 275\,^{\circ}\mathrm{C}$

These results show no difference during an up-shift manoeuvre at higher temperature with respect to the same one at reference temperature. This effect is due to the engagement condition reached for low values of the throwout bearing position, see Figures 4.16(b) and 4.17(b). In fact, for these values there is a superposition of the cushion spring curves at different temperature and consequently the cushion spring load is nearly the same, see Figure 3.26.

4.2.3   MODEL PREDICTIVE CONTROL (MPC)

In this section the MPC approach is developed since it provides numerous advantages over the conventional control algorithms. Indeed, it naturally handles multivariable control problem; it can take into account of actua-

tor limitations; it allows the system to operate closer to constraints than conventional control; and finally control update rates are relatively low in these applications, so that there is plenty of time for the necessary on-line computations [54]. One of the main factors which has led to use the MPC approach could be found in its ability to explicitly handle the constraints. This means that the controller allows for input constraints, like for example actuator saturation constraints, and it never generates input signal that attempt to violate them. Thus, with predictive control the wind-up problem does not arise [54]. Furthermore, with the rapid development of computing, MPC becomes more and more attractive feedback strategy in fast dynamics systems [55]. Some attempts have been made for designing various control systems in aerospace, automotive and network systems [56–58]. A Segway-like robot system modeled by a linear time-invariant system with 8 states and 2 inputs subject to input constraints has been tested by using a MPC with a sampling period of 4 ms and a low-cost embedded controller with limited CPU time and memory [59]. Instead, in [60] a constrained MPC has been introduced for the servo design of fast mechatronic systems.

The solution here proposed is based on the design of a multiple controller working in sequence according to the powertrain operating conditions. These controllers are designed to comply with some constraints, both on the "plant" inputs and on the "plant" outputs, which allow the comfort to be improved during the engagement process and increase the safety of the system. In particular, on the plant inputs saturation constraints have been imposed both on the torques and on their variation rates:

$$T_e \in \left[T_e^{\min}, T_e^{\max}\right] \tag{4.20}$$

$$T_{fc} \in \left[T_{fc}^{\min}, T_{fc}^{\max}\right] \tag{4.21}$$

$$\dot{T}_e \in \left[\dot{T}_e^{\min}, \dot{T}_e^{\max}\right] \tag{4.22}$$

where $T_e^{\min} = -20$ Nm is the minimum engine torque value during the vehicle launch, $T_e^{\max} = 250$ Nm is the maximum engine torque value, $T_{fc}^{\min} = 0$ Nm is the minimum torque value transmitted by the clutch, $T_{fc}^{\max} = 315$ Nm is the maximum torque value that the clutch can transmit, $\dot{T}_e^{\min} = -500$ Nm/s is the maximum decrease (≤ 0) in one step and $\dot{T}_e^{\max} = 500$ Nm/s is the maximum increase (≥ 0) in one step.

Instead, on the "plant" outputs, engine and clutch angular speeds, the

following constraints hold:

$$\omega_e \in \left[\omega_e^{kill}, \omega_e^{\max}\right] \tag{4.23}$$

$$\omega_c \geq \omega_c^{\min} \tag{4.24}$$

where $\omega_e^{kill} = 80 \ rad/s$ represents the so-called no-kill condition [52], $\omega_e^{\max} = 600 \ rad/s$ is the maximum value of the engine speed before attaining critical conditions and $\omega_c^{\min} = 0 \ rad/s$ is the minimum value of clutch speed during the vehicle launch. It is worth noting that it is not necessary to impose a maximum clutch angular speed, because it is equal to the engine angular speed during the engaged phase and it can only decrease for passive resistance during the idle phase.

As explained above, the clutch operates in two different working conditions: the slipping phase and the engaged phase. That is why two different controllers for each phase have been designed. The switching parameter d selects the controller by considering the absolute value of the difference between the engine and the clutch angular speed. Particularly, the switching condition is attained when $\omega_{sl} = |\omega_e - \omega_c| \leq 1 \ rad/s$. It is important to emphasize that in no way the two controllers can work simultaneously and so any conflict between them is avoided prior. An alternative mathematical representation of the driveline useful for the Model Predictive Control (MPC) approach is the State-Space representation. In the continuous the driveline model can be written as follows:

$$\dot{\mathbf{x}}(t) = [\mathbf{A}_{sl}d + \mathbf{A}_{eng}(1-d)]\mathbf{x}(t) + [\mathbf{B}_{sl}d + \mathbf{B}_{eng}(1-d)]\mathbf{u}(t)$$
$$\mathbf{y}(t) = \mathbf{C}\mathbf{x}(t) \tag{4.25}$$

where the state, input and output vectors are respectively:

$$\mathbf{x} = \left\{ \ \omega_e \quad \vartheta_e \quad \omega_c \quad \vartheta_c \ \right\}^T$$

$$\mathbf{u} = \left\{ \ T_e \quad T_{fc} \quad T_w \ \right\}^T$$

$$\mathbf{y} = \left\{ \ \omega_e \quad \omega_c \ \right\}^T$$

and d is a switching variable equal to 1 when the system is in the slipping phase and 0 otherwise. The subscript sl and eng indicate the slipping and the engaged system matrices, respectively, and the matrices can be simply deduced from equation (4.1)-(4.15), see Appendix B. The MPC has been

designed with the discrete time version of the driveline model (4.25) obtained by using the zero-order hold method with a sampling time of 0.01 s. This value is compatible for automotive applications. In fact, as reported in [61], the computational cycle adopted for these applications is set as 5 to 10 ms.

$$\mathbf{x}_{k+1} = \left[\bar{\mathbf{A}}_{sl}d + \bar{\mathbf{A}}_{eng}\left(1 - d\right) \right] \mathbf{x}_k + \left[\bar{\mathbf{B}}_{sl}d + \bar{\mathbf{B}}_{eng}\left(1 - d\right) \right] \mathbf{u}_k$$
$$\mathbf{y}_k = \bar{\mathbf{C}}\mathbf{x}_k \tag{4.26}$$

The MPC aims at finding the output $\mathbf{y}_k$ by tracking the reference trajectory $\mathbf{r}_k$ and fulfilling the constraints seen above for any time step $k \geq 0$. Under the assumption that the estimate of $\mathbf{x}_k$ is available at time k, the cost function to be optimized is:

$$J_i\left(\Delta u, \varepsilon\right) = \mathbf{u}_i^T \mathbf{W}_{u,i}^2 \mathbf{u}_i + \Delta \mathbf{u}_i^T \mathbf{W}_{\Delta u,i}^2 \Delta \mathbf{u}_i + ...$$
$$+[\mathbf{y}_i - \mathbf{r}_i]^T \mathbf{W}_{y,i}^2 [\mathbf{y}_i - \mathbf{r}_i] + \rho_\varepsilon \varepsilon \tag{4.27}$$

where:

$\mathbf{u}_i = \left[\begin{array}{ccc} u_i\left(0\right) & ... & u_i\left(P - 1\right) \end{array} \right]^T$ is the input vector;

$\Delta \mathbf{u}_i = \left[\begin{array}{ccc} \Delta u_i\left(0\right) & ... & \Delta u_i\left(P - 1\right) \end{array} \right]^T$ is the input increment vector;

$\mathbf{y}_i = \left[\begin{array}{ccc} y_i\left(0\right) & ... & y_i\left(P\right) \end{array} \right]^T$ is the output vector;

$\mathbf{r}_i = \left[\begin{array}{ccc} r_i\left(0\right) & ... & r_i\left(P\right) \end{array} \right]^T$ is the reference trajectory vector;

$\mathbf{W}_{u,i}$, $\mathbf{W}_{\Delta u,i}$ and $\mathbf{W}_{y,i}$ are, respectively, the input, input increment and output weights matrices (diagonals and squares);

the subscript $i = 1, 2$ accounts for the two inputs and two outputs of the "plant".

The constraints on $\mathbf{u}$, $\Delta \mathbf{u}$, and $\mathbf{y}$ are softened by introducing the slack variable $\varepsilon \geq 0$. In (4.27), the weight ρ_ε on the slack variable ε penalizes the violation of the constraints. As ρ_ε increases with respect to the input and output weights, the controller gives a higher priority to the minimization of constraint violations. The optimization accounts for the constrains as

follows:

$$
\begin{cases}
u_{\min,i}\left(j\right) - \varepsilon V_{\min,i}^{u}\left(j\right) \leq u_i\left(k+j\left|k\right.\right) \leq u_{\max,i}\left(j\right) + ... \\
\quad + \varepsilon V_{\max,i}^{u}\left(j\right) \\[4pt]
\Delta u_{\min,i}\left(j\right) - \varepsilon V_{\min,i}^{\Delta u}\left(j\right) \leq \Delta u_i\left(k+j\left|k\right.\right) \leq \Delta u_{\max,i}\left(j\right) + ... \\
\quad + \varepsilon V_{\max,i}^{\Delta u}\left(j\right) \\[4pt]
y_{\min,i}\left(j\right) - \varepsilon V_{\min,i}^{y}\left(j\right) \leq y_i\left(k+j+1\left|k\right.\right) \leq y_{\max,i}\left(j\right) + ... \\
\quad + \varepsilon V_{\max,i}^{y}\left(j\right) \\[4pt]
\Delta u_i\left(k+h\left|k\right.\right) = 0 \\[4pt]
\varepsilon \geq 0
\end{cases} \tag{4.28}
$$

where $j = 0, ..., P-1$, $h = m, ..., P-1$, P is the prediction horizon, m is the control horizon, the vectors $V_{\min,i}^{u}$, $V_{\max,i}^{u}$, $V_{\min,i}^{\Delta u}$, $V_{\max,i}^{\Delta u}$, $V_{\min,i}^{y}$, $V_{\max,i}^{y}$ have non-negative entries that quantify the concern for relaxing the corresponding constraint; the larger V, the softer the constraint. $V = 0$ means that the constraint is hard and cannot be violated. The following constraints have been considered hard for the input and input increments: $V_{\min,i}^{u} = V_{\max,i}^{u} = V_{\min,i}^{\Delta u} = V_{\max,i}^{\Delta u} = 0$, whereas the soft constraints for the outputs are $V_{\min,i}^{y} = V_{\max,i}^{y} = 1$.

The parameters to be tuned are the prediction horizon P, the control horizon m, the weights W_u, $W_{\Delta u}$, W_y, respectively, the input, the input increments, the output weights matrices, and the overall penalty weight ρ_ε. The parameters have been tuned by trial and error procedure by using Simulink$^{©}$ and the MPC Toolbox. The driving criteria adopted to select these parameters have been a trade-off between fast engagement and comfortable lock-up. In particular, this goal has been easily achieved by a suitably choice of the weights W_u, $W_{\Delta u}$ and W_y. Instead, the prediction and the control horizon, together with the inputs weights, have allowed to improve the steady-state solution. The parameters used during the simulations are defined in Tables 4.1 and 4.2. A sensitive analysis has been carried out to evaluate the performance of the controller by changing the weights both for plant inputs (engine and clutch torque) and plant outputs (engine and clutch angular velocity). The results have highlighted the need of a resolution equal to one hundredth even on the outputs. During the engaged phase, i.e. when the engine is synchronized with the transmission, the clutch torque value (second input) does not influence the plant. Indeed,

MPC1 - SLIPPING PHASE			
Symbol	**Description**	**Value**	
		1	**2**
W_u	Input weight	0.00	0.00
$W_{\Delta u}$	Input rate weight	0.10	0.50
W_y	Output weight	1.00	0.40
P	Prediction horizon	10	
m	Control horizon	3	
ρ_ϵ	Overall penalty weight	0.8	

Table 4.1: MPC1 parameters, slipping phase

MPC2 - ENGAGED PHASE			
Symbol	**Description**	**Value**	
		1	**2**
W_u	Input weight	0.00	0.00
$W_{\Delta u}$	Input rate weight	1.00	0.00
W_y	Output weight	1.00	1.00
P	Prediction horizon	10	
m	Control horizon	3	
ρ_ϵ	Overall penalty weight	0.8	

Table 4.2: MPC2 parameters, engaged phase

in these conditions the driveline has a degree of freedom lesser than during the slipping phase and the plant model is represented by equation (4.15) which has been obtained by adding the equations (4.2) and (4.3). In particular, when the clutch is engaged the engine angular velocity (first plant output) and the clutch angular velocity (second plant output) are the same and the system has one degree of freedom less than the slipping phase. Zero value has been used both for $W_u(2)$ and $W_{\Delta u}(2)$ by taking into account that the second plant input does not influence the plant. Instead, for $W_u(1)$, a smaller value has been used to avoid singularity problem on the Hessian matrix (the nominal zero value has been listed in the Table 4.2). A lower value of the weight means that the first plant input account for weaker influence on the behaviour of overall performance.

The simulations are carried out by using a closed loop system with two MPCs as described in the previous paragraph for the slipping and engaged phases. The set point inputs are the $\omega_{e,sp}$ and the $\omega_{c,sp}$ (see Figure 4.18 for details). The set point about clutch angular speed $\omega_{c,sp}$ and engine speed $\omega_{e,sp}$ are compared with the output of the driveline model. The parameters of the MPC are shown in Tables 4.1 and 4.2, respectively. The controller has been designed by considering only the driveline dynamics described by equations (4.1)-(4.16) or, in the discrete state-space representation, by equation (4.26). The first output of the MPC, the engine torque T_e is fed directly into the driveline model. Instead, the second output of the MPC, the clutch torque T_{fc}, has been inverted by using a look-up table which represents the cushion spring load-deflection characteristic and by considering a constant friction coefficient μ_0 in order to obtain the reference throwout bearing position x_{to}^{ref}. The latter variable has been modified by means of an actuator which has been represented by considering the discrete time model of a unitary gain first-order transfer function with a time constant equal to 0.1 s. The actuator dynamics has been modelled by the transfer function is $A(z) = \frac{0.0952}{z-0.905}$ but it has not been considered in the control design. The output of $A(z)$, i.e. the throwout bearing position, has been used as input of the clutch torque map to obtain the clutch torque which is the second input of the plant. In Figure 4.18 the control scheme is reported. In the numerical algorithm, the cushion spring characteristics has been introduced through a look-up table, whereas the friction coefficient, function of the contact pressure and of the sliding speed, has been obtained as explained in the Chapter 3.
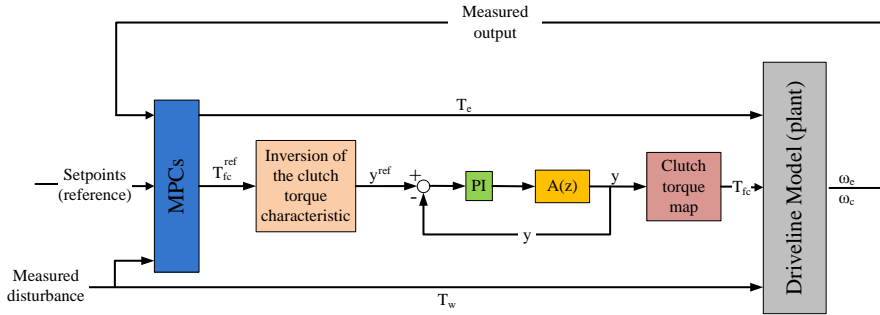
Figure 4.18: Closed loop control scheme

SIMULATIONS RESULTS: VEHICLE LAUNCH

This section describes the results of the simulations about the performances of MPC during the vehicle launch manoeuvres at different pairs of temperatures. The clutch is considered to be engaged when the slip speed is less than $1\ rads^{-1}$. The Figures below point out the results of a typical fast torque request manoeuvre. Figure 4.19 shows the plots of a start-up manoeuvre at $\theta_{cs} = 80\,°C$ and $\theta_{cm} = 80\,°C$. In particular, Figure 4.19(a) represents the engine torque (red line) and the clutch torque (blue dashed line). Figure 4.19(b) represents the reference throwout bearing position (red line) and the true position (blue dashed line). Figure 4.19(c) shows the comparison between the engine and the clutch set points angular speeds (blue and red line, respectively) and the engine and the clutch driveline outputs angular speeds (blue and red dashed line, respectively). Finally, Figure 4.19(d) represents the lock up signal. The start-up manoeuvre is completed in 2.32 s. When the clutch is engaged the controller gives to the throwout bearing the signal to reach the rest position, i.e. clutch closed, Figure 4.19(d). This means that the clutch can transimt its maximum value as highlighted in Figure 4.19(a). Figure 4.20 displays the plots of a start-up manoeuvre at $\theta_{cs} = 213\,°C$ and $\theta_{cm} = 275\,°C$. Figure 4.20(a) represents the engine torque (red line) and the clutch torque (blue dashed line). Figure 4.20(b) represents the reference throwout bearing position (red line) and the true position (blue dashed line). Figure 4.20(c) shows the comparison between the engine and the clutch set points angular speeds (blue and red line, respectively) and the engine and the clutch driveline outputs angular speeds (blue and red dashed line, respectively). Finally, Figure 4.20(d) represents the lock up signal. In this case the start-up manoeuvre is completed in 2.23 s. Also by

(a) Torques vs. time

(b) Throwout bearing position vs. time

(c) Angular velocity vs. time

(d) Lock up condition vs. time
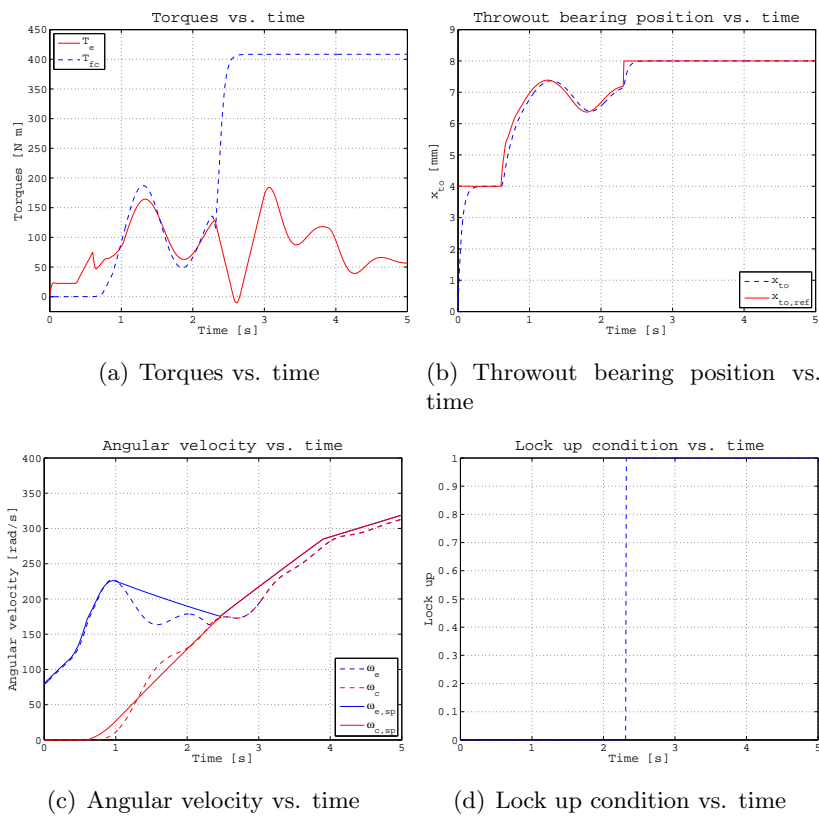
Figure 4.19: Start up manoeuvre at $\theta_{cs} = 80\,^\circ\text{C}$ and $\theta_{cm} = 80\,^\circ\text{C}$

using a controller more complex than the PI is proved that the uncertainty of the clutch torque map due to the temperature induces jerks as exhibited by the comparison between the figures 4.19(c) and 4.20(c). This results in a uncomfortable launch manoeuvre and consequently in a poor engagement. As explained in the previous paragraph 4.2.2 these phenomena are due to the backward travel of the kiss point at higher temperatures, making the start-up manoeuvre faster.

(a) Torques vs. time

(b) Throwout bearing position vs. time

(c) Angular velocity vs. time

(d) Lock up condition vs. time
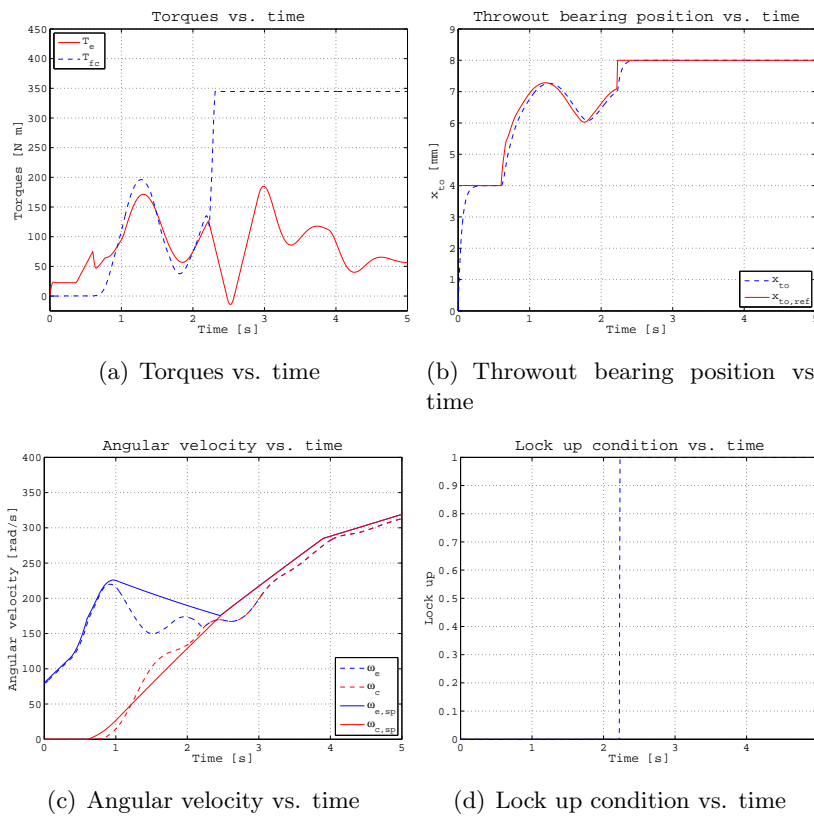
Figure 4.20: Start up manoeuvre at $\theta_{cs} = 213\,^{\circ}\mathrm{C}$ and $\theta_{cm} = 275\,^{\circ}\mathrm{C}$

4.3 HIGH-ORDER DRIVELINE MODEL

The high-order model analysed in this section is shown in Figure 4.3 and represented by equations (4.1)-(4.15). The continuous State-Space representation is formally the same used for the reduced-order driveline model,

equation (4.25). The matrices and the state vector change.

The state, input and output vectors are respectively:

$$\mathbf{x} = \left\{ \begin{array}{cccccccccc} \omega_e & \vartheta_e & \omega_f & \vartheta_f & \omega_c & \vartheta_c & \omega_g & \vartheta_g & \omega_w & \vartheta_w \end{array} \right\}^T$$

$$\mathbf{u} = \left\{ \begin{array}{ccc} T_e & T_{fc} & T_w \end{array} \right\}^T$$

$$\mathbf{y} = \left\{ \begin{array}{cc} \omega_e & \omega_c \end{array} \right\}^T$$

The matrices can be simply deduced from equation (4.1)-(4.15), see Appendix B.

4.3.1 MODEL PREDICTIVE CONTROL (MPC)

All the considerations viewed for the constraints and the tuning of the MPCs used for the reduced-order driveline model are valid also for a high-order driveline model. So, for the sake of brevity in this section are reported only the parameters used for the simulations. The reader could find in the previous paragraph more details on the choice of these parameters. The

MPC1 - SLIPPING PHASE			
Symbol	**Description**	**Value**	
		1	**2**
W_u	Input weight	0.18	0.12
$W_{\Delta u}$	Input rate weight	0.15	0.35
W_y	Output weight	1.00	1.15
P	Prediction horizon	10	
m	Control horizon	2	
ρ_ϵ	Overall penalty weight	0.8	

Table 4.3: MPC1 parameters, slipping phase

simulations have been carried out by using the same closed loop system with two MPCs described in the previous paragraph for the reduced-order driveline model (see Figure 4.18 for details). In particular, a comparison between the unconstrained and the constrained MPCs has been proposed in this section to highlight the effectiveness of the constrained controllers to achieve better performance in terms of safety of the system and comfortable engagement process.

MPC2 - ENGAGED PHASE			
Symbol	Description	Value	
		1	2
W_u	Input weight	0.00	0.00
$W_{\Delta u}$	Input rate weight	1.00	0.00
W_y	Output weight	1.00	1.00
P	Prediction horizon	15	
m	Control horizon	5	
ρ_ϵ	Overall penalty weight	0.8	

Table 4.4: MPC2 parameters, engaged phase

SIMULATIONS RESULTS: VEHICLE LAUNCH

This section describes the results of the simulations to stress the differences between the constrained and the unconstrained MPC algorithms during the vehicle launch. The clutch is considered to be engaged when the slip speed is less than 1 $rads^{-1}$. Once the clutch is engaged, the throwout bearing position is rapidly increased to its maximum value by the control algorithm. The sub-paragraphs below show the results for two different launch manoeuvres.

MANOEUVRE 1   The following figures show the results of a typical launch manoeuvre. Figure 4.21 shows the plots of the engine 4.21(a) and the clutch 4.21(b), angular speeds, respectively. The dashed blue lines represent the set points $\omega_{e,sp}$ and $\omega_{c,sp}$, the solid red lines represent the output of the constrained model $\omega_{e,C}$ and $\omega_{c,C}$ whereas the black dash-dot lines represent the output of the unconstrained model $\omega_{e,U}$ and $\omega_{c,U}$. For the clutch speed there are not differences between the outputs of the two models. Instead, for the engine speed there are some little differences as shown in Figure 4.21(a)). Figure 4.22 shows the MPC outputs $T_{e,MPC}$ and $T_{fc,MPC}$, the torque load T_{load} and the clutch torque output of the clutch model map block T_{fc}. This picture highlights that both MPC outputs do not violate their lower bounds Figure 4.22(a). Instead, this violation instead occurs in the unconstrained model Figure 4.22(b). The green dotted line represents the clutch torque output of the clutch torque map block. After that the engaged condition is attained, the throwout bearing position reaches its maximum value, as shown in Figure 4.23, corresponding to the maximum torque transmittable by the clutch by considering the frictional map and

(a) Engine angular speed vs. time   (b) Clutch angular speed vs. time
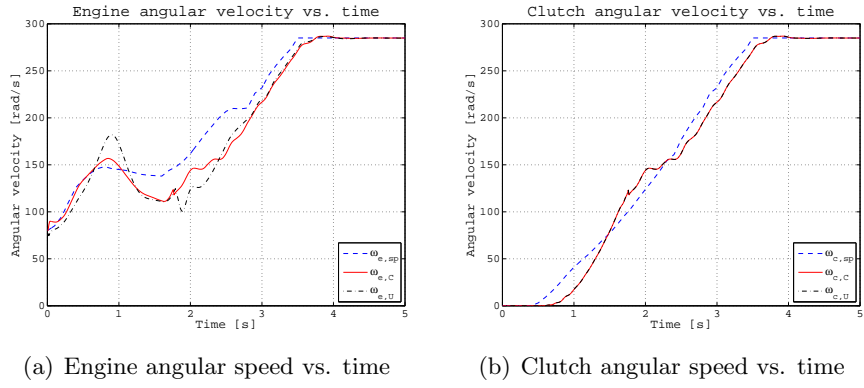
Figure 4.21: Engine (a) and Clutch (b) angular speed

(a) Constrained   (b) Unconstrained
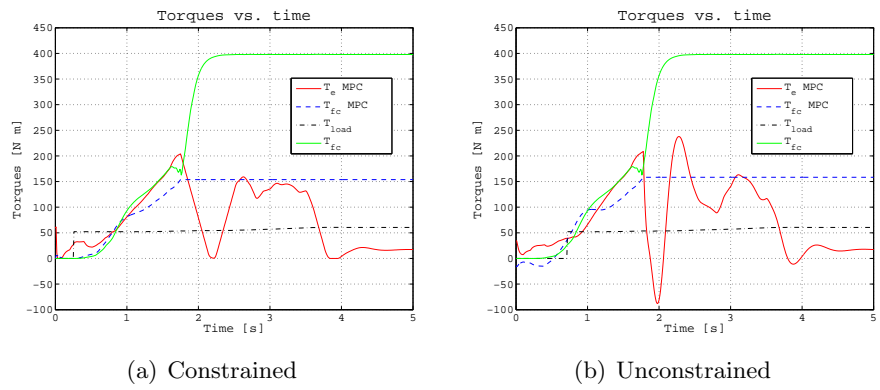
Figure 4.22: Torques (a) Constrained and (b) Unconstrained

the cushion spring characteristic. Moreover, it is worth noting that the un-

(a) Constrained
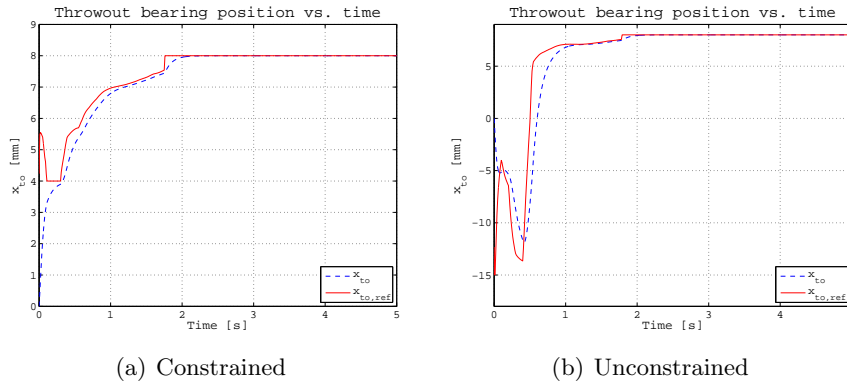
(b) Unconstrained

Figure 4.23: Throwout bearing position (a) Constrained and (b) Unconstrained

constrained MPC imposes negatives values to the throwout bearing position resulting in a dangerous and unwanted condition, i.e. excessive stress on the actuator that may be damaged. Saturation on the actuator output is necessary to avoid this drawback. On the other hand the constrained controllers never reach negative values making this saturation unnecessary. Figure 4.24

(a) Set points vs. time

(b) Plant outputs vs. time
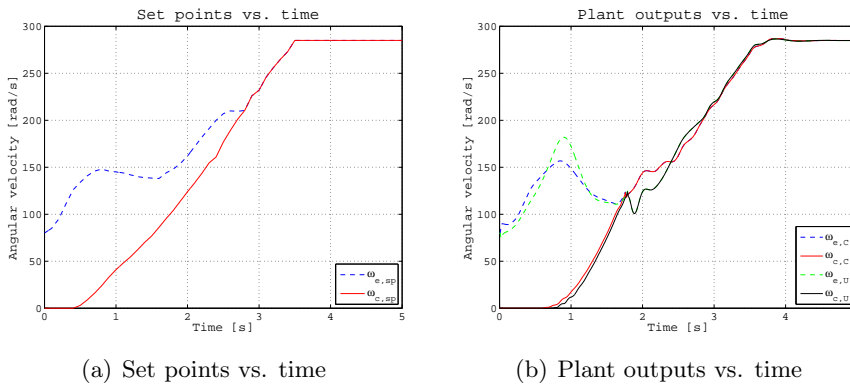
Figure 4.24: Engine and clutch speed (a) Set points (b) Plant outputs

describes the engine and clutch angular speed set point, Figure 4.24(a), and the outputs of the driveline both for the unconstrained and the constrained model, Figure 4.24(b). It shows that the engagement time is 2.8 s for the

set points and 1.7 s for the driveline outputs: this results in reduction of wear of frictional facings, less energy and fuel consumptions. Moreover, it is worth noting that the start up manoeuvre with the unconstrained model yields to an engine speed spike, with consequent noise, and undesired jerks. Finally, Figure 4.25 shows the input/output trajectories both for the con-
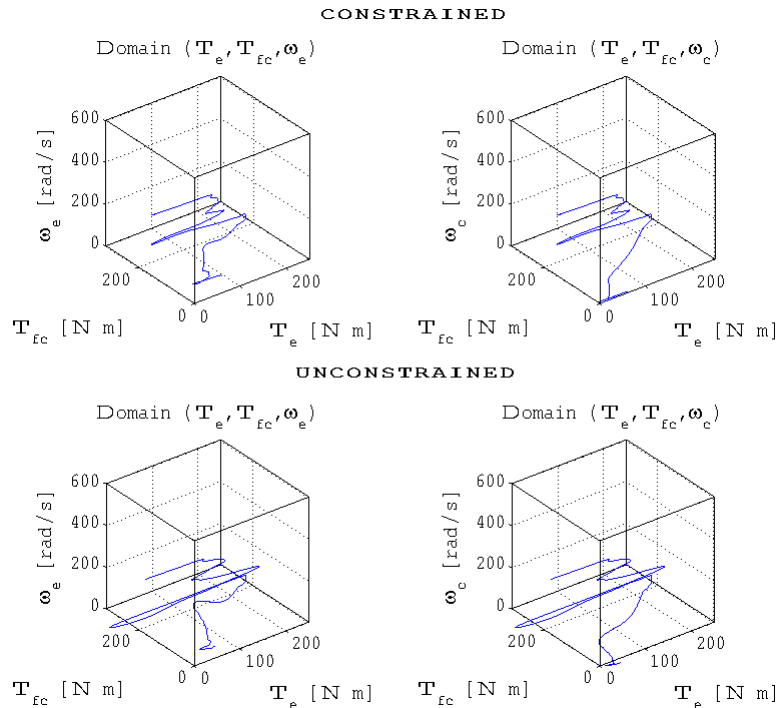
Figure 4.25: Input/Output trajectories

strained model and for the unconstrained model. In this picture it is evident that the constrained MPC keeps both the input and the output within the limits, represented by the black parallelepipeds.

MANOEUVRE 2   This section presents the results of a fast launch manoeuvre. Figure 4.26 points out the engine 4.26(a) and the clutch 4.26(b) angular speeds, respectively. Also in this case there are no differences for the clutch speed between the two models. However there is a remarkable difference between the engine speed of the constrained and unconstrained model (Figure 4.26(a)). This is due to the fast torque demanded for this

manoeuvre as highlighted also in Figure 4.27. Actually, in this figure, by comparing the image 4.27(a) with the image 4.27(b), it is worth to note how the constraints, both on the engine torque and on its rate, play an important role to prevent the violation of the limits (red solid lines). In the same figure it underlined that the clutch torque in both cases is nearly the same (blue dashed lines).   In this case the unconstrained MPC imposes high

(a) Engine angular speed vs. time   (b) Clutch angular speed vs. time
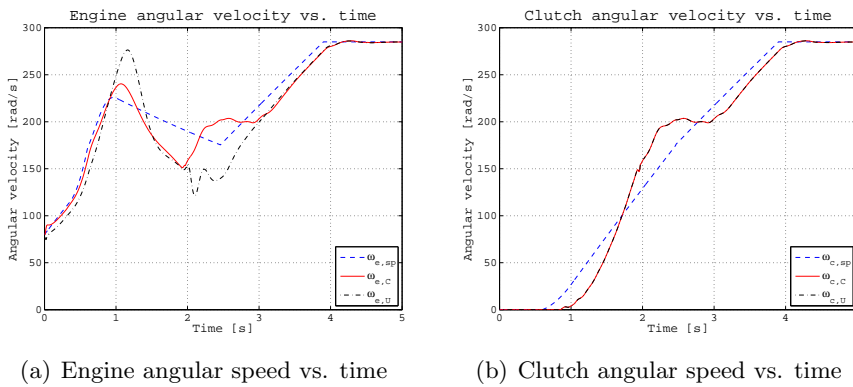
Figure 4.26: Engine (a) and Clutch (b) angular speed

(a) Constrained   (b) Unconstrained
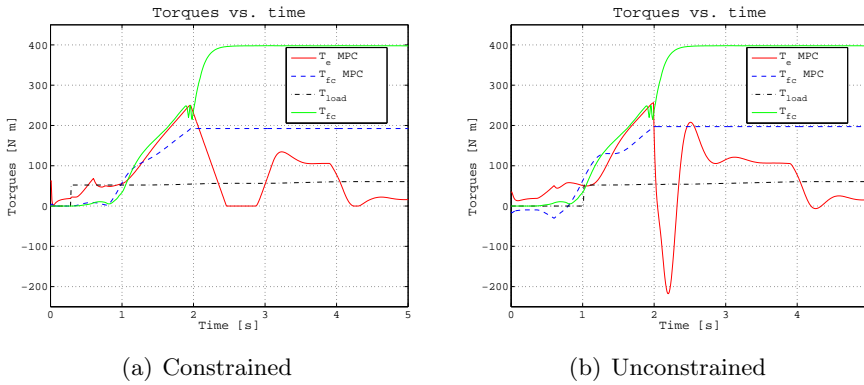
Figure 4.27: Torques (a) Constrained and (b) Unconstrained

negatives values to the throwout bearing, which compromises the system security. Figure 4.28(a) exhibits that the constrained controllers, also for a fast torque demand, never reach negatives values of x_{to}.   Finally, Figure 4.30 highlights the good performance of the constrained MPC preventing
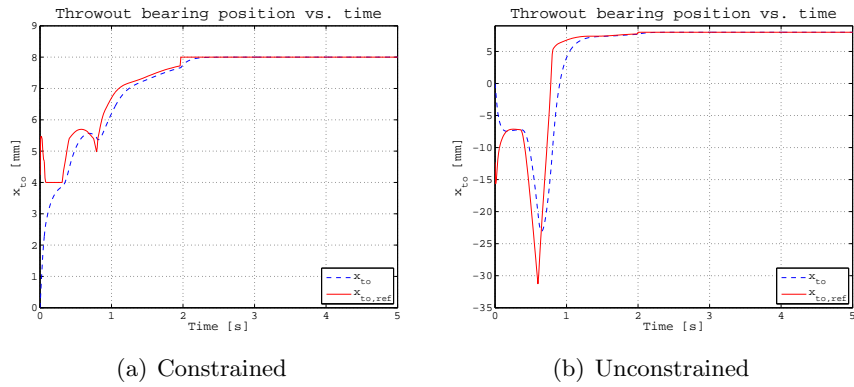
Figure 4.28: Throwout bearing position (a) Constrained and (b) Unconstrained
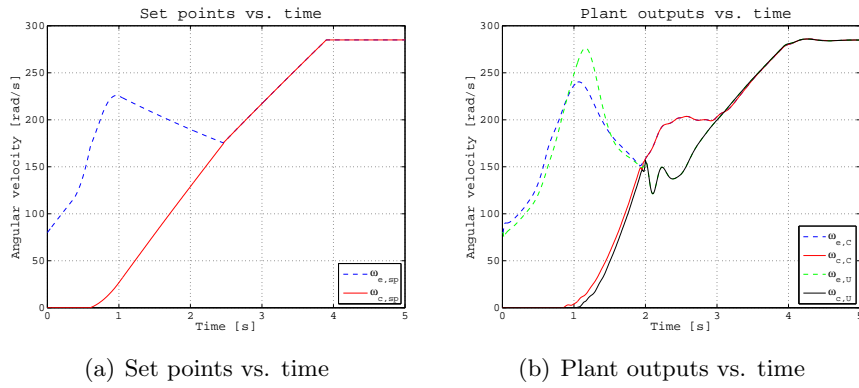
Figure 4.29: Engine and clutch speed (a) Set points (b) Plant outputs

the limits to be exceeded.
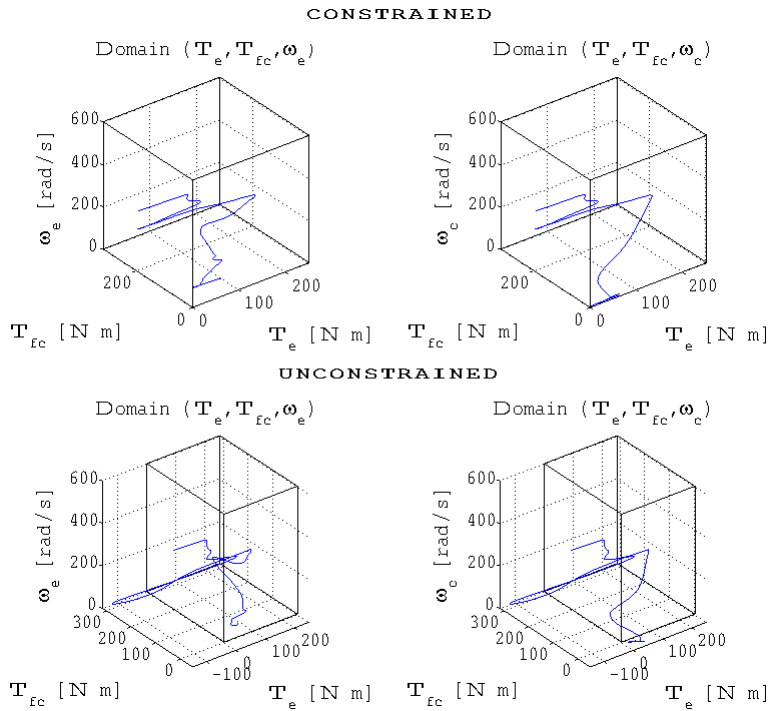
Figure 4.30: Input/Output trajectories

OPTIMIZED MPCs FOR A REDUCED-ORDER MODEL OF THE DRIVELINE This sub-paragraph shows the simulations results of the constrained MPCs tuned for a reduced-order driveline, but used to control the high-order driveline described in the previous paragraph, which better represents the real system. As explained in [62], [63] the reduced-order model of the driveline can be controlled by using only one MPC. However the simulations carried out demonstrate that it is impossible to control a real system by using only one controller. The reduced-order model can be obtained from the high-order one, as explained in the previous paragraph, by assuming the rigidity of the crankshaft $\omega_e = \omega_f$, of the mainshaft $\omega_c = \omega_g$ and of the driveshaft $\omega_g = r\omega_w$. The reduced-order model requires a less number of states to estimate. Consequently, the computational effort is reduced by permitting to implement the MPC in real-time applications.

Actually, Figures 4.31, 4.32, 4.33 and 4.34 illustrate that, after that the engagement condition is reached, the controller cannot manage the lock-up phase at the same time.

(a) Engine angular speed vs. time   (b) Clutch angular speed vs. time
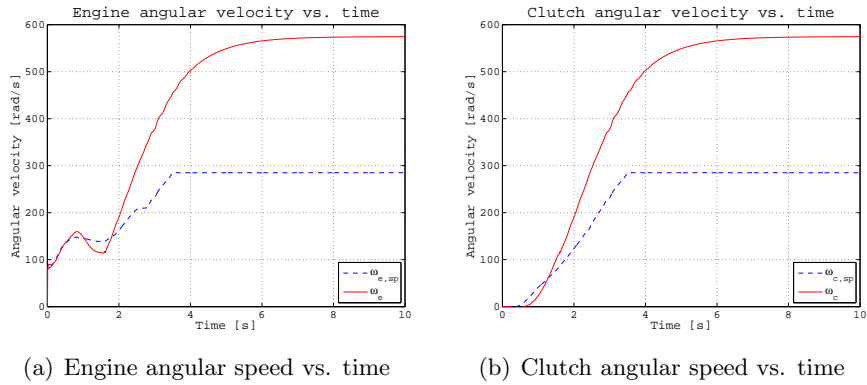
Figure 4.31: Manoeuvre 1: Engine (a) and Clutch (b) angular speed

(a) Set points vs. time   (b) Plant outputs vs. time

Figure 4.32: Manoeuvre 1: Engine and clutch speed (a) Set points (b) Plant outputs

Thus, a second controller is necessary to overcome this problem. As shown later, by introducing an optimized second controller also on the reduced-order model, it is possible to control a high-order model. Table 4.5 shows the parameters used for the MPC optimized for a reduced-order model during the slipping phase: Table 4.6 lists the parameters used for the MPC optimized for a reduced-order model during the engaged phase:
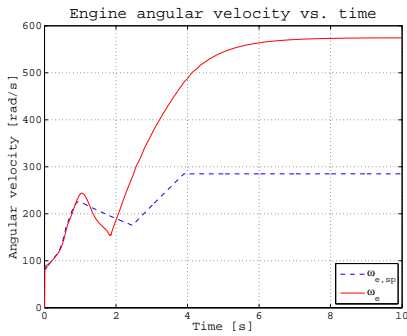
(a) Engine angular speed vs. time
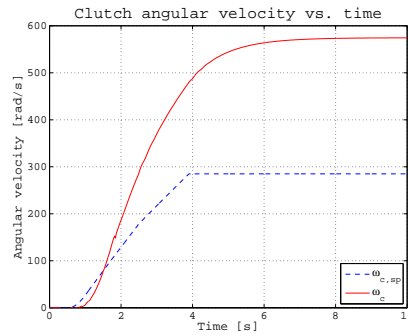
(b) Clutch angular speed vs. time

Figure 4.33: Manoeuvre 2: Engine (a) and Clutch (b) angular speed
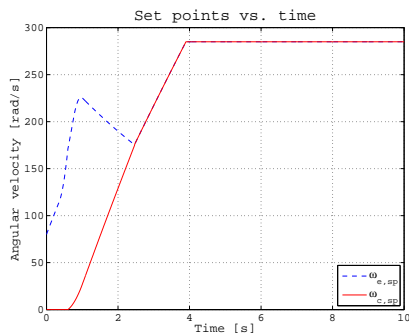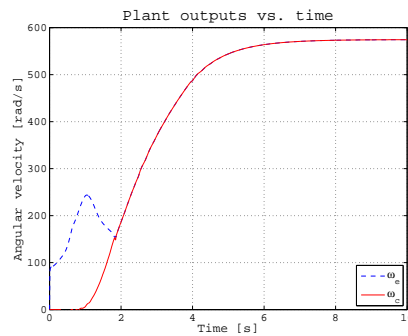
(a) Set points vs. time

(b) Plant outputs vs. time

Figure 4.34: Manoeuvre 2: Engine and clutch speed (a) Set points (b) Plant outputs

MPC1 - SLIPPING PHASE			
Symbol	Description	Value	
		1	2
W_u	Input weight	0.10	0.10
$W_{\Delta u}$	Input rate weight	0.10	0.10
W_y	Output weight	1.00	1.00
P	Prediction horizon	10	
m	Control horizon	2	
ρ_ϵ	Overall penalty weight	0.8	

Table 4.5: MPC1 parameters, slipping phase

As previously explained zero value has been used for $W_u(2)$ and $W_{\Delta u}(2)$

MPC2 - ENGAGED PHASE			
Symbol	Description	Value	
		1	2
W_u	Input weight	0.00	0.00
$W_{\Delta u}$	Input rate weight	1.00	0.00
W_y	Output weight	1.00	1.00
P	Prediction horizon	15	
m	Control horizon	5	
ρ_ϵ	Overall penalty weight	0.8	

Table 4.6: MPC2 parameters, engaged phase

because the second input does not influence the plant during the engaged phase. Instead, for $W_u(1)$ a small value has been used to avoid singularity problem on the Hessian matrix (the nominal zero value has been listed in the table).

MANOEUVRE 1 Figure 4.35 displays the comparison between the engine angular speed, set point and plant output, 4.35(a), and the clutch angular speed set point and plant output, 4.35(b). It is noteworthy the start-up manoeuvre with the constrained controllers optimized for a reduced-order model produces a slight increase of the jerks, Figures 4.35 and 4.36. Finally, Figure 4.37 points out the torque values as a function of the time.
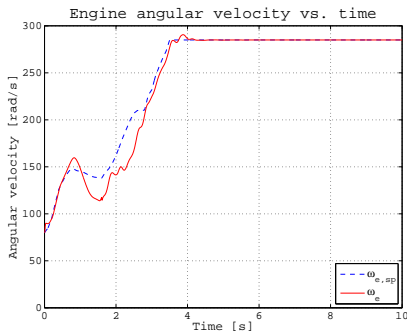
(a) Engine angular speed vs. time
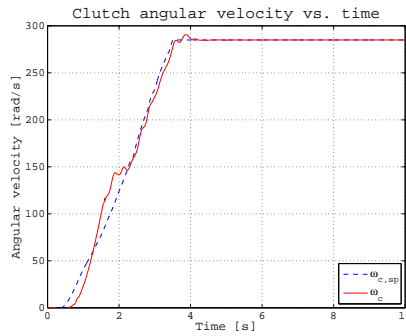
(b) Clutch angular speed vs. time

Figure 4.35: Engine (a) and Clutch (b) angular speed
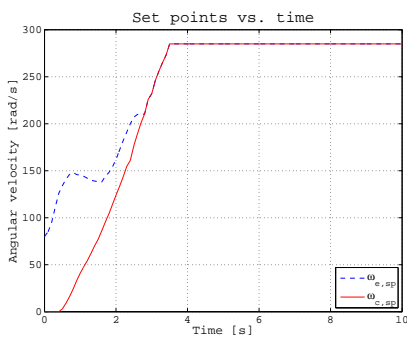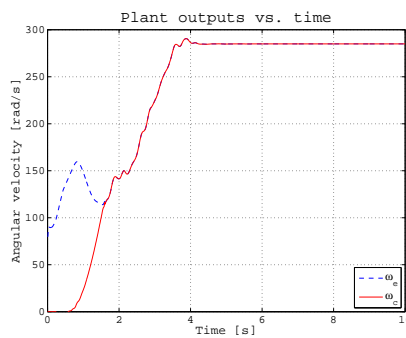
(a) Set points vs. time

(b) Plant outputs vs. time

Figure 4.36: Engine and clutch speed (a) Set points (b) Plant outputs
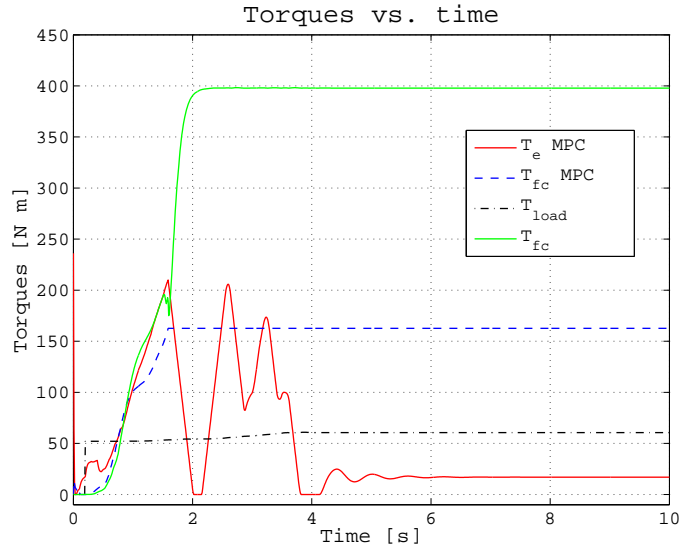
Figure 4.37: Torques vs. time

MANOEUVRE 2   Figure 4.38 exhibits the comparison between the engine angular speed, set point and plant output, 4.38(a), and the clutch angular speed set point and plant output, 4.38(b). Also in this case it is possible to note that the start-up manoeuvre with the constrained controllers optimized for a reduced-order model produces a slight increase of the jerks, Figures 4.38 and 4.39.   Finally, Figure 4.40 shows the torque values as a function of the time. This graph, together with Figure 4.37, highlights that controllers yield sudden changes of the engine torque during the launch manoeuvre, which results in increase of the jerks. A controller-order reduction leads up to a decrease of its computational effort. In fact, a reduced-order plant requires fewer states to estimate than a high-order plant. From this standpoint, the evaluation of the performance of the reduced-order controllers can be useful for evaluating the opportunity to implement the model predictive controller in real-time applications.
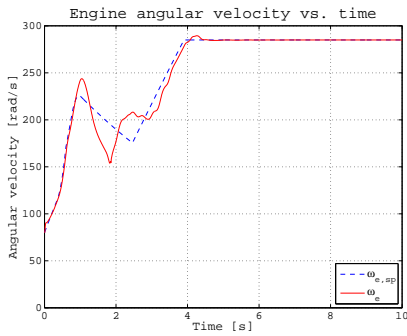
(a) Engine angular speed vs. time
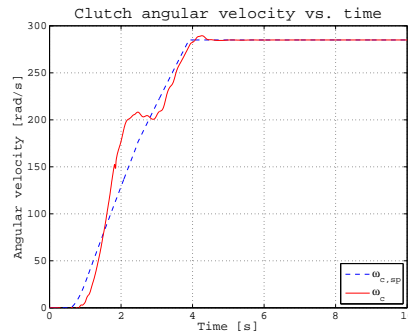
(b) Clutch angular speed vs. time

Figure 4.38: Engine (a) and Clutch (b) angular speed
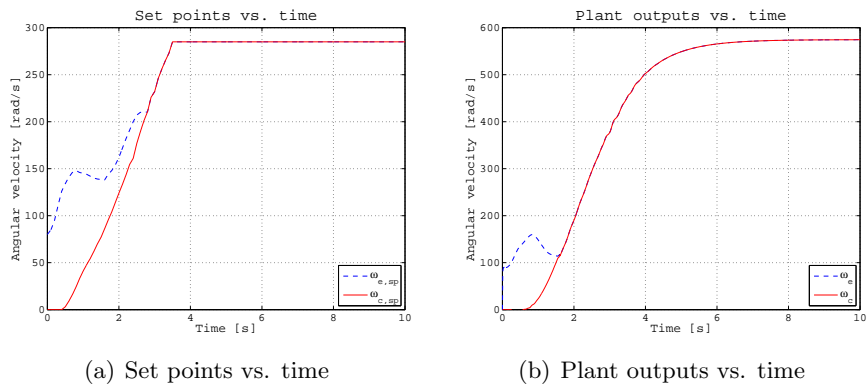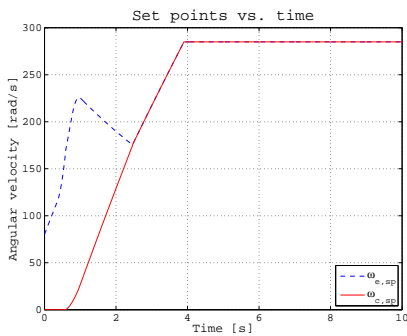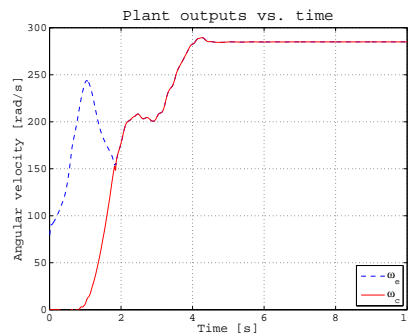
(a) Set points vs. time

(b) Plant outputs vs. time

Figure 4.39: Engine and clutch speed (a) Set points (b) Plant outputs
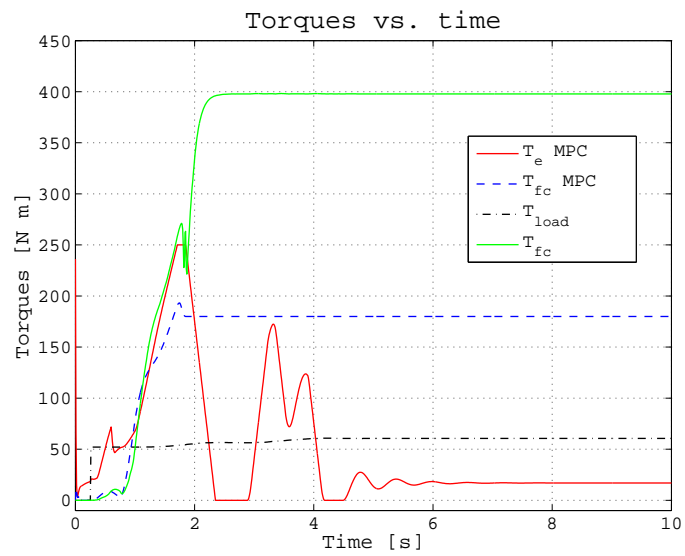
Figure 4.40: Torques vs. time

Chapter 5

CONCLUDING REMARKS

This Ph.D dissertation focuses on the analysis of dry clutches used in AMTs/DCTs. In particular, the mechanical behaviour and the role of the main elastic components, such as the the diaphragm spring, the cushion spring and the drive straps, on the clutch torque characteristic have been studied. Furthermore, a deep analysis on the friction coefficient has been carried out to find the main factors that affect the facing material behaviour.

Since the thermal influence plays a crucial role in a dry clutch system an investigation on how the temperature affects the clutch torque characteristic has been done. The inference of the temperature on the cushion spring, on the diaphragm spring and on the friction coefficient has been analysed separately to empathize the influence of the temperature during the vehicle launch and gear-shifts manoeuvres in dry clutch AMTs/DCTs after repetitive engagements. It has been shown that after repeated engagements the temperature of the facings rises and this influences the friction coefficient behaviour. In fact, the friction coefficient exhibits a smooth variation within a wide range of temperature, whereas it begins to decline at temperature higher than 250 °C. This effect is due to the decomposition of the phenol resin of the clutch facings at high temperature. In fact, when the temperature reaches very high values this mechanism leads to friction coefficient drop. The sliding speed and the contact pressure also influence the friction coefficient. In particular the friction coefficient tends to an asymptotic value at higher sliding speed, and this value is higher for higher contact pressure level. This means that the contact pressure has a nearly linear influence on the friction coefficient. No significant influence of the temperature on the diaphragm spring load-deflection characteristic has been found. Instead, the

temperature influences the throwout bearing characteristic position because the axial thermal expansion and the cushion spring load-deflection curve lead to a variation of the kiss point. In particular the temperature affects in two ways the cushion spring load deflection curve. Indeed, by increasing the temperature level, the material stiffness changes and this results in local modification of the load-deflection characteristic slope. Conversely, the thermal load induces a thermal expansion with axial size increasing.

The effects of the temperature during the vehicle launch have been highlighted simulating two typical manoeuvre, a slow-torque request and a fast-torque request. The results have demonstrated that the open loop controller, which does not take into account the thermal effects, selects a wrong position for the throwout bearing causing the switching off of the engine in the first case, and a poor engagement in the second one. The same vehicle launch manoeuvres along with an up-shift gear request have been simulated with a decoupling PI closed loop controller. Also in this case the results have highlighted that during a vehicle launch the thermal effects influence the engagement time. It is due to the higher temperature that induces a thermal expansion of the cushion spring and this results in an backward travel of the position of the kiss point. Consequently, at higher temperature the TCU, which does not take into account the thermal effects, assigns a given position of the throwout bearing which corresponds to an unexpected higher torque value. In the second case the results have shown that the up-shift manoeuvre is only lightly influenced by the temperature because the engagement condition is reached for low values of the throwout bearing position to which corresponds a nearly same cushion spring load. Consequently, it results in a similar value of the clutch torque transmitted by the clutch. Finally, a multiple model predictive controller (mMPC) for dry clutch engagement problem during vehicle launch has been proposed. Two controllers, the first for the slipping phase and the second for the engaged phase, have been designed to achieve a good trade-off between a fast engagement and a comfortable manoeuvre by complying with the imposed limits both on the input and the output variables. Simulation results have shown that a good choice of the MPC parameters and the adoption of constrained controllers make it possible to achieve better performance in terms of safety of the system and comfortable engagement process. Even tough using a more complex controller is proven that the uncertainty of the clutch torque map due to the temperature induces jerks. This results in a uncomfortable launch manoeuvre and consequently in poor engagements. As previously explained, these phenomena are related to the backward travel of the kiss

point at higher temperatures making the start-up manoeuvre faster. It is worth to highlight that the thermal disturbance can not be compensated by an inner loop on the throwout bearing position. Indeed, if the clutch torque transmissibility model implemented in the TCU does not take into account the thermal effects it generates a wrong reference throwout bearing position frustrating the controller role on the inner loop. Moreover, for this reasons a sensor on the throwout bearing is worthless and unjustified.

By concluding, for these reasons, the availability of a dependable model about the thermal effects on the dry clutch assembly is crucial to improve engagement performance exhibited by AMTs/DCTs especially during start up manoeuvres after repetitive gear shifts.

References

[1] M. Pisaturo, "Relazione Geometria-Caratteristica Elastica di un Disco Elemento in Frizioni a Secco Automotive", Master Thesis, University of Salerno, 2008/09.

[2] F. Vasca, L. Iannelli, A. Senatore, and M. Scafati, "Modeling Torque Transmissibility for Automotive Dry Clutch Engagement", in *American Control Conference, 2008*, 2008, pp. 306–311.

[3] A. Senatore, "Advances in the Automotive Systems: An Overview of Dual-Clutch Transmissions", *Recent Patents on Mechanical Engineering*, vol. 2, pp. 93–101, 2 2009, ISSN: 2212-7976.

[4] (2009). Global Automotive Industry News, Market Research and Expert Analysis, [Online]. Available: `www.just-auto.com` (visited on 12/27/2009).

[5] C. Worldwide. (2009). Source for Automotive Market Forecasting and Automotive Market Foresight, [Online]. Available: `www.csmauto.com` (visited on 12/27/2009).

[6] E. Vitale, *Le Frizioni Manuali*, 2005.

[7] (2013). Special Tuning Clutches, [Online]. Available: `www.apracing.com` (visited on 12/27/2013).

[8] P. Dolcini, C. Canudas de Wit, and H. Béchart, *Dry Clutch Control for Automotive Applications*, Springer, Ed. 2010.

[9] W. Reik, R. Seebacher, and A. Kooy, "Dual Mass Flywheel", LuK, 6th LuK Symposium, 1998.

[10] K.-L. Kimming, "The Self-Adjusting Clutch SAC of the 2nd Generation", LuK, 6th LuK Symposium, 1998.

[11] R. Felger, C. Spandern, M. Häßler, and H.-D. Elison, "Innovative Clutch Facing Materials", LuK, LuK Symposium, 2006.

[12] "LuK Clutch Course: An Introduction to Clutch Technology for Passenger Cars", LuK, 2012.

[13] (2013). Manual Transmission, [Online]. Available: `en.wiki-pedia.org/wiki/Manual_transmission` (visited on 09/02/2013).

[14] (2013). Manual Transmission, [Online]. Available: `www.thecarsecrets.net/manual-transmission/` (visited on 12/01/2013).

[15] G. Lucente, M. Montanari, and C. Rossi, "Modelling of an Automated Manual Transmission System", *Mechatronics*, vol. 17, no. 2-3, pp. 73–91, 2007, ISSN: 0957-4158.

[16] Fisher and Berger, "Automation of Manual Trasmission", LuK, 6th LuK Symposium, 1998.

[17] Kimming and Agner, "Double Clutch: Wet or Dry, this is the question", LuK, LuK Symposium, 2006.

[18] (2013). Automatic Transmission, [Online]. Available: `en.wikipedia.org/wiki/Automatic_transmission` (visited on 09/06/2013).

[19] (2013). Automatic Transmission, [Online]. Available: `www.oscars-automatictransmission.com/` (visited on 09/06/2013).

[20] (2013). Continuously Variable Transmission, [Online]. Available: `en.wikipedia.org/wiki/Continuously_variable_transmission` (visited on 09/06/2013).

[21] Faust and Linnenbrugger, "CVT Development at LuK", LuK, 6th LuK Symposium, 1998.

[22] F. Vasca, L. Iannelli, A. Senatore, and G. Reale, "Torque Transmissibility Assessment for Automotive Dry-Clutch Engagement", *Mechatronics, IEEE/ASME Transactions on*, vol. 16, no. 3, pp. 564–573, 2011, ISSN: 1083-4435.

[23] S. Mauro, G. Mattiazzo, M. Velardocchia, G. Serra, F. Amisano, and G. Ercole, "The Influence of the Push-plate Mechanical Characteristic on Torque Transmissibility in Diaphragm Spring Clutches", in *AIMETA International Tribology Conference*, September, 18-20, Vietri sul Mare, Italy, 2002.

[24] G. La Rosa, M. Messina, and A. Risitano, "Stiffness of Variable Thickness Belleville Springs", *Journal of Mechanical Design*, vol. 123, pp. 294–299, 2 1998.

[25] N. Cappetti, M. Pisaturo, and A. Senatore, "Temperature Influence on the Engagement Uncertainty in Dry Clutch-AMT", in *Proceedings of Global Powertrain Congress*, May, 9-10, Frankfurt am Main, Germany, 2012.

[26] S. Sfarni, E. Bellenger, J. Fortin, and M. Malley, "Finite Element Analysis of Automotive Cushion Discs", *Thin-Walled Structures*, vol. 47, no. 4, pp. 474–483, 2009, ISSN: 0263-8231.

[27] N. Cappetti, M. Pisaturo, and A. Senatore, "Load-Deflection Curve Sensitivity to Main Shape Parameters in a Dry Clutch Cushion Spring", in *Proceedings of the Seventh International Conference on Engineering Computational Technology*, September 14-17, Valencia, Espagna, 2010.

[28] N. Cappetti, M. Pisaturo, and A. Senatore, "Modelling the Cushion Spring Characteristic to Enhance the Automated Dry-Clutch Performance: The Temperature Effect", *Proceedings of the Institution of Mechanical Engineers, Part D: Journal of Automobile Engineering*, vol. 226, no. 11, pp. 1472–1482, 2012.

[29] N. Cappetti, M. Pisaturo, and A. Senatore, "Cushion Spring Sensitivity to the Temperature Rise in Automotive Dry Clutch and Effects on the Frictional Torque Characteristic", *Mechanical Testing and Diagnosis*, vol. 3, pp. 28–38, 2012.

[30] H. Feng, M. Yimin, and L. Juncheng, "Study on Heat Fading of Phenolic Resin Friction Material for Micro-automobile Clutch", in *Measuring Technology and Mechatronics Automation (ICMTMA), 2010 International Conference on*, vol. 3, 2010, pp. 596–599.

[31] B. Czél, K. Váradi, A. Albers, and M. Mitariu, "FE Thermal Analysis of a Ceramic Clutch", *Tribology International*, vol. 42, no. 5, pp. 714–723, 2009, ISSN: 0301-679X.

[32] LuK, *Technical Data Sheet for Friction Material R-233*.

[33] V. D'Agostino, N. Cappetti, M. Pisaturo, and A. Senatore, "Improving the Engagement Smoothness Through Multi-Variable Frictional Map in Automated Dry Clutch Control", in *Proceedings of the ASME2012 International Mechanical Engineering Congress & Exposition, Transportation Systems*, November, 9-15, vol. 11, Houston, Texas, USA, 2012, pp. 9–19, ISBN: 978-0-7918-4527-1.

[34] C. Duan and R. Singh, "Dynamics of a 3DoF Torsional System with a Dry Friction Controlled Path", *Journal of Sound and Vibration*, vol. 289, no. 4-5, pp. 657–688, 2006, ISSN: 0022-460X.

[35] A. Senatore, V. D'Agostino, R. D. Giuda, and V. Petrone, "Experimental Investigation and Neural Network Prediction of Brakes and Clutch Material Frictional Behaviour Considering the Sliding Acceleration Influence", *Tribology International*, vol. 44, no. 10, pp. 1199–1207, 2011, ISSN: 0301-679X.

[36] V. D'Agostino, M. Pisaturo, and A. Senatore, "Improving the Engagement Performance of Automated dry Clutch Through the Analysis of the Influence of the Main Parameters on the Frictional Map", in *5th World Tribology Congress*, September, 8-13, Turin, Italy, 2013.

[37] A. Senatore, A. Ruggiero, and M. Pisaturo, "Models for Pressure Control of Automated dry Clutches: Temperature Influence on Frictional and Elastic Behaviour", *ACTA TECHNICA CORVININESIS*, vol. 4, pp. 55–58, 2013, ISSN: 2067-3809.

[38] Nam, Lee, Chai, and Kwon, "Finite Element Analysis and Optimal Design of Automobile Clutch Diaphragm Spring", F. W. A. Congress, Ed., 2000.

[39] D. H. Johnson, "Principles of Simulating Contact Between Parts using ANSYS", *ANSYS*, 2002.

[40] *ANSYS Contact Tecnology Guide*, 2007.

[41] V. D'Agostino, N. Cappetti, M. Pisaturo, and A. Senatore, "Dry Clutch Models for Control of AMTs/DCTs: Influence of the Temperature Level on Frictional and Elastic Characteristics", *International Journal of Mechanical Engineering and Industrial Design*, vol. 1, no. 1, pp. 106–111, 2012, ISSN: 2280-6407.

[42] B. Armstrong-Helouvry, "Stick Slip and Control in Low Speed Motion", *IEEE Trans. Autom. Control*, 1993.

[43] J. Heap, "Application of Variable Coefficient of Friction and Wear to Block Brakes and Clutches", *J Mech Eng Sci*, 1993.

[44] S. Herscovici, "Determining the Static and Dynamic Coefficient of Friction and its Causes for Variation", *SAE Paper 690570*, 1969.

[45] M. Raghavan and R. Jayachandran, "Analysis of the Performance Characteristics of a Two-Inertia Power Transmission System with a Plate Clutch", *J Mech Mach Theory*, 1989.

[46] K. Poser, K.-H. Z. Gahr, and J. Schneider, "Development of Al2O3 based ceramics for dry friction systems", *Wear*, vol. 259, no. 1-6, pp. 529–538, 2005, 15th International Conference on Wear of Materials, ISSN: 0043-1648.

[47] D. Centea, H. Rahnejat, and M. T. Menday, "The Influence of the Interface Coefficient of Friction upon the Propensity to Judder in Automotive Clutches", *Proceedings of the Institution of Mechanical Engineers, Part D: Journal of Automobile Engineering*, vol. 213, no. 3, pp. 245–258, 1999.

[48] P. Maucher, "Clutch Chatter", in *Proceedings of the 4th International Symposium on Torsional Vibrations in the Drivetrain*, Baden-Baden, Germany, 1990.

[49] A. Yevtushenko, A. Adamowicz, and P. Grzes, "Three-dimensional {FE} Model for the Calculation of Temperature of a Disc Brake at Temperature-dependent Coefficients of Friction", *International Communications in Heat and Mass Transfer*, vol. 42, no. 0, pp. 18–24, 2013, ISSN: 0735-1933.

[50] D. Dane Quinn, "A New Regularization of Coulomb Friction", *ASME Journal of Vibration and Acoustics*, vol. 126, no. 3, pp. 391 –397, 2004, ISSN: 2280-6407.

[51] B. Bhushan, *Modern Tribology Handbook*, C. Press, Ed. 2001, vol. 1- Principles of Tribology.

[52] L. Glielmo, L. Iannelli, V. Vacca, and F. Vasca, "Gearshift Control for Automated Manual Transmissions", *Mechatronics, IEEE/ASME Transactions on*, vol. 11, no. 1, pp. 17–26, 2006, ISSN: 1083-4435.

[53] F. Garofalo, L. Glielmo, L. Iannelli, and F. Vasca, "Smooth Engagement for Automotive Dry Clutch", in *Decision and Control, 2001. Proceedings of the 40th IEEE Conference on*, vol. 1, 2001, pp. 529–534.

[54] J. M. Maciejowski, *Predictive Control with Constraints*, P. Hall, Ed. 2000.

[55] X. Lu, P. Wang, B. Gao, and H. Chen, "Model Predictive Control of AMT clutch during start-up process", in *Control and Decision Conference (CCDC), 2011 Chinese*, 2011, pp. 3204–3209.

[56] R. Bhattacharya, G. J. Balas, M. A. Kaya, and A. Packard, "Nonlinear Receding Horizon Control of an F-16 Aircraft", *Journal of Guidance, Control, and Dynamics*, vol. 25, no. 5, pp. 924–931, 2002, ISSN: 0731-5090.

[57] G. Goodwin, H. Haimovich, D. Quevedo, and J. Welsh, "A Moving Horizon Approach to Networked Control System Design", *Automatic Control, IEEE Transactions on*, vol. 49, no. 9, pp. 1427–1445, 2004, ISSN: 0018-9286.

[58] M. Cychowski and K. Szabat, "Efficient Real-time Model Predictive Control of the Drive System with Elastic Transmission", *Control Theory Applications, IET*, vol. 4, no. 1, pp. 37–49, 2010, ISSN: 1751-8644.

[59] P. Zometa, M. Kogel, T. Faulwasser, and R. Findeisen, "Implementation Aspects of Model Predictive Control for Embedded Systems", in *American Control Conference (ACC), 2012*, 2012, pp. 1205–1210.

[60] C.-Y. Lin and Y.-C. Liu, "Precision Tracking Control and Constraint Handling of Mechatronic Servo Systems Using Model Predictive Control", *Mechatronics, IEEE/ASME Transactions on*, vol. 17, no. 4, pp. 5 93–605, 2012, ISSN: 1083-4435.

[61] H. Quanan, S. Jian, and L. Lei, "Research on Rapid Testing Platform for TCU of Automated Manual Transmission", in *Proceedings of the 2011 Third International Conference on Measuring Technology and Mechatronics Automation - Volume 03*, ser. ICMTMA '11, Washington, DC, USA: IEEE Computer Society, 2011, pp. 67–70, ISBN: 978-0-7695-4296-6.

[62] A. Bemporad, F. Borrelli, L. Glielmo, and F. Vasca, "Hybrid Control of Dry Clutch Engagement", in *European Control Conference*, Porto, Portugal, 2001, pp. 635–639.

[63] R. Amari, M. Alamir, and P. Tona, "Unified MPC Strategy for Idle Speed Control, Vehicle Start-up and Gearing Applied to an Automated Manual Transmission", in *17th IFAC World Congress*, July, 6-11, Seoul, South Korea, 2008.

Appendix A

DRIVELINE PARAMETERS

DRIVELINE PARAMETERS		
Symbol	**Description**	**Value**
Δ	$\mu_d - \mu_s$	-
ρ_a	Air density	$1.2\ kgm^{-3}$
$\dot{\omega}_c$	Clutch angular acceleration	$rads^{-2}$
ω_c	Clutch angular speed	$rads^{-1}$
$\dot{\omega}_{c,SP}$	Set point clutch angular speed	$rads^{-1}$
$\dot{\omega}_e$	Engine angular acceleration	$rads^{-2}$
$\omega_e,\ \dot{\vartheta}_e$	Engine angular speed	$rads^{-1}$
$\dot{\omega}_{e,SP}$	Set point engine angular speed	$rads^{-1}$
$\dot{\omega}_f$	Flywheel angular acceleration	$rads^{-2}$
$\omega_{ef},\ \dot{\vartheta}_{ef}$	Crankshaft angular speed	$rads^{-1}$
ϑ_{ef}	Crankshaft angle	rad
$\dot{\omega}_g$	Main-shaft angular acceleration	$rads^{-2}$
$\omega_g,\ \omega_{cg},\ \dot{\vartheta}_{cg}$	Main-shaft angular speed	$rads^{-1}$
ϑ_{cg}	Main-shaft angle	rad
$\dot{\omega}_w$	Wheel angular acceleration	$rads^{-2}$
$\omega_{gw},\ \dot{\vartheta}_{gw}$	Driveshaft angular speed	$rads^{-1}$
ϑ_{gw}	Driveshaft angle	rad
δ_f	Cushion spring compression	mm
$\mu_s,\ \mu_d$	Static (dynamic) friction coefficient	$-$
A	Front surface vehicle area	$2.12\ m^2$
c_d	Air resistance coefficient	0.367
F_{fc}	Reaction of the cushion spring	N
J_c	Equivalent clutch disc inertia	$0.0159\ kgm^2$
J_e	Equivalent engine inertia	$0.159\ kgm^2$
J_f	Equivalent flywheel inertia	$0.0159\ kgm^2$
J_g	$J_{g1} + J_{g2}/r^2$	kgm^2
J_{g1}	Equivalent gearbox primary shaft	$0.039\ kgm^2$
J_{g2}	Equivalent gearbox secondary shaft	$0.039\ kgm^2$
J_v	Equivalent vehicle inertia at main-shaft	$0.942\ kgm^2$
J_w	Equivalent wheel inertia	$133\ kgm^2$
n	Number of friction surfaces on the clutch disc	2

DRIVELINE PARAMETERS		
Symbol	**Description**	**Value**
R_{eq}	Equivalent radius of the contact surface	$0.089\ m$
R_w	Wheel radius	$0.32\ m$
t	Time	s
T_{cg}	Main-shaft torque	Nm
$T_e^{ref},\ T_e$	Engine torque	Nm
T_{ef}	Engine-flywheel torque	Nm
T_{fc}	Torque transmitted by clutch	Nm
T_{fc}^{ref}	Reference torque transmitted by clutch	Nm
T_{gw}	Driveshaft torque	Nm
T_w	Equivalent torque load at wheel	Nm
T_{w0}	Load torque	Nm
v	Sliding speed	ms^{-1}
b_e	Engine friction coefficient	$0.03\ Nmsrad^{-1}$
b_g	Main-shaft friction coefficient	$0.012\ Nmsrad^{-1}$
b_{ef}	Crankshaft viscous damping	$100\ Nmsrad^{-1}$
b_{cg}	Main-shaft viscous damping	$4\ Nmsrad^{-1}$
k_{ef}	Crankshaft torsional stiffness coefficient	$32 \cdot 10^3\ Nmrad^{-1}$
k_{cg}	Main-shaft torsional stiffness coefficient	$3.2 \cdot 10^3\ Nmrad^{-1}$
k_{gw}	Driveshaft torsional stiffness coefficient	$16 \cdot 10^3\ Nmrad^{-1}$
r	Gear ratio (included the final conversion ratio)	$-$
x_{pp}	Pressure plate position	mm
x_{to}	Throwout bearing position	mm
x_{to}^{ref}	Reference throwout bearing position	mm
x_{to}^{cnt}	Throwout bearing position at kiss point	mm
x_{to}^{cls}	Throwout bearing position at clutch closed	mm
x_{to}^{max}	Throwout bearing maximum position	mm

Appendix B

CONTINUOUS STATE-SPACE REPRESENTATION

$$\dot{\mathbf{x}}(t) = [\mathbf{A}_{sl}d + \mathbf{A}_{eng}(1-d)]\mathbf{x}(t) + [\mathbf{B}_{sl}d + \mathbf{B}_{eng}(1-d)]\mathbf{u}(t)$$

$$\mathbf{y}(t) = \mathbf{C}\mathbf{x}(t)$$

(B.1)

where d is a switching variable equal to 1 when the system is in the slipping phase and 0 otherwise. The subscript sl and eng indicate the slipping and the engaged system matrices, respectively.

B.1   2 DoF

The state, input and output vectors are respectively:

$$\mathbf{x} = \left\{ \begin{array}{cccc} \omega_e & \vartheta_e & \omega_c & \vartheta_c \end{array} \right\}^T$$

$$\mathbf{u} = \left\{ \begin{array}{ccc} T_e & T_{fc} & T_w \end{array} \right\}^T$$

$$\mathbf{y} = \left\{ \begin{array}{cc} \omega_e & \omega_c \end{array} \right\}^T$$

and the matrices are:

$$
\mathbf{A_{sl}} = \begin{bmatrix} \frac{-b_e}{J_e+J_f} & 0 & 0 & 0 \\ 1 & 0 & 0 & 0 \\ 0 & 0 & \frac{-b_g}{J_c+J_v(r)} & 0 \\ 0 & 0 & 1 & 0 \end{bmatrix}
\tag{B.2}
$$

$$
\mathbf{A_{eng}} = \begin{bmatrix} -\frac{b_e+b_g}{J_e+J_f+J_c+J_v(r)} & 0 & 0 & 0 \\ 1 & & 0 & 0 & 0 \end{bmatrix}
\tag{B.3}
$$

$$
\mathbf{B_{sl}} = \begin{bmatrix} \frac{1}{J_e+J_f} & \frac{-1}{J_e+J_f} & 0 \\ 0 & 0 & 0 \\ 0 & \frac{1}{J_c+J_v(r)} & \frac{1}{J_c+r\cdot J_v(r)} \\ 0 & 0 & 0 \end{bmatrix}
\tag{B.4}
$$

$$
\mathbf{B_{eng}} = \begin{bmatrix} \frac{1}{J_e+J_f+J_c+J_v(r)} & 0 & \frac{-1}{J_e+J_f+J_c+J_v(r)} \\ 0 & 0 & 0 \end{bmatrix}
\tag{B.5}
$$

$$
\mathbf{C} = \begin{bmatrix} 1 & 0 & 0 & 0 \\ 0 & 0 & 1 & 0 \end{bmatrix}
\tag{B.6}
$$

$$
\mathbf{D} = \begin{bmatrix} 0 & 0 & 0 \\ 0 & 0 & 0 \end{bmatrix}
\tag{B.7}
$$

B.2 5 DoF

The state, input and output vectors are respectively:

$$
\mathbf{x} = \left\{ \begin{matrix} \omega_e & \vartheta_e & \omega_f & \vartheta_f & \omega_c & \vartheta_c & \omega_g & \vartheta_g & \omega_w & \vartheta_w \end{matrix} \right\}^T
$$

$$
\mathbf{u} = \left\{ \begin{matrix} T_e & T_{fc} & T_w \end{matrix} \right\}^T
$$

$$
\mathbf{y} = \left\{ \begin{matrix} \omega_e & \omega_c \end{matrix} \right\}^T
$$

and the matrices are:

$$
\mathbf{A}_{sl} =
\begin{bmatrix}
-\left(\frac{b_e+b_{ef}}{J_e}\right) & -\frac{k_{ef}}{J_e} & \frac{b_{ef}}{J_e} & \frac{k_{ef}}{J_e} & 0 & 0 & 0 & 0 & 0 & 0 \\
1 & 0 & 0 & 0 & 0 & 0 & 0 & 0 & 0 & 0 \\
\frac{b_{ef}}{J_f} & \frac{k_{ef}}{J_f} & -\frac{b_{ef}}{J_f} & -\frac{k_{ef}}{J_f} & 0 & 0 & 0 & 0 & 0 & 0 \\
0 & 0 & 1 & 0 & 0 & 0 & 0 & 0 & 0 & 0 \\
0 & 0 & 0 & 0 & -\frac{b_{cg}}{J_c} & -\frac{k_{cg}}{J_c} & \frac{b_{cg}}{J_c} & \frac{k_{cg}}{J_c} & 0 & 0 \\
0 & 0 & 0 & 0 & 1 & 0 & 0 & 0 & 0 & 0 \\
0 & 0 & 0 & 0 & \frac{b_{cg}}{J_g} & \frac{k_{cg}}{J_g} & -\left(\frac{b_g+b_{cg}+\frac{b_{gw}}{r2}}{J_g}\right) & -\left(\frac{k_{cg}+\frac{k_{gw}}{r2}}{J_g}\right) & \frac{b_{gw}}{J_g r} & \frac{k_{gw}}{J_g r} \\
0 & 0 & 0 & 0 & 0 & 0 & 1 & 0 & 0 & 0 \\
0 & 0 & 0 & 0 & 0 & 0 & \frac{b_{gw}}{J_w r} & \frac{k_{gw}}{J_w r} & -\frac{b_{gw}}{J_w} & -\frac{k_{gw}}{J_w} \\
0 & 0 & 0 & 0 & 0 & 0 & 0 & 0 & 1 & 0
\end{bmatrix}
$$

$$(\text{B.8})$$

$$
\mathbf{B}_{sl} =
\begin{bmatrix}
\frac{1}{J_e} & 0 & 0 & 0 & 0 & 0 & 0 & 0 & 0 & 0 \\
0 & 0 & -\frac{1}{J_f} & 0 & \frac{1}{J_c} & 0 & 0 & 0 & 0 & 0 \\
0 & 0 & 0 & 0 & 0 & 0 & 0 & 0 & -\frac{1}{J_w} & 0
\end{bmatrix}^{T}
$$

$$(\text{B.9})$$

$$\mathbf{A}_{eng} = \begin{bmatrix} -\left(\dfrac{b_e+b_{ef}}{J_e}\right) & -\dfrac{k_{ef}}{J_e} & \dfrac{b_{ef}}{J_e} & \dfrac{k_{ef}}{J_e} & 0 \\ 1 & 0 & 0 & 0 & 0 \\ \dfrac{b_{ef}}{J_c+J_f} & \dfrac{k_{ef}}{J_c+J_f} & 0 & 0 & -\left(\dfrac{b_{ef}+b_{cg}}{J_c+J_f}\right) \\ 0 & 0 & 0 & 0 & 1 \\ \dfrac{b_{ef}}{J_c+J_f} & \dfrac{k_{ef}}{J_c+J_f} & 0 & 0 & -\left(\dfrac{b_{ef}+b_{cg}}{J_c+J_f}\right) \\ 0 & 0 & 0 & 0 & 1 \\ 0 & 0 & 0 & 0 & \dfrac{b_{cg}}{J_g} \\ 0 & 0 & 0 & 0 & 0 \\ 0 & 0 & 0 & 0 & 0 \\ 0 & 0 & 0 & 0 & 0 \end{bmatrix} \dots$$

$$(B.10)$$

$$\begin{bmatrix} 0 & 0 & 0 & 0 & 0 \\ 0 & 0 & 0 & 0 & 0 \\ -\left(\dfrac{k_{ef}+k_{cg}}{J_c+J_f}\right) & \dfrac{b_{cg}}{J_c+J_f} & \dfrac{k_{cg}}{J_c+J_f} & 0 & 0 \\ 0 & 0 & 0 & 0 & 0 \\ -\left(\dfrac{k_{ef}+k_{cg}}{J_c+J_f}\right) & \dfrac{b_{cg}}{J_c+J_f} & \dfrac{k_{cg}}{J_c+J_f} & 0 & 0 \\ 0 & 0 & 0 & 0 & 0 \\ \dfrac{k_{cg}}{J_g} & -\left(\dfrac{b_g+b_{cg}+\frac{b_{gw}}{r^2}}{J_g}\right) & -\left(\dfrac{k_{cg}+\frac{k_{gw}}{r^2}}{J_g}\right) & \dfrac{b_{gw}}{J_g r} & \dfrac{k_{gw}}{J_g r} \\ 0 & 1 & 0 & 0 & 0 \\ 0 & \dfrac{b_{gw}}{J_w r} & \dfrac{k_{gw}}{J_w r} & -\dfrac{b_{gw}}{J_w} & -\dfrac{k_{gw}}{J_w} \\ 0 & 0 & 0 & 1 & 0 \end{bmatrix}$$

$$\mathbf{B}_{eng} = \begin{bmatrix} \dfrac{1}{J_e} & 0 & 0 & 0 & 0 & 0 & 0 & 0 & 0 & 0 \\ 0 & 0 & 0 & 0 & 0 & 0 & 0 & 0 & 0 & 0 \\ 0 & 0 & 0 & 0 & 0 & 0 & 0 & 0 & -\dfrac{1}{J_w} & 0 \end{bmatrix}^T \qquad (B.11)$$

$$\mathbf{C} = \begin{bmatrix} 1 & 0 & 0 & 0 & 0 & 0 & 0 & 0 & 0 & 0 \\ 0 & 0 & 0 & 0 & 1 & 0 & 0 & 0 & 0 & 0 \end{bmatrix} \qquad (B.12)$$

$$\mathbf{D} = \begin{bmatrix} 0 & 0 & 0 \\ 0 & 0 & 0 \end{bmatrix} \qquad (B.13)$$